

Research on Rain Attenuation Mitigation Technologies for High Throughput Satellite Communication

PEERAMED CHODKAVEEKITYADA

DEPARTMENT OF AEROSPACE ENGINEERING
GRADUATE SCHOOL OF SYSTEM DESIGN
TOKYO METROPOLITAN UNIVERSITY
SEPTEMBER 2016

Research on Rain Attenuation Mitigation Technologies for High Throughput
Satellite Communication

by

Peeramed Chodkaveekityada

Student ID 13991571

Submitted to the Department of Aerospace Engineering,
Graduate School of System Design,
in partial fulfillment of the requirements for the degree of
Doctor of Philosophy in Aerospace Engineering
at the

TOKYO METROPOLITAN UNIVERSITY

September 2016

Certified by advisor

Professor Hajime Fukuchi

Department of Aerospace Engineering

Graduate School of System Design

Tokyo Metropolitan University

Doctoral thesis committee:

Professor Hironori Sahara

Tokyo Metropolitan University

Professor Makoto Abo

Tokyo Metropolitan University

Professor Yoshihisa Takayama

Tokai University

Associate Professor Noboru Takeichi

Tokyo Metropolitan University

Acknowledgements

I would like to express my very appreciation and thanks to my supervisor Prof. Hajime Fukuchi of Tokyo Metropolitan University for his all support.

I would like to thank to Tokyo Metropolitan Government for providing me the Asian Human Resources Fund during my doctoral study in Japan.

My special thanks are extend to Assoc. Prof. Pramote Wardkien, Assoc. Prof. Jeerasuda Koseeyaporn, Prof. Pornchai Supnithi and Asst. Prof. Tulaya Limpiti of King Mongkut's Institute of Technology Ladkrabang, who are behind this successfulness.

Finally, I wish to thank my parents and friends for their support and encouragement throughout my study.

September 30, 2016

Peeramed Chodkaveekityada

Abstract

Since the first satellite was launched in the 20th century, satellite communication technology has been undergoing constant improvement and development to support the growing user demand. The use of satellite broadcasting in the 22 GHz band was recently proposed to transmit high-capacity signals, such as Super Hi-Vision TV. According to ITU frequency allocation, such a band is available in Regions 1 (Europe, the Middle East, Russia, and Africa) and 3 (Asia, Australia, and Oceania). Region 3 includes Japan. In these high throughput satellite and future satellite broadcasting system, rain attenuation has a strong effect on satellite communication systems that use frequencies above 10 GHz, including the Ku- and Ka-bands. Several impairment mitigation strategies including site diversity, time diversity, adaptive satellite power control, and modulation or coding control, can be used to reduce the influence of rain attenuation. Each method has unique advantages and disadvantages depending on its services.

The above mentioned methods may be based on qualitative proposals or empirical knowledge. It is needed to evaluate above future methods quantitatively in order to realize efficient practical link impairments mitigation. This thesis deals mainly three rain attenuation mitigation methods to maintain satellite link service: time diversity, adaptive satellite power control and site diversity. The evaluations of these methods are done by using

measured rainfall rate data all over Japan and Thailand, and measured received level data of satellite signals in Japan and Thailand. Time diversity is shown to likely be the most effective method. The adaptive satellite power control method can be used to improve satellite communication or broadcasting performance in narrow targeted areas. Regarding site diversity method, spatial correlation property of rainfall rate is investigated precisely. It is found that the spatial correlation of rainfall rates has anisotropic characteristics. This is useful to design efficient site diversity design.

This thesis also re-considers the theoretical relationships among rainfall rate, attenuation and depolarization due to rain up to 100 GHz using latest rain model such a Gamma distribution raindrop size distribution. Dual polarization wireless communication link is useful to increase link capacity twice as much. However, the above mentioned depolarization effect is expected to play a more significant role in such a dual-polarized link design.

Contents

Abstract	i
Contents	iii
List of Figures	vi
List of Tables	xi
1. Introduction	1
1.1 Trend of High Throughput Satellite (HTS) System	1
1.2 Future Broadcasting Satellite in Japan	2
1.3 Rain Attenuation Countermeasure Methods	4
1.4 Objectives of This Thesis	6
1.5 Organization	7
2 Theoretical Consideration of Rain Effect on Radio Wave	13
2.1 Introduction	13
2.2 Parameters Consideration	15
2.2.1 Raindrop Size Distribution	15
2.2.2 Rainfall Rate Calculation	17
2.3 Formula for Prediction of XPD	19
2.3.1 Relationship between Attenuation and XPD	19
2.3.2 Relationship between Rainfall Rate and XPD	25
2.4 Effect of Inhomogeneity of the Rainfall Rate	27

3.3.2.3	Rain Rate Diversity Gain	72
3.3.3	Time Diversity Gain Prediction Model	79
3.4	Summary of Chapter 3	81
4	Adaptive Satellite Power Control Method	89
4.1	Concept and System Configuration	89
4.2	Rain Rate Observation and Simulation Parameters	91
4.3	Simulation Results	94
4.3.1	Boost Beam Efficiency	94
4.3.2	Effective Rainfall Rate Reduction Factor throughout Japan	98
4.3.3	ERF and Boost Parameters	101
4.4	Summary of Chapter 4	104
5	Site Diversity Improvement Derived by Rain Gauge Network in Thailand	108
5.1	Overview	108
5.2	Rain Gauge Network	109
5.3	Spatial Correlation Estimation	110
5.3.1	Spatial Correlation Coefficient	110
5.3.2	Spatial Correlation Pattern Analysis	114
5.4	Site Diversity Gain Improvement	116
5.5	Summary of Chapter 5	117
6	Conclusion	120
6.1	Summary of Preceding Chapters	120
6.2	Comparison of attenuation mitigation technologies	123
6.3	Future Work	123
A	List of Publications	125

List of Figures

1.1	Japanese satellite broadcasting roadmap	3
1.2	Highlighted areas of heavy rain	3
1.3	Flowchart of the research	7
1.4	Outline of the thesis	9
2.1	Frequency dependence of parameters	15
2.2	Comparison of the MP and gamma models with various values of $\mu = 0, 3, 6$	17
2.3	Errors of derived rainfall rates of the MP and gamma models with various values of $\mu = 0, 3, 6$	19
2.4	Frequency dependence of V	21
2.5	Frequency dependence of u	21
2.6	Depolarization comparison of theoretical and proposed approximation: (a) MP DSD, (b) gamma DSD	24
2.7	Comparison of XPD of the MP and gamma models with various values of $\mu = 0, 3, 6$	25
2.8	Homogeneous and inhomogeneous rain models	27
2.9	Derivation of XPD correction value for (a) path length dependence, and (b) frequency dependence	29
3.1	The methodology of time diversity and frequency configuration	37

3.2	The flows of time diversity process	38
3.3	Example of time diversity using CS beacon attenuation time series. (blue : original data, red : delayed data, green : time diversity result)	40
3.4	Annual cumulative time percentage of rainfall rate between Kashima, Japan and Bangkok, Thailand	42
3.5	Rain attenuation sample of Thaicom 2 and 3 compared between frequency of 12.57 and 12.59 GHz, and 19.45 GHz	44
3.6	Yearly cumulative time percentage (P) against rain attenuation of Thaicom 2, 3 and CS	46
3.7	Sample of CS beacon attenuation time series with example of the attenuation threshold, fade duration and illustrated fade slope	48
3.8	Fade duration statistic of CS beacon observed at 19.45 GHz. (a) event number of rain fade, (b) total time of rain fade in percentage	50
3.9	Fade duration statistic of Thaicom 2 beacon observed at 19.45 GHz. (a) event number of rain fade, (b) total time of rain fade in percentage	52
3.10	Fade duration statistic of Thaicom 3 beacon observed at 19.45 GHz. (a) event number of rain fade, (b) total time of rain fade in percentage	54
3.11	Rain attenuation comparison of Thaicom 2 and 3. (a) sample of consideration period, (b) scatterplot of attenuation	55
3.12	Fade slope comparison of Thaicom 2, 3 and CS	56
3.13	Comparison of fade slope of Thaicom 2, 3 and CS with ITU prediction model	58

3.14 Performance of time diversity of CS beacon with several time delays 59

3.15 Performance of time diversity of Thaicom 2 for vertical polarization with several time delays. (a) In Ku-band at frequency 12.57 GHz, (b) In Ka-band at frequency 19.45 GHz 61

3.16 Performance of time diversity of Thaicom 3 vertical polarization with several time delays. (a) In Ku-band at frequency 12.59 GHz, (b) In Ka-band at frequency 19.45 GHz 63

3.17 Diversity gain observed at 0.1% of cumulative time percentage against time delays. TC2 and TC3 results represent the diversity gain of Figs 8(b) and 9(b) at 19.45 GHz 64

3.18 Simulation analysis flow 66

3.19 23 observation points on (a) mainland and (b) southwestern islands of Japan 67

3.20 Four-year cumulative distribution of rain intensity for $P = 0.01\%$ with no time diversity for (a) mainland and (b) southwestern islands of Japan 68

3.21 Four-year cumulative distribution of rain intensity for $P = 0.1\%$ with no time diversity for (a) mainland and (b) southwestern islands of Japan 69

3.22 Four-year cumulative distribution of rain intensity for $P = 0.01\%$ with a time diversity of 10 min for (a) mainland and (b) southwestern islands of Japan 70

3.23 Diversity gain vs. rainfall rate for $P = 0.01\%$ with a time diversity of (a) 10 min and (b) 120 min 71

3.24	Cumulative rainfall occurrence rate by location for $P = 0.01\%$ and various time delays	72
3.25	Cumulative time percentage of rainfall rate over four years at Owase for various time delays	75
3.26	Cumulative time percentage versus rain attenuation for (a) rain attenuation in Owase with time delays at 22 GHz and (b) comparison of ITU and Capsoni's parameters in Owase and Tokyo at 20 GHz	75
3.27	Diversity gain versus rain attenuation for 23 observation points in Japan for $P = 0.1\%$ with various time delays at 22 GHz . . .	77
3.28	Comparison prediction of time diversity gain between our proposed and Matricciani models for $P = 0.1\%$ for (a) 10 min, proposed model used $\alpha = 0.585$ and $\beta = 0.739$, and (b) 120 min, proposed model used $\alpha = 0.746$ and $\beta = 0.869$	79
3.29	Cumulative time percentage versus rainfall rate for no time delay, a time delay of 120 min, and the probability maximum gain at (a) Matsumoto and (b) Niigata	80
4.1	Attenuation mitigation using boost beam concept	91
4.2	Analysis flow	93
4.3	Rain intensity for cumulative time percentage of (a) 0.01% and (b) 0.1%	95
4.4	Rain intensity for case 1-1 with cumulative time percentage of (a) 0.01% and (b) 0.1%	96
4.5	Rain intensity for case 4-4 with cumulative time percentage of (a) 0.01% and (b) 0.1%	97
4.6	Rain intensity for cumulative time percentage of 0.01% with (a) case 1-4 and (b) case 4-2	98

4.7	ERFs in case 1-1 for a constant boost beam of 20 mm/h at a cumulative time percentage of 0.01%	99
4.8	ERFs in case 4-4 for a constant boost beam of 20 mm/h at a cumulative time percentage of 0.01%	100
4.9	ERFs in case 1-4 for a constant boost beam of 20 mm/h at a cumulative time percentage of 0.01%	100
4.10	ERFs in case 4-2 for a constant boost beam of 20 mm/h at a cumulative time percentage of 0.01%	101
4.11	Cumulative place percentage in case 1-m	103
4.12	Cumulative place percentage in case 4-m	103
4.13	EFRs for cumulative time percentages of (a) 0.01% and (b) 0.1%	104
5.1	Map of locations of rain gauges	109
5.2	Example of rainfall rate scattergram between station no. 1 and no. 2	111
5.3	Relationship of spatial correlation and distance on a linear scale	112
5.4	Comparison of approximation formula and spatial correlation coefficients of rainfall rate	113
5.5	Rainfall spatial correlation pattern in the center of Thailand .	115

List of Tables

1.1	Classification of attenuation countermeasure.	5
2.1	DSD parameters.	16
2.2	V and u for the relationship between attenuation and XPD . . .	22
2.3	Values of u for the relationship between rainfall rate and XPD	26
2.4	Comparison of propagation for homogeneous and inhomogeneous rainfall models	28
3.1	Geographical and radio links parameters of rain attenuation measurements. Rain attenuation sampling time is 1 s	39
3.2	Event number of CS beacon derived for 2 years	49
3.3	Event number of Thaicom 2 beacon derived for 1 years	51
3.4	Event number of Thaicom 3 beacon derived for 1 years	53
3.5	Parameters describes the rain attenuation behavior derived from fade slope	56
3.6	Diversity gain with various cumulative time percentage of CS beacon	60
3.7	Diversity gain with various cumulative time percentage of Thaicom 2 beacon	62
3.8	Diversity gain with various cumulative time percentage of Thaicom 3 beacon	63

3.9	Rainfall rate and rain attenuation at 22 GHz of 23 observation points of 0.01% and 0.1% of time	76
3.10	Frequency-dependent coefficients of time delays for P = 0.1% at 22 GHz	78
3.11	Prediction errors comparison	79
5.1	Site specifications of Rain gauges	110
5.2	Distance, spatial correlation and azimuth angle parameters .	114
6.1	Advantage and disadvantage of 3 mitigation methods	123

Chapter 1

Introduction

1.1 Trend of High Throughput Satellite (HTS) System

For rapid demand of large capacity and high speed satellite communication and broadcasting, radio wave in higher frequency bands such as Ku- and Ka-bands will be used and high throughput satellite communication system (HTS) can be realized. For example, WINDS(Japan) is a one of HTS for demonstrates the technologies related to ultra-high-speed and large-volume data communication. There are other HTS such as ViaSat-1(US), Eutelsat(France), IPSTAR(Thailand), etc. However, rain influence such as rain attenuation has a strong effect on satellite communication systems that use frequencies above 10 GHz, including the Ku-, Ka-bands or higher bands. Several impairment mitigation strategies including time diversity, adaptive satellite power control, site diversity, or adaptive channel coding and modulation control, are proposed or have been used to reduce the influence of rain attenuation. Each method has unique advantages and disadvantages depending on its services.

1.2 Future Broadcasting Satellite in Japan

In this era, the number of communication networks around the world is increasing rapidly. With the increasing volume of information, faster and higher quality communication links are in demand. To meet these requirements, satellite communications in frequency bands higher than the Ku-band [1][2] are expected to provide existing C-band and Ku-band exchanges, primarily because higher bands have more bandwidth available to support the growing number of users and can thus facilitate high-resolution information exchanges. The International Telecommunications Union (ITU) released a new broadcasting band for use within the last decade. This band spans 21.4–22 GHz [3] in the Ka-band for Region 1 (Europe, Africa) and Region 3 (Asia, Pacific). As a preliminary service, Japanese satellite operators intend to use the 21 GHz slot to broadcast high-quality 8k Super Hi-Vision TV in the year of the Tokyo Olympics (2020) and they plan to start testing in the current year (2016), as presented in Figure1.1.

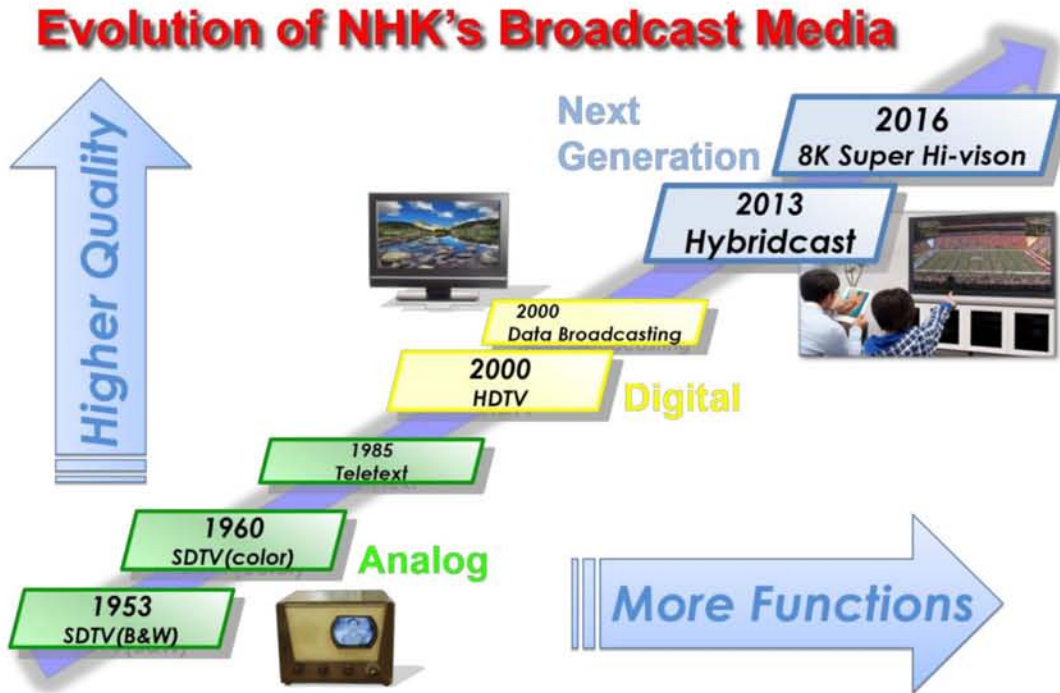


Figure 1.1: Japanese satellite broadcasting roadmap.

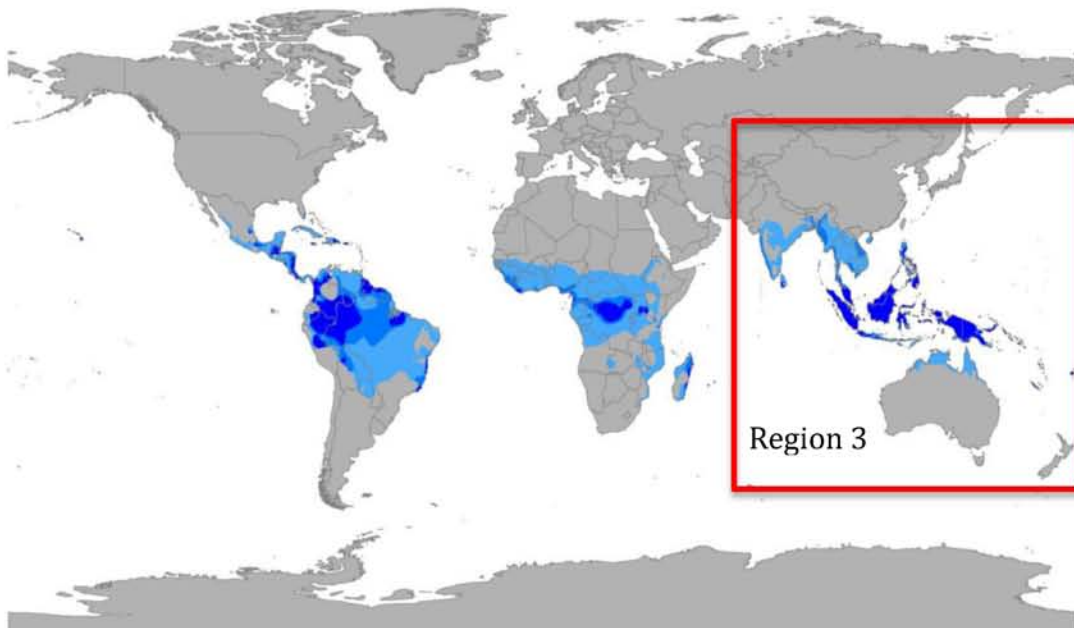


Figure 1.2: Highlighted areas of heavy rain.

However, in ITU Region 3, many countries face severe signal attenuation due to rain, as shown in Figure 1.2. These countries, most of which are located in the tropical zone near the equatorial line, include the Philippines, Indonesia, Malaysia, Singapore, and Thailand. Equatorial climatic conditions almost always produce convective rainfall [4][5], which particularly degrades the satellite signal propagation property.

1.3 Rain Attenuation Countermeasure Methods

Mitigation techniques [6] for rain attenuation have been widely investigated to compensate for the effects of rain degradation on satellite communications. Rain attenuation countermeasures are classified into three categories, as shown in Table 1.1.

The first category is static methods, which improve the received signal strength by increasing the transmission power. However, these methods are limited by the satellite power generation capacity, and they are ineffective in the presence of strong rain attenuation.

The second is adaptive methods, such as adaptive coding and modulation control, which are effective when the link becomes unstable as a result of rain. In these methods, the code or modulation type automatically changes to increase the power margin. Another adaptive method is adaptive power control [7], which boosts the satellite signal in specific areas suffering from rain attenuation. In this case, an adjustable phase-array antenna and a backup power source are installed on the satellite. However, when the degree of attenuation is large, particularly at higher frequencies, these adaptive methods are also limited by satellite resources such as power and bandwidth.

The third category of countermeasures is diversity methods, which are popular and useful methods that have always been used in satellite communication systems. Several diversity techniques, including site, time, frequency, and orbit diversity, are available. One method that can be used when large attenuation is present is site diversity [8]-[10], which involves two or more stations. The distance between the main and diversity sites should be sufficiently large to overcome the effects of rain attenuation, but as short as possible to reduce unnecessary costs. Recently, a novel mitigation approach based on time diversity was proposed as an efficient method to solve the data loss during severe rainfall [11]-[16]. Because of recent advances in technology, complex receivers that have a fast processor and a high storage capacity can be constructed, so this approach is now becoming feasible.

Table 1.1: Classification of attenuation countermeasure.

Type	Principle and Feature	Examples
Statistic	- Margin addition	- EIRP, G/T increase
	- Hierarchical channel	- Hierarchical coding & modulation
	- Waste of resource	
Dynamic	- Adaptive distribution of link resourced	- Power control
	- Good for point to point	- Bandwidth control
		- Coding rate control
Diversity	- Prepare channels with low attenuation correlation	- Site diversity
		- Time diversity
	- Good for large attenuation	- Frequency diversity
		- Orbit diversity

1.4 Objectives of This Thesis

This thesis proposes three rain attenuation mitigation methods and considers theoretical relations among propagation parameters such as attenuation, depolarization due to rain which affect the next generation of satellite communication operating in the Ka-band, as shown in Figure 1.3. The main objectives of the thesis are as follows:

- To enhance the accuracy of the prediction formula of cross-polarization up to 100 GHz in order to support the next generation of satellite communication.
- To evaluate the time diversity method, which maybe the most effective method to mitigate rain attenuation in Japan as well as in areas in the tropical region.
- To propose an adaptive satellite power control method as a new technology of attenuation mitigation.
- To improve the site diversity method by considering the direction-dependent factor.

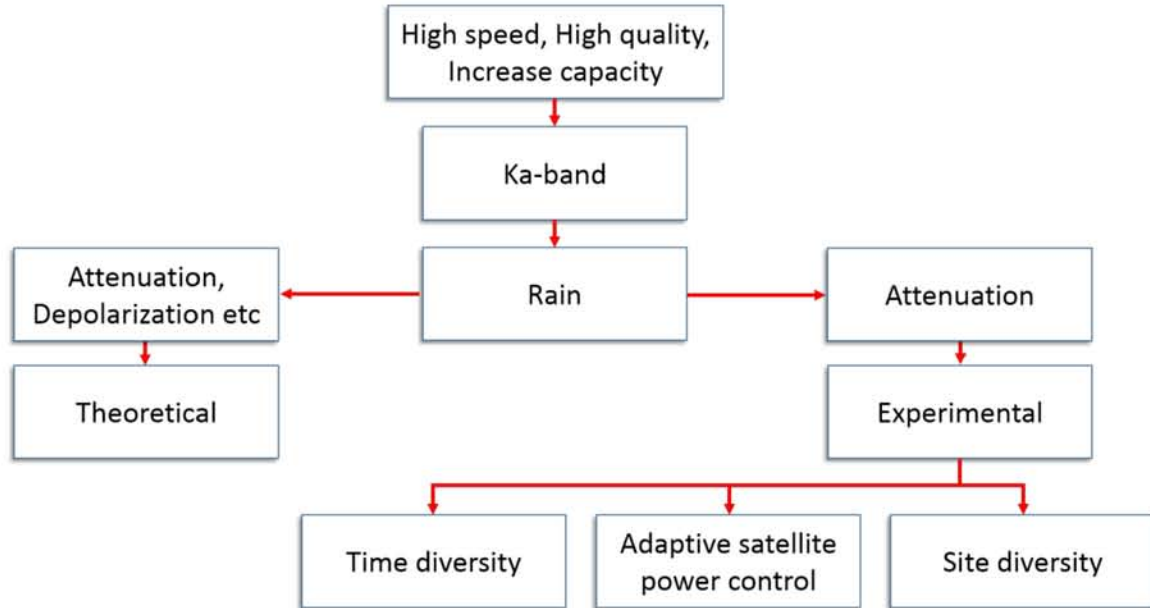


Figure 1.3: Flowchart of the research.

1.5 Organization

This thesis consists of the following 6 chapters as shown in Figure 1.4 and each chapter contents is as follows:

Chapter 1 reviews recent rapid demand of large capacity and high speed communication performance in satellite communication and broadcasting systems. Necessity of much higher radio wave frequency bands is mentioned and as a result importance of rain effect mitigation technology is mentioned especially in Asian region where rain may happen seriously in comparison to USA and Europe. Introduction of rain attenuation mitigation methods are shown by using classification of the methods into 3 categories

Chapter 2 derives theoretical relationships among rainfall rate, attenuation and depolarization using latest rain model. And practically useful

approximated relations are derived to predict depolarization due to rainfall based on the assumption of a gamma raindrop size distribution and Marshall-and-Palmer raindrop size distribution from 10-100 GHz. Moreover, the differences in the relation of rainfall rates between the homogeneity and the inhomogeneity rain models are described.

Chapter 3 evaluates the time diversity method derived by using two different kinds of information. The first one is beacon signal data from satellites and the second one is rain radar data. For beacon data, beacon data from Thailand and Japan represent the rain attenuation behavior in tropical and non-tropical areas, respectively. Moreover, beacon data can be used to analyze the dynamic properties of rain fade, such as fade duration and fade slope. By using high resolution rainfall rate data in time and space all over Japan produced by Japanese Meteorological Office, time diversity effect is evaluated and it is found the method is quite effective especially in broadcasting application.

Chapter 4 evaluates the adaptive satellite power control method using above mentioned rain data all over Japan. It is simulated that the power boost is done by several boost beams with several sizes. The optimal control parameters are derived or suggested to recover service availability throughout Japan.

Chapter 5 evaluates the site diversity method by using the rain gauge network at the center of Thailand. The spatial correlation is investigated site-by-site and is presented as a 2-dimensional spatial correlation map. It is

found that to enhance the performance of site diversity gain, the direction factor should be taken into account.

Chapter 6 concludes the thesis and presents areas for future work to continuously improve rain effect mitigation technologies.

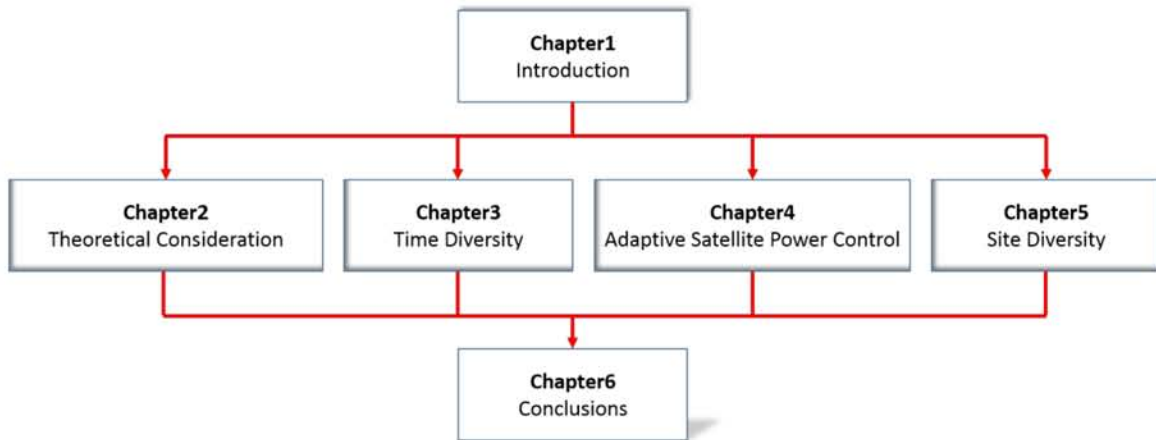


Figure 1.4: Outline of the thesis.

References of Chapter 1

- [1] Y. Abdulrahman, T. A. Rahman, R. M. Islam, B. J. Olufeagba and J. Chebil, “Comparison of Measured Rain Attenuation in the 10.982-GHz Band with Predictions and Sensitivity Analysis,”. *Int. J. Satell. Commun. Network.* 2015; **33**:185-195. doi:10.1002/sat.1082.
- [2] T. Boonchuk, N. Hemmakorn, P. Supnithi, M. Iida, K. Tanaka, K. Igarashi and Y. Moriya, “Rain Attenuation of Satellite link in Ku-band At Bangkok,” *Proc. Int. Conf. Information, Commun. Signal Process. (ICICS)*, pp. 1093-1095, 2005.
- [3] T. Nomoto, “Toward the Realization of a 21-GHz-Band Satellite Broadcasting System,” *Broadcast Technol.*, no.20, Autumn 2004.
- [4] C. Capsoni, L. Luini, A. Paraboni, C. Riva and A. Martellucci, “Stratiform and Convective Rain Discrimination Deduced From Local P(R),” *IEEE Trans. Antennas Propag.*, vol. 54, no. 11, pp. 3566-3569, 2006.
- [5] C. Capsoni, L. Luini, A. Paraboni, C. Riva and A. Martellucci, “A New Prediction Model of Rain Attenuation That Separately Accounts for Stratiform and Convective Rain,” *IEEE Trans. Antennas Propag.*, vol. 57, no. 1, pp. 196-204, 2009.

- [6] A. D. Panagopoulos, P. D. M. Arapoglou and P. G. Cottis, "Satellite Communication at Ku, Ka and V Bands, Propagation Impairments and Mitigation Techniques," *IEEE Commun. Surveys and Tutorial*, 3rd Quarter, vol. 6, no. 3, pp. 1-13, 2004.
- [7] H. Fukuchi, Y. Suzuki and S. Maeda, "Attenuation Mitigation in 21GHz Band Satellite Broadcasting Service," *Proc. Int. Symp. Space Technol. Sci. (ISTS)*, 2013.
- [8] Garcia-del-Pino P, Benarroch A and Riera JM, "Large-scale correlation of rainfall rate based on data from Spanish sites," *Int. J. Satell. Commun. Network*. 2015; **33**:43-56. doi:10.1002/sat.1070.
- [9] T. Hatsuda, Y. Aoki, H. Echigo, F. Takahata, Y. Maekawa and K. Fujisaki, "Ku-Band Long Distance Site-Diversity (SD) Characteristics Using New Measuring System," *IEEE Trans. Antennas Propag.*, vol. 52, no. 6, pp. 1481-1491, 2004.
- [10] H. Fukuchi, "Correlation properties of rainfall rates in the United Kingdom," *IEE proc.*, vol. 135, no. 2, pp. 83-88, 1988.
- [11] V. Fabbro, L. Castanet, S. Croce and C. Riva, "Characterization and Modelling of Time Diversity Statistics for Satellite Communications from 12 to 50 GHz," *Int. J. Commun. Syst. Network*, pp. 87-101, 2009.
- [12] H. Fukuchi, "Slant Path Attenuation Analysis at 20 GHz for Time Diversity Reception of Future Satellite Broadcasting," *URSI-F Open Symp. Colloque*, pp. 6.5.1-6.5.4, 1992.
- [13] E. Matriccioni, "Time Diversity as a Rain Attenuation Countermeasure in Satellite Links in The 10-100 GHz Frequency

- Bands,” *Proc. European Conference on Antennas and Propagation (EuCAP)*, 2006.
- [14] H. Fukuchi and T. Nakayama, “Quantitative Evaluation of Time Diversity as a Novel Attenuation Mitigation Technology for Future High Speed Satellite Communication,” *IEICE Trans. Commun.*, vol. E87-B, no. 8, pp. 2119-2123, 2004.
- [15] P. D. M. Arapoglou, A. D. Panagopoulos and P. G. Cottis, “An Analytical Prediction Model of Time Diversity Performance for Earth-Space Fade Mitigation,” *Int. J. Antennas Propag.*, 2008; Article ID 142497, 5 pages, doi:10.1255/2008/142497.
- [16] C. Kourogorgas, A. D. Panagopoulos, S. N. Livieratos and G. E. Chatzarakis, “On The Outage Probability Prediction of Time Diversity Scheme in Broadband Satellite Communication Systems,” *Progress in Electromagnetics Research C*, vol. 44, pp. 175-184, 2013.

Chapter 2

Theoretical Consideration of Rain Effect on Radio Wave

2.1 Introduction

It is well known that rainfall affects satellite communication. Recently, communications technology has developed rapidly in the direction of connecting everyone everywhere. For example, this year 2016, Facebook will launch their own satellite (AMOS-6; a cooperative venture with Spacecom) [1]. Many Ka-band beams will be used to deliver broadband internet to much of Africa. Although the Ka-band can contain much information and can lead to high-speed communication, it is highly sensitive to rain [2][3]. The reason for this sensitivity is that rain not only attenuates the power of the signal along the propagation path, but it also can change the polarization of the signal due to the shape of the raindrops, as shown in Figure 2.1. The degree of depolarization is expressed as the cross-polarization discrimination (XPD) [4].

In 1948, Marshall and Palmer (MP) [5] derived a well-known exponential raindrop size distribution (DSD) formula and proposed appropriate parameters. Many years later, Ulbrich [6] presented an accurate model of the DSD that was based on the gamma distribution. In order to reflect rain patterns characteristic of particular regions, many researchers have developed their own formula for the DSD, based on the exponential or gamma distribution with various parameters [7]–[9]. In 1991, Kozi [10] investigated the gamma DSD for Japan, using multiparameter radar measurements and considering microwave attenuation. Kozi's formula is very useful for representing the DSD in Japan. Lakshmi *et al.* [11] proposed a model for Singapore's DSD that was based on the gamma distribution with the shape parameter $\mu = 3$.

In a parallel study, Nowland *et al.* [12] proposed a formula for the relationship between rain attenuation and XPD by using a small argument approximation. The cross-polarization can be calculated theoretically, using the rainfall rate, the attenuation due to rain, the DSD, the forward scattering amplitude of the raindrops [13][14], the velocity of the rainfall [15], and the raindrop diameters [16]. Then, Fukuchi [17][18] improved Nowland's equation by using many DSDs, such as the MP DSD, the Joss thunderstorm DSD, and the Joss drizzle DSD, which they calculated up to 40 GHz. In this paper, in order to support the future use of a higher frequency band, we use a new DSD model to calculate the cross-polarization approximation up to 100 GHz.

In order to calculate the rainfall rate to the rain attenuation by ITU-R P. 618-12 [19], the approximation formula of cross-polarization is considered base on the homogeneous rain model. Although we will assume that the rainfall rate is constant along the propagation path, we note that the

rainfall spatial correlation results of many studies have shown that the rainfall rate is not constant in a block with a given slant path length, and it may depend on the amount of rainfall, wind direction, and surrounding environment.

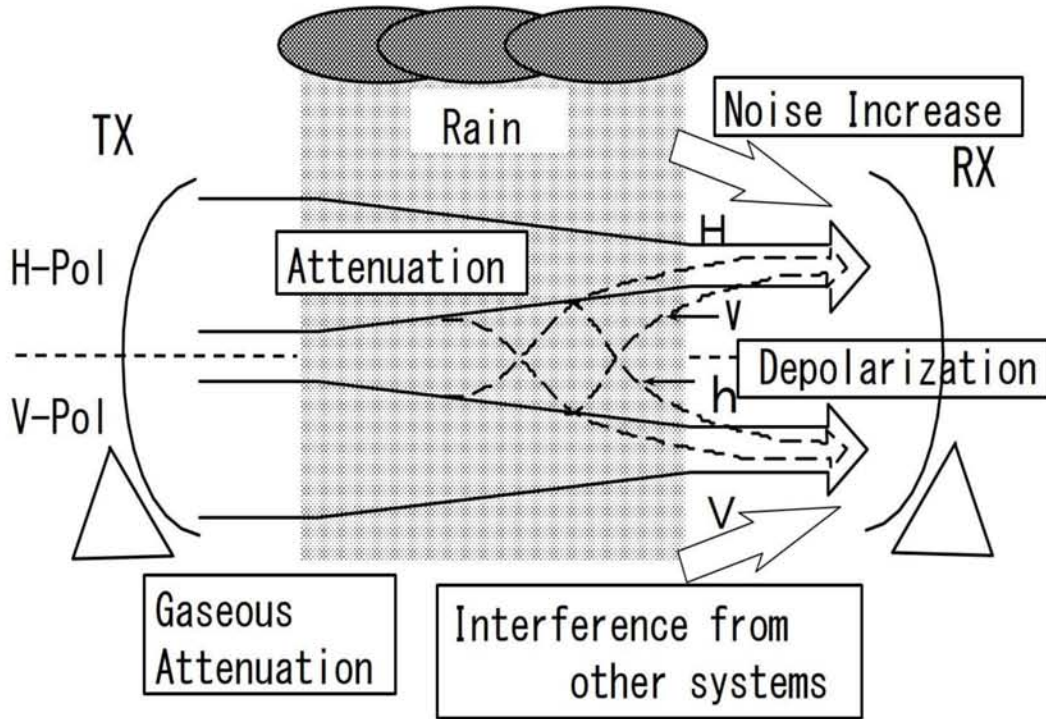


Figure 2.1: Frequency dependence of parameters.

2.2 Parameters Consideration

2.2.1 Raindrop Size Distribution

The MP and gamma DSD models are as follows:

$$\text{MP} \quad N(D) = N_0 e^{(-\Lambda D)} \quad (2.1)$$

$$\text{Gamma} \quad N(D) = N_0 D^\mu e^{(-\Lambda D)} \quad (2.2)$$

where N_0 is the number of droplets in unit volume, μ determines the shape of the distribution, Λ determines the slope of the distribution, D (mm) is the size of the raindrops, and R (mm/h) is the rainfall rate. We note that all parameters have already been determined for the original MP DSD model and the gamma DSD model investigated by Kozi [10]; these are shown in Table 2.1.

In Figure 2.2, the DSDs are compared, and it can be seen that compared to the MP DSD, because of the shape parameter μ , the gamma model is able to more accurately express the behavior of raindrops with small diameters, which are more common than those with large diameters. Many studies have suggested that $\mu = 3$ is the most suitable choice for the gamma model, and the obtained data is in good agreement with this. The results shown in Figure 2.2 were calculated with a rainfall rate of 20 mm/h; other rainfall rates are not shown, but their results were similar.

Table 2.1: DSD parameters.

DSD type	μ	N_0 ($\text{m}^{-3}\text{mm}^{-1-\mu}$)	Λ (mm^{-1})
MP	0	8000	$4.1R^{-0.21}$
	0	$9057R^{0.177}$	$4.37R^{-0.21}$
Gamma	3	$1.19 \times 10^5 R^{-0.352}$	$6.78R^{-0.176}$
	6	$1.44 \times 10^6 R^{-0.880}$	$9.16R^{-0.176}$

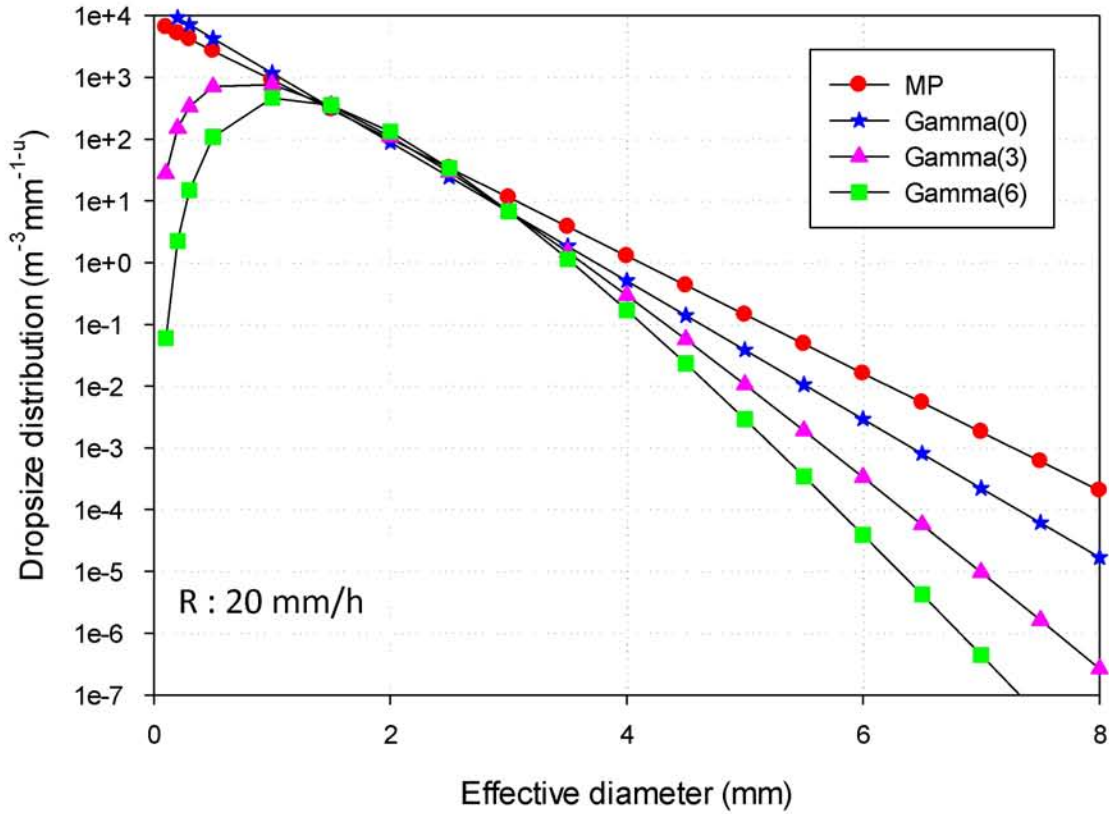


Figure 2.2: Comparison of the MP and gamma models with various values of $\mu = 0, 3$ and 6 .

2.2.2 Rainfall Rate Calculation

In order to investigate the DSD of the MP and gamma models, the rainfall rate (mm/h) is calculated as

$$R = 6 \times 10^{-3} \pi \int_0^{\infty} N(D) v(D) D^3 dD \quad (2.3)$$

where $N(D)$ is the raindrop size distribution for the particular model, and $v(D)$ is the falling velocity of the rain (m/s), which is defined according to Ulbrich [15]:

$$v(D) = 3.78D^{0.67} \quad (2.4)$$

where D is the diameter of the drop (mm) and falls in the following range:

$$0.1 \leq D(mm) \leq 8 \quad (2.5)$$

Figure 2.3 compares the errors of the rainfall rate as calculated in each of the DSD models. The ordinate is expressed as the relative difference (%) calculated by Eq. (2.6) with respect to the rainfall rate of Eq. (2.7):

$$Error(\%) = (R'_{est} - R_{real}) / R_{real} * 100 \quad (2.6)$$

$$0 \leq R(mm/h) \leq 200 \quad (2.7)$$

where R' is the rainfall rate estimated by Eq. (2.3), and R is the rainfall rate used in the DSD calculation.

As can be seen in Figure 2.3, the rainfall rate calculated using the MP DSD model has the largest error (ranging from 10% to 40%), and the error is particularly large when the rainfall rate is low (1 to 10 mm/h). The gamma models with various values of μ have smaller errors; in particular, when $\mu = 3$, the errors are between -2% and 0%. Therefore, it is appropriate to use the gamma model with $\mu = 3$ to approximate the XPD. In the following, we will show only the results for the MP DSD and for the gamma DSD with $\mu = 3$.

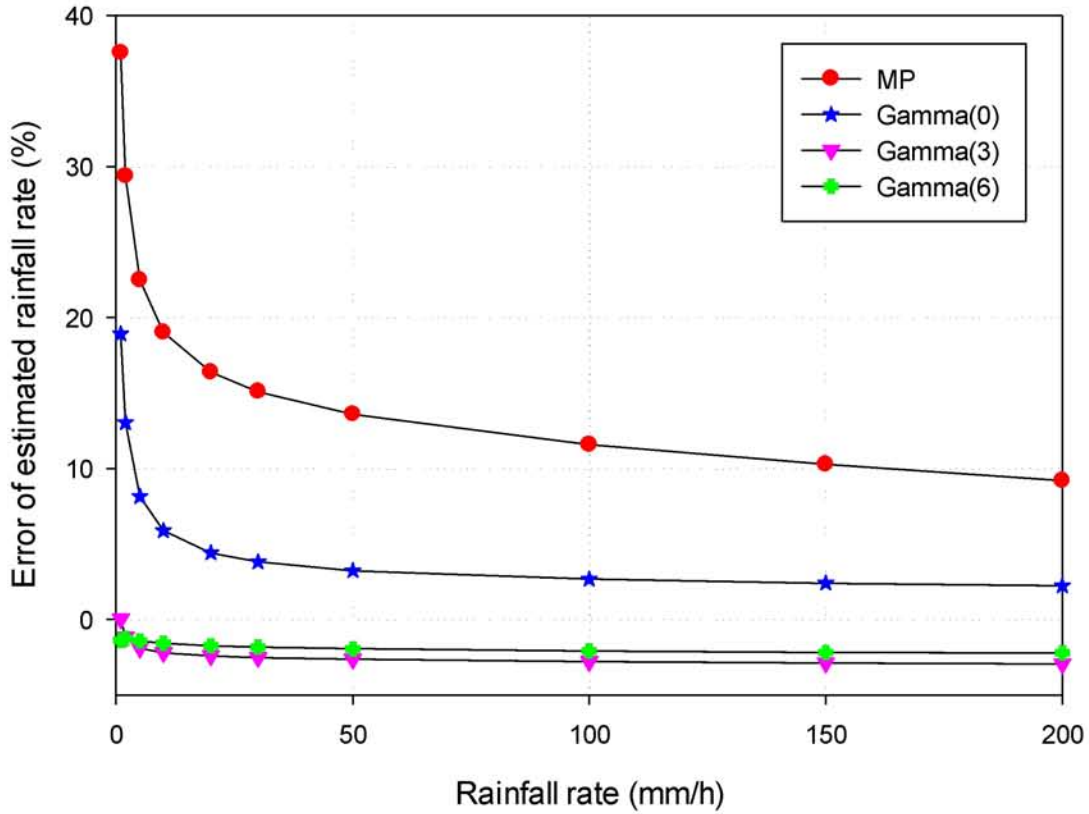


Figure 2.3: Errors of derived rainfall rates of the MP and gamma models with various values of $\mu = 0, 3, 6$.

2.3 Formula for Prediction of XPD

2.3.1 Relationship between Attenuation and XPD

Nowland *et al.* [12] proposed a theoretical basis for approximating the cross-polarization; they derived a formula by applying small-argument approximations and the attenuation A (dB) and XPD (dB) [20] induced by deformed raindrops, as follows:

$$A = aR^bL \quad (2.8)$$

$$\begin{aligned}
 XPD = & -20\log(|\Delta k / 2|) - 20\log(\sin 2|\phi - \tau|) \\
 & -40\log(\cos \varepsilon) - 20\log L + 0.0053\sigma^2
 \end{aligned} \tag{2.9}$$

where XPD is the ratio of co- and cross-polarized received components of the same signal.

Following this, Dissanayake et al. [21], Chu [22], and Fukuchi et al. [23][24] improved this, as follows:

$$XPD = U - V \log A \tag{2.10}$$

where the following assumptions are made:

$$\gamma = aR^b \tag{2.11}$$

$$|\Delta k| = cR^d \tag{2.12}$$

where

$$V = 20d / b \tag{2.13}$$

$$\begin{aligned}
 U = & 0.0053\sigma^2 - 20\log(\sin 2|\phi - \tau|) \\
 & -40\log(\cos \varepsilon) + u
 \end{aligned} \tag{2.14}$$

$$u = -20\log\left(\frac{c}{2a^{d/b}}\right) + (V - 20)\log L \tag{2.15}$$

where A (dB) is the attenuation, R (mm/h) is the rainfall rate, ε (degree) is the elevation angle, ϕ (degree) is the effective raindrop canting angle, τ (degree) is the polarization tilt angle of the incident wave relative to the horizontal direction, L (m) is the path length through the rain, and σ (degree) is an effective standard deviation of the raindrop canting angle distribution. In the case of circular polarization, the term $(\phi-\tau)$ in Eq. (2.14) should be 45 degrees. The parameters a , b , c , and d are constants obtained from the specific attenuation, γ , and the differential propagation constant, $|\Delta k|$.

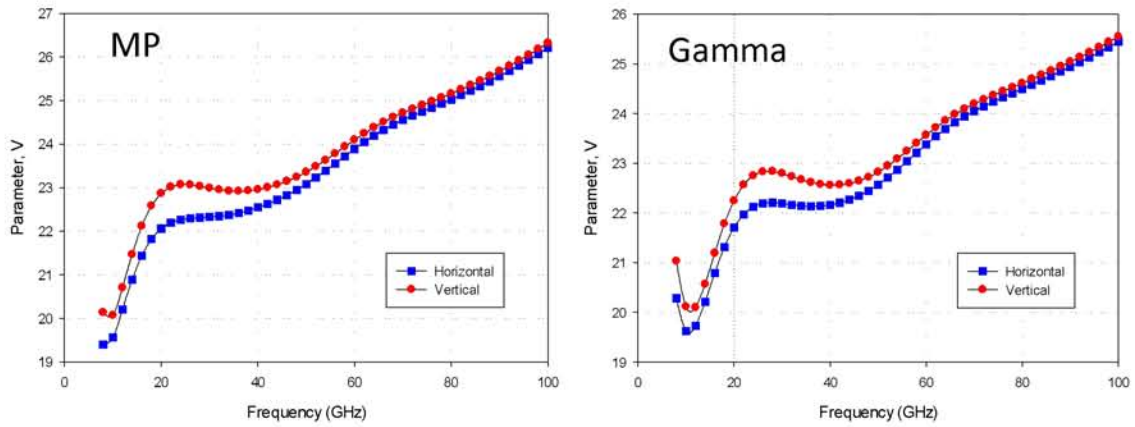


Figure 2.4: Frequency dependence of V .

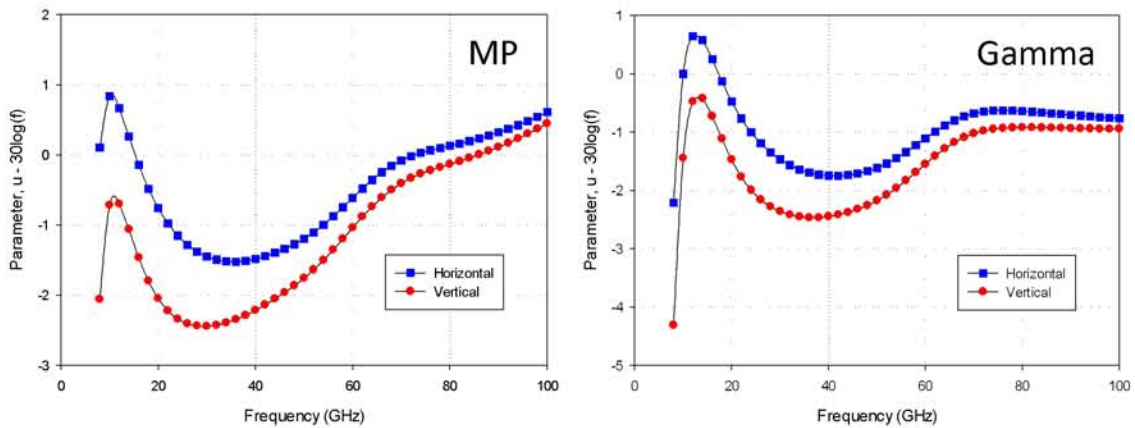


Figure 2.5: Frequency dependence of u .

Figures 2.4 and 2.5 show the frequency dependence of V and u from 10 to 100 GHz. The results are derived from the parameters a , b , c , and d , which were obtained from specific attenuation and difference propagation constants. It can be seen that for both V and u , the frequency depends on the raindrop size distribution in both the MP and gamma models.

The least-squares method was used to approximate the frequency dependence of V and u , which were obtained from the results shown in Figures 2.4 and 2.5; the resulting equations are shown in Table 2.2. We note that the frequency ranges of V and u were calculated separately in order to obtain a precise approximation for an equation for XPD for both horizontal and vertical polarization.

Table 2.2: V and u for the relationship between attenuation and XPD.

Raindrop size distribution	Parameter V	Frequency (GHz)		Parameter $U_0 - (V - 20)\log L$	Frequency (GHz)	
		($f_1 < f < f_2$)			($f_1 < f < f_2$)	
		f_1	f_2		f_1	f_2
MP (Hor)	$14.29f^{0.142}$	10	26	$25.28\log f + 5.54$	10	36
	$20.58f^{0.024}$	26	40	$35.42\log f - 10.23$	36	100
	$12.02f^{0.168}$	40	100			
MP (Ver)	$14.21f^{0.155}$	10	26	$26.44\log f + 2.83$	10	36
	$24.05f^{-0.013}$	26	40	$36.89\log f - 13.28$	36	100
	$12.85f^{0.154}$	40	100			
Gamma ($\mu = 0$) (Hor)	$15.23f^{0.119}$	10	24	$25.69\log f + 5.38$	12	34
	$22.41f^{-0.005}$	24	38	$33.99\log f - 7.49$	34	70
	$13.91f^{0.122}$	38	100	$33.95\log f - 7.32$	70	100
Gamma ($\mu = 0$) (Ver)	$15.33f^{0.124}$	10	24	$26.45\log f + 3.38$	12	34
	$24.90f^{-0.029}$	24	38	$35.48\log f - 10.54$	34	70
	$14.72f^{0.111}$	38	100	$34.93\log f - 9.43$	70	100
Gamma ($\mu = 3$) (Hor)	$13.78f^{0.149}$	10	26	$24.80\log f + 6.33$	12	40
	$22.66f^{-0.006}$	26	40	$35.01\log f - 10$	40	74
	$12.11f^{0.161}$	40	100	$28.87\log f + 1.49$	74	100

Gamma ($\mu = 3$) (Ver)	13.77f ^{0.157}	10	26	25.46logf + 4.5	12	20
	25.40f ^{-0.032}	26	40	36.49logf - 13.07	40	74
	12.92f ^{0.147}	40	100	29.90logf - 0.74	74	100
Gamma ($\mu = 6$) (Hor)	11.95f ^{0.195}	12	26	24.03logf + 7.31	14	42
	23.35f ^{-0.013}	26	40	36.19logf - 12.41	42	74
	10.58f ^{0.197}	40	100	25.67logf + 7.33	74	100
Gamma ($\mu = 6$) (Ver)	11.58f ^{0.214}	12	26	24.57logf + 5.66	14	42
	26.68f ^{-0.044}	26	40	37.69logf - 15.55	42	74
	11.28f ^{0.184}	40	100	26.70logf + 5.08	74	100

We also used this equation to calculate the XPD and compared these values with the theoretical results. The basic formula for transmitting and receiving a wave through the rain [25] is

$$V_a = \left[V_h \sin^2(\phi - \tau) + V_v \cos^2(\phi - \tau) \right] \cos^2 \varepsilon + V_z \sin^2 \varepsilon \quad (2.16)$$

where V_a is the parameter of the polarized wave, and V_h , V_v , and V_z are the parameters for polarization in the h , v , and z directions, respectively. When computing a circularly polarized XPD with a horizontal propagation path, the term $(\phi - \tau)$ equals 45 degrees and ε equals zero; V and u can then be approximated as follows:

$$V_c = \frac{V_h + V_v}{2} \quad (2.17)$$

$$u'_c = \frac{u'_h + u'_v}{2} \quad (2.18)$$

where V_c and u'_c are the parameters for circular polarization.

Figure 2.6 shows the relationship of XPD to the attenuation of frequency at 20 and 100 GHz for both the MP and gamma models. The

parameters in this calculation are set as follows: $L = 10$ km, $\sigma = 0^\circ$, $\varepsilon = 0^\circ$, and $(\phi - \tau) = 45^\circ$.

In Figure 2.6, the theoretically calculated and approximated results are indicated by dots and solid lines, respectively. The two results are in good agreement. We note that the XPD will be small when the attenuation is large, and this is due to the negative sign in the following equation:

$$XPD_H = -20 \log \left(\frac{E_V}{E_H} \right) \quad (2.19)$$

where E_V is the cross-polarized received field in the vertical polarization and E_H is the co-polarized received field in the horizontal directions.

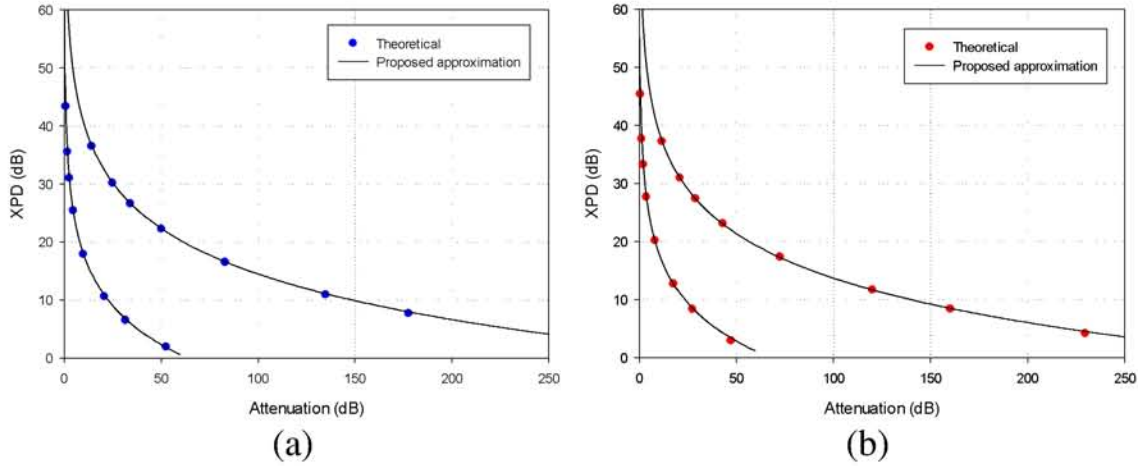


Figure 2.6: Depolarization comparison of theoretical and proposed approximation: (a) MP DSD, (b) gamma DSD.

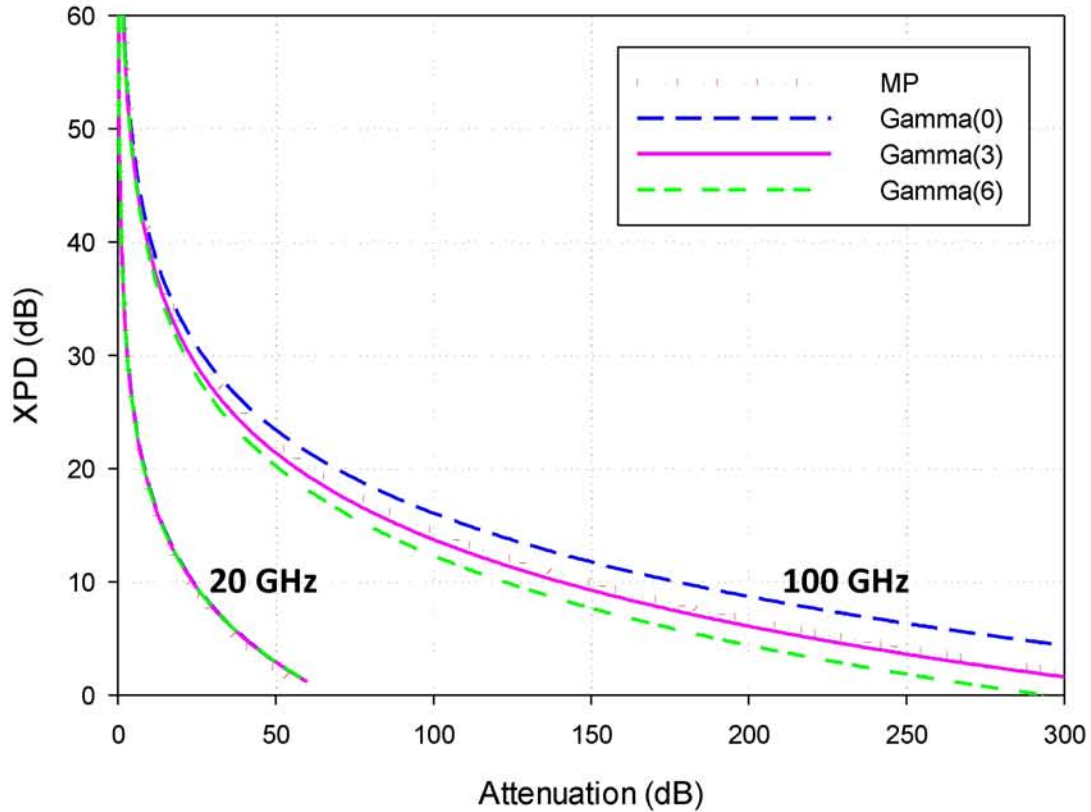


Figure 2.7: Comparison of XPD of the MP and gamma models with various values of $\mu = 0, 3, 6$.

Figure 2.7 presents the results for the XPD for the MP and the gamma models with various values of μ . It can be seen that there is no significant difference between them in the lower frequency band, but in the higher frequency band, the shape of the droplet (μ) becomes a significant factor in the attenuation due to the XPD.

2.3.2 Relationship between Rainfall Rate and XPD

The rainfall rate can be used to approximate the XPD [26] by using the parameters c and d in Eq. (2.12); the differential propagation constant Δk can be approximated as follows:

$$-20\log(|\Delta k|) = u_1 - u_2 \log f - (u_3 - u_4 f) \log R \quad (2.20)$$

where u_1 , u_2 , u_3 , and u_4 are approximated as constants, and their values are shown in Table 2.3.

Substituting Eq. (2.20) into Eq. (2.9), the relationship between rainfall rate and XPD is obtained as follows:

$$\begin{aligned} XPD = & u_1 - u_2 \log f - (u_3 - u_4 f) \log R \\ & -20\log(\sin 2|\phi - \tau|) - 40\log(\cos \varepsilon) \\ & -20\log L + 0.0053\sigma^2 \end{aligned} \quad (2.21)$$

Table 2.3: Values of u for the relationship between rainfall rate and XPD.

Raindrop size distribution	Parameter		Frequency (GHz)		Parameter		Frequency (GHz)	
	u_1	u_2	f_1	f_2	u_3	u_4	f_1	f_2
MP	90.02	20.46	8	52	25.22	-0.0096	8	24
	57.93	1.34	52	82	29.83	0.1665	24	52
	31.57	-12.41	82	100	25.29	0.0661	52	82
					20.07	0.0014	82	100
Gamma ($\mu=0$)	92.34	20.43	8	56	24.73	-0.0204	8	24
	62.72	2.94	56	80	29.04	0.1347	24	56
	32.5	-12.84	80	100	25.66	0.0623	56	80
					20.27	-0.0049	80	100
Gamma ($\mu=3$)	93.19	21.43	8	56	25.04	-0.0043	8	28
	61.83	3.01	56	80	30.04	0.1551	28	56
	31.66	-12.74	80	100	26.87	0.0876	56	80
					19.64	-0.0019	80	100
Gamma ($\mu=6$)	93.56	22.13	8	54	25.37	0.0176	8	24
	60.30	2.63	54	82	29.39	0.1413	24	54
	29.11	-13.60	82	100	27.52	0.1029	54	82
					18.92	-0.0017	82	100

2.4 Effect of Inhomogeneity of the Rainfall Rate

In previous studies of the theoretical relationship between XPD and attenuation, rainfall rate has been assumed to be constant due to the lack of information. There are now several kinds of information available, such as rain-gauge, radar, and even beacon signal data. Integration of this information into the model will improve our estimates of the attenuation due to rain attenuation and the XPD characteristics and propagation. Figure 2.8 shows a comparison of the calculation of the propagation properties when using homogeneous and inhomogeneous rain models. The formula for the model with inhomogeneous rain is shown in Table 2.4.

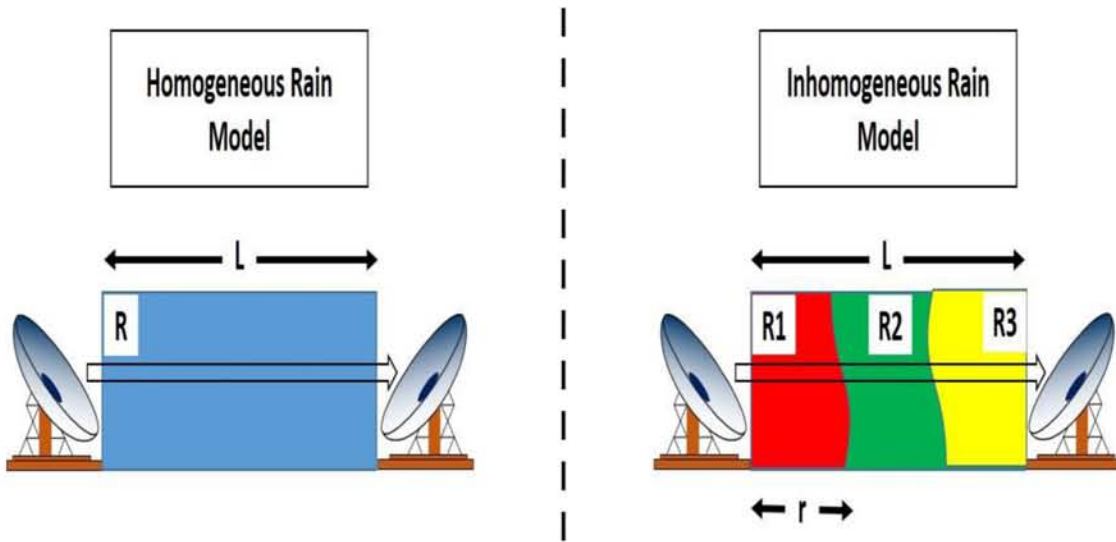


Figure 2.8: Homogeneous and inhomogeneous rain models.

Table 2.4: Comparison of propagation for homogeneous and inhomogeneous rainfall models.

Propagation characteristics	Homogeneous rain	Inhomogeneous rain
Rain attenuation	aR^bL	$a \int_0^L R(r)^b dr$
Depolarization (XPD)	$-20 \log(cR^dL) + X_0$	$-20 \log \left(c \int_0^L R(r)^d dr \right) + X_0$

In order to determine the effect of inhomogeneity on the XPD prediction, we introduce a correction value that expresses the difference between the XPD values of the two models. Compared to the results from Fukuchi [27], as shown in Figure 2.9, it can be seen that the correction value is very small and does not significantly affect the approximation. Figure 2.9(a) shows the XPD correction value as a function of the path length and calculated at 19.45 GHz. The absolute value of the correction is less than 0.5 dB when the XPD is derived by using the attenuation relationship. This is because the rainfall inhomogeneity affects both the attenuation and the XPD in nearly the same way. Figure 2.9(b) shows the XPD correction value derived as a function of the frequency. Both results show that the rainfall rate inhomogeneity is not significant. In these figures, the parameter α expresses the degree of inhomogeneity, which is used in the spatial correlation of the rainfall rate, as follows:

$$\rho = \exp^{-\alpha\sqrt{D}} \quad (2.22)$$

where ρ is the spatial correlation and D is distance between two locations. In Figures 2.9(a) and 2.9(b), the shaded area and range bars indicate the variation due to the cumulative distribution attenuation.

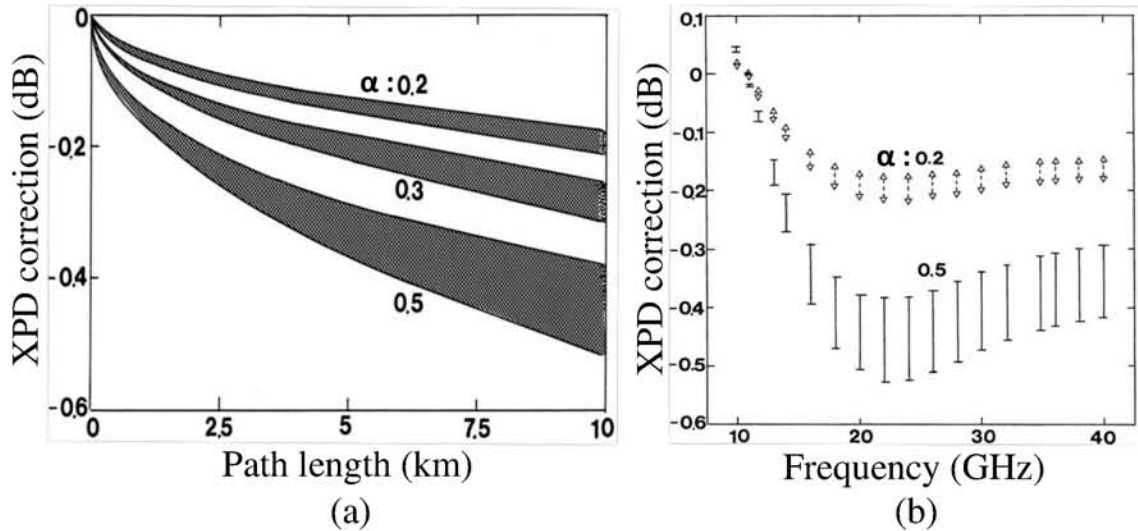


Figure 2.9: Derivation of XPD correction value for (a) path length dependence, and (b) frequency dependence.

2.5 Summary of Chapter 2

This chapter proposes a formula for approximating the cross-polarization and the relevant parameters up to 100 GHz in order to support the future design of communication satellites. The cross-polarization strongly depends on the rainfall rate and frequency, because the rainfall rate can be used to determine the attenuation due to rain, and XPD will be more dominant when there is a high precipitation rate and at high frequencies. We compared the parameters for these relationships using a gamma distribution for the raindrop size, and we compared the results for various μ values and with the results of an exponential model (MP DSD). The shape parameter $\mu = 3$ resulted in the smallest error, and thus it seems to be the most suitable value,

as has been previously stated in other studies.

The formula for approximating the relation between the attenuation and the XPD or the rainfall rate are very useful for predicting the cross-polarization. Moreover, our proposed approximation formula can be used over a wide frequency range up to 100 GHz.

Usually, the cross-polarization formula is calculated based on the homogeneous rain model for a high elevation angle or a short slant path distance. For a lower elevation angle or a longer slant path distance, the signal may pass through many rain regions. In that case, the homogeneity approximation formula can be applied, since the inhomogeneity has little effect on the relationship between the XPD and the attenuation.

References of Chapter 2

- [1] P. B. de. Selding, “Facebook-Eutelsat Internat Deal Leaves Industry Awaiting Encore,” *Spacenews*, 17 Oct 2015.
- [2] W. L. Stutzman, “Prediction of Rain Effects on Earth-Space Communication Links Operating in the 10 to 35 GHz Frequency Range,” *Int. J. Satell. Commun. Network.* 1989; 7:37-45. doi:10.1002/sat.4600070107.
- [3] R. Howell and P. Thompson, “A Review of Ka and Ku Band Propagation Measurements on Satellite Paths Made at the BT Laboratories in the U.K.,” *Int. J. Satell. Commun. Network.* 1992; 10:71-79. doi:10.1002/sat.4600100204.
- [4] A. Ghorbani and N. J. McEwan, “Propagation Theory in Adaptive Cancellation of Cross-Polarization,” *Int. J. Satell. Commun. Network.* 1988; 6:41-52. doi:10.1002/sat.4600060107.
- [5] J. S. Marshall and W. M. Palmer, “The Distribution of Raindrop with Size,” *J. Meteor.*, vol. 5, pp. 165-166, 1948.
- [6] C. W. Ulbrich, “Natural Variation in the Analytical Form of the Raindrop Size Distribution,” *J. Cilm. Appl. Meteorol.*, vol. 22, no. 10, pp. 1764-1775, 1983.

- [7] L. S. Kumar, Y. H. Lee and J. T. Ong, "Truncated Gamma Drop Size Distribution Models for Rain Attenuation in Singapore," *IEEE Trans. Antennas Propag.*, vol. 58, no. 4, pp. 1325-1335, 2010.
- [8] D. Tokay and A. Short, "Evidence from tropical raindrop spectra of the origin of rain from stratiform versus convective clouds," *J. App. Meteorol.*, vol. 37, no. 9, pp. 912-923, 1998.
- [9] V. N. Bringi, T. A. Selgia and W. A. Cooper, "Analysis of aircraft hydrometeor spectra and differential reflectivity (Z_{DR}) radar measurements during the cooperative precipitation experiment," *Radio Sci.*, vol. 19, no. 1, pp. 157-167, 1984.
- [10] T. Kozu and K. Nakamura, "Rainfall Parameter Estimation from Dual-Radar Measurements Combining Reflectivity Profile and Path-integrated Attenuation," *J. Atmos. Oceanic Technol.*, 8, pp. 259-270, 1991.
- [11] L. S. Kumar, Y. H. Lee and J. T. Ong, "Two-Parameter Gamma Drop Size Distribution Models for Singapore," *IEEE Trans. Antennas Propag.*, vol. 49, no. 9, pp. 3371-3380, 2011.
- [12] W. L. Nowland, R. L. Olsen and I. P. Shkarofsky, "Theoretical Relationship Between Rain Depolarisation and Attenuation," *Electron. Lett.*, vol. 13, no. 22, pp. 676-678, 1977.
- [13] T. Oguchi, "Scattering properties of Pruppacher and Pitter form raindrops and cross-polarization due to rain: calculations at 11, 13, 19.3 and 34.8 GHz," *Radio Sci.*, vol. 12, pp. 41-51, 1977.
- [14] T. Oguchi, "Summary of Studies on Scattering of Centimetre and Millimetre Waves Due to Rain and Hail," *Ann. Telecommunic.*, vol. 36, no. 7, pp. 383-399, 1981.

- [15] N. I. Fox, "The representation of rainfall drop-size distribution and kinetic energy," *Hydrol. Earth Syst. Sci.*, 8(5), pp. 1001-1007, 2004
- [16] H. R. Pruppacher and R. L. Pitter, "A Semi-Empirical Determination of the Shape of Cloud and Rain Drops," *J. Atmos. Sci.*, pp. 86-94, 1971.
- [17] H. Fukuchi, J. Awaka and T. Oguchi, "Improved Theoretical Formula for the Relationship Between Rain Attenuation and Depolarisation," *Electron. Lett.*, vol. 20, no. 21, pp. 859-860, 1984.
- [18] H. Fukuchi, J. Awaka and T. Oguchi, "Approximate Theoretical Formula for the Prediction of Depolarization Due to Rain," *Denshi Tokyo*, no. 24, pp. 36-40, 1985.
- [19] ITU-R, "Propagation data and prediction methods required for the design of Earth-space telecommunication systems," *Recommendation*, P.618-12, 2015.
- [20] J. S. Mandeep, "Microwave Depolarization Versus Rain Attenuation on Earth Space in Malaysia," *Int. J. Satell. Commun. Network*. 2008; **26**:523-533. doi:10.1002/sat.923.
- [21] A. W. Dissanayake, D. P. Haworth and P. A. Watson, "Analytical Models for Cross-Polarization on Earth-Space Radio Paths for Frequency Range 9-30 GHz," *Ann. Telecommun.*, 35, pp. 398-404, 1980.
- [22] T. S. Chu, "A Semi-Empirical Formula for Microwave Depolarization Versus Rain Attenuation on Earth-Space Paths," *IEEE Trans.*, vol. COM-30, no. 12, pp. 2550-2554, 1982.
- [23] H. Fukuchi, "Relationship between rain attenuation and depolarisation up to 100GHz," *Int. Symp. Ant. And Prop. (ISAP2008)*, October 2008.

- [24] P. Chodkaveekityada and H. Fukuchi, "Improvement of Depolarization Formula Using Gamma Raindrop Size Distribution Up to 100GHz," *Proc. Asia-Pacific Con. Antennas. Propag. (APCAP)*, 2015.
- [25] I. J. Dilworth and B. G. Evans, "Cumulative Crosspolarisation and Canting Angle Distributions," *Electron. Lett.*, vol. 15, no. 19, pp. 603-604, 1979.
- [26] M. M. J. L. van de Kamp, "Depolarization Due to Rain: the XPD-CPA Relation," *Int. J. Satell. Commun. Network.* 2001; **19**:285-301. doi:10.1002/sat.672.
- [27] H. Fukuchi, "Effect of Rainfall Rate Inhomogeneity on Relations Among Propagation Properties," *Proc. Int. Symp. Antennas. Propag. (ISAP)*, 2006.

Chapter 3

Time Diversity Method

3.1 Methodology

Time diversity method [1]-[4] will be used in the next generation broadcasting satellite service using high frequency of Ka-band in order to reduce the effect of severe rain attenuation. Figure 3.1 shows an example of time diversity method in both time domain and frequency domain. Most simple time diversity method requires bandwidth twice as much because of repeated transmission of the programs with time difference. However, frequency bandwidth is valuable resource of transmission, one example of realization of time diversity uses information compressed transmission. For example, as shown in Figure 3.1, one additional transponder is adopted to transmit several compressed programs with time difference to the original programs. The compressed programs need relatively small bandwidth and transmitted with time delays or time advances.

Use of the time diversity method requires ground precipitation information coverage for all target areas in order to determine where rain attenuation problems are occurring. Ground precipitation stations measure

and record weather parameters such as rainfall rates, wind, humidity, and temperature in real time, then pass that information to all parties involved, especially gateway and broadcast stations. When it is determined that rainfall in affected areas has reached the point where communications are unreliable, time diversity gateways will be applied. Time diversity from 1 minute to more than 1 hour can be used, and the method works by transmitting the same information twice. The first transmission, which is the same as a normal real-time transmission, is done in order to maintain satellite input power and will later be used for information processing. The second transmission is time delayed (t_d) but contains the same information when time diversity is applied. Each receiver will collect and use both information types independently.

Receivers will also be required to prepare and maintain large-capacity central processing unit (CPUs) and memory because some time diversity method cases will take considerable time to process. Additionally, memory space will be needed to store received information before processing. Once both information sets have been obtained, the receiver will extract the clearest information from each segment in order to assemble the clearest version of the transmitted data.

In the following analysis, we used a simple time diversity model in which all information is transmitted twice with a delay between the two transmissions. The first signal is like a normal transmission to maintain the satellite input power during heavy rainfall events. The second is applied in certain areas of concern, which are determined using the method described above; a second delayed signal is used only for these troublesome areas. The factor that can be used to express the performance of time diversity is diversity gain. In general, the diversity gain can be determined both rain rate

and rain attenuation, which can be calculated by the use of different rain rate or attenuation values between the “no time delay” and each of the time delay created via Eq. (3.1).

$$G_{d,R} = R_0 - R_d \quad \text{or} \quad G_{d,A} = A_0 - A_d \quad (3.1)$$

where R_0, A_0 is the “no time delay” rain rate and attenuation value and R_d, A_d is the rain rate and attenuation value for each of the time delays. Both attenuation values are estimated at 0.1% or 0.01% of cumulative time percentage.

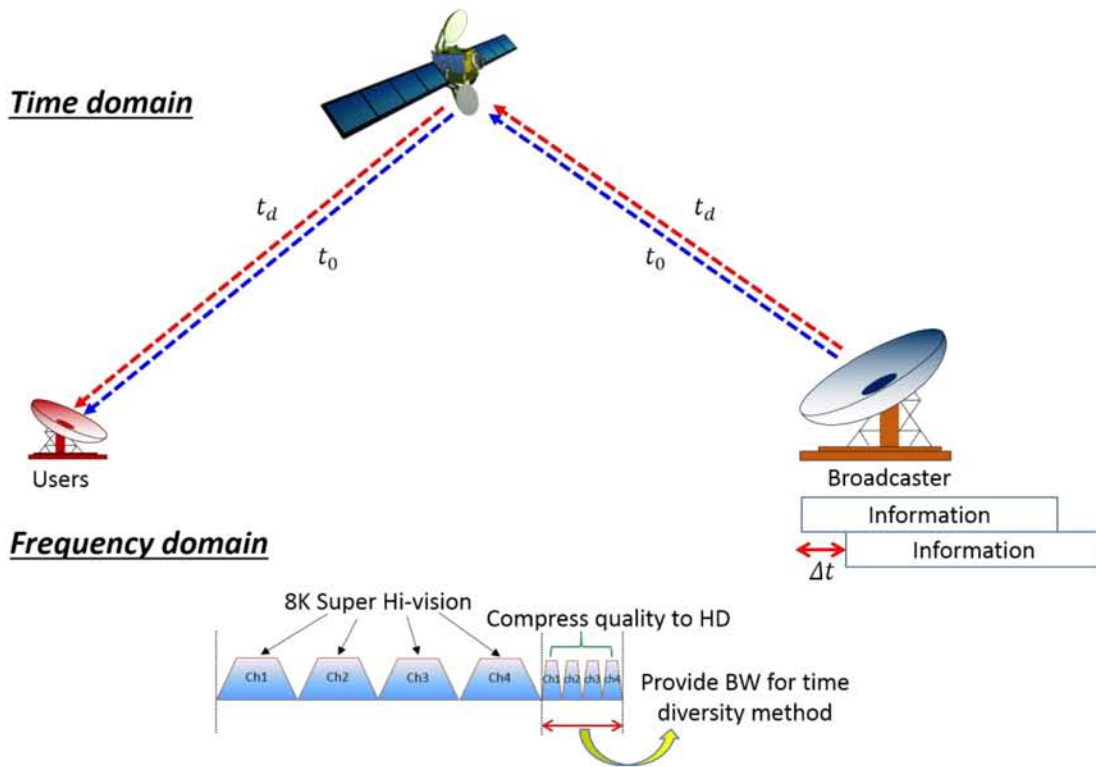


Figure 3.1: The methodology of time diversity and frequency configuration.

In this chapter, there are two kind of information in order to evaluate time diversity performance. First information is beacon received data from

both Thailand and Japan to represent rain behavior in tropical and non-tropical regions. And second information is rain radar data across Japan. Each information has different process to get the results of time diversity and parameter involves as shown in Figure 3.2.

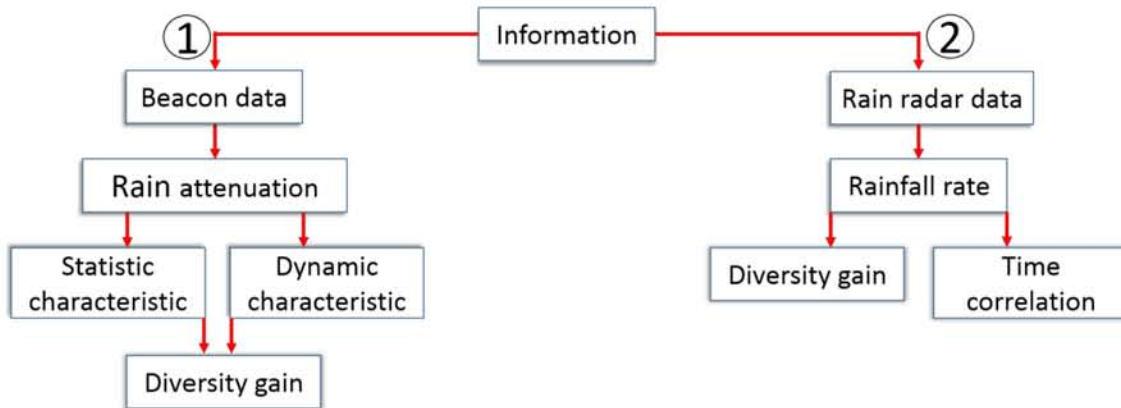


Figure 3.2: The flows of time diversity process.

3.2 Time Diversity Method Apply with Beacon Data

3.2.1 Measurement Data Analysis

The time diversity method is based on the received beacon data. This section used two different sites, one in a tropical area and another one in a non-tropical area. The parameters involved are listed in Table 3.1. In the case of the tropical zone, the beacon reception site was located at KMITL (13.7257° N, 100.7778° E), Thailand and receives transmissions from the Thaicom 2 beacon at an operating frequency of 12.57 GHz with vertical polarization, and the Thaicom 3 beacon operating at a frequency of 12.59 GHz with horizontal polarization. These satellites are co-located at 78.5° E longitude in geostationary orbit.

For the non-tropical zone, the beacon reception site was located at Kashima Space Technology Center (35.9657° N, 140.6448° E), Japan and received the beacon of a CS satellite operating at a frequency of 19.45 GHz with circular polarization and in geostationary orbit at 135° E longitude. We could only obtain 1 year (2006) for Thaicom 2 & 3 beacon received data at 1-second time intervals, but obtained 2 years for CS beacon received data covering the period between Apr 1981 and Mar 1983, also at 1-second time intervals.

It should be noted that the elevation angle of the received antenna for the receiving antenna for the CS beacon at KSTC was set at 48° , while the receiving antenna for the Thaicom 2 and 3 beacon located at KMITL was set at 59.83° . These values relate to the slant path length (km), where lower elevation angle values will add significantly more distance to the slant path when compared to the nearby locations.

Table 3.1: Geographical and radio links parameters of rain attenuation measurements. Rain attenuation sampling time is 1 s.

Satellite	Site	Frequency (GHz)	Elevation (deg)	Polarization	Duration
Communication Satellite (CS) (GEO, 135.0° E)	Kashima (Japan) 35.97° N, 140.65° E	19.45	48.0°	Circular	April 1981- March 1983
Thaicom 2 (GEO, 78.5° E)	Bangkok (Thailand) 13.73° N, 100.78° E	12.57	59.8	Vertical	2006
Thaicom 3 (GEO, 78.5° E)	Bangkok (Thailand) 13.73° N, 100.78° E	12.59	59.8	Horizontal	2006

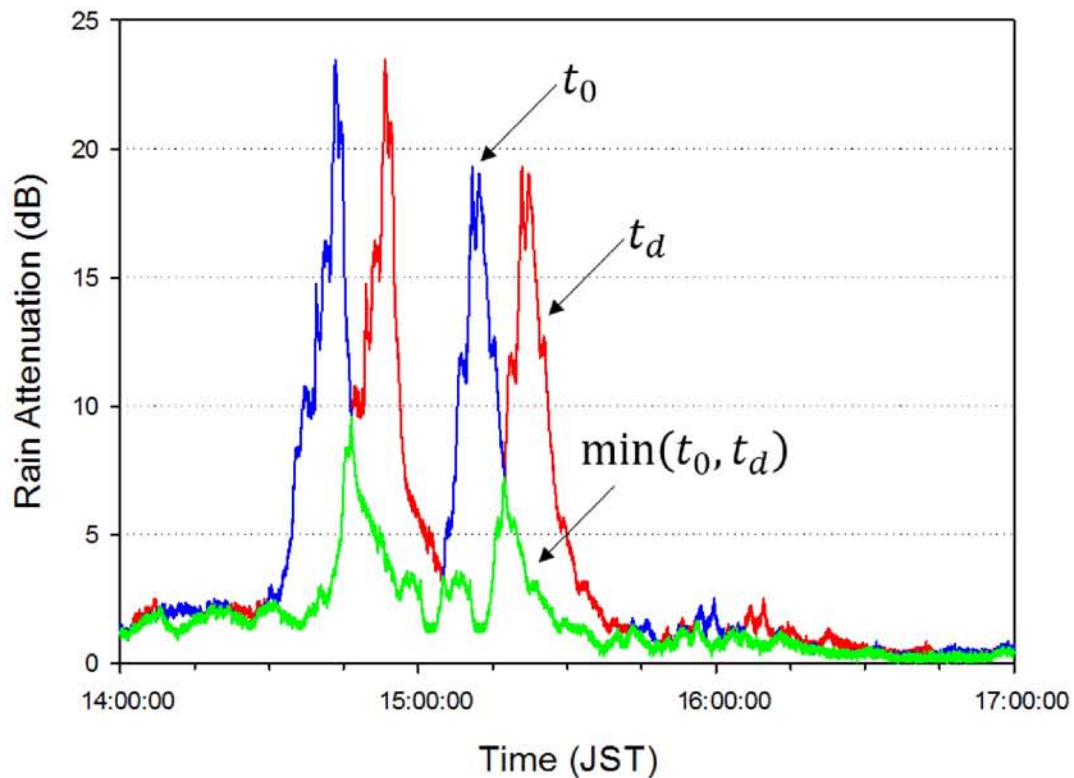


Figure 3.3: Example of time diversity using CS beacon attenuation time series. (blue : original data, red : delayed data, green : time diversity result)

In this case, due to the difference in latitudes, we calculated the slant path length of the CS beacon and determined that it is about 5.9 km, while the Thaicom 2 and path is 6.2 km. This means the slant path length of the received Thaicom 2 and 3 beacons is longer than the slant path length of the received CS beacon if it is assumed that these two stations are located at the same height (0 km) above mean sea level. As a result, when compared to the CS beacon, the Thaicom 2 and 3 beacon will be more affected by rain attenuation due to the longer distance between the receiver antenna and the rain height.

Figure 3.3 shows sample of receiver beacon rain attenuation data collected over 3 hours with time delay and time diversity result. The CS beacon operating in the Ka-band in Figure 3.3 shows that rainfall has degraded the KSTC receiver beacon more than 20 dB at the non-tropical Kashima site. In contrast, the results of Thaicom 2 beacon and Thaicom 3 beacon operating in Ku-band indicate that KMITL in Bangkok, which is located in a tropical zone, is being hit by severe rain and that signal attenuation will become more dominant over the Ka band satellite signal.

The measurement comparison shows an approximately dB difference in rain attenuation between the Thaicom 2 and Thaicom 3 receiver beacons. More specifically, these two satellites were placed near the same location in order to back up each other. However, to avoid interference and maximize utilization, they were designed to use different polarizations. From the measurement results, it can be seen that the horizontally polarized waves suffer more degradation due to rainfall than vertically polarized waves, and that the rain intensity in the reception areas affected Thaicom 3 beacon by about 12 dB and Thaicom 2 beacon by approximately 9 dB.

However to confirm the behavior of rain between temperate and tropical regions, the rain statistics in both areas are needed. Figure 3.4 shows the cumulative rainfall rate of Kashima, Japan by rain gauge data from April 1978 to March 1982, and Bangkok, Thailand using data from ITU-R P.837-6 [5]. This comparison result shows the rainfall rate in Bangkok, Thailand is much higher than in Kashima, Japan when observed at 0.01% or 0.1% of time. It shows clear difference of the effect of rain attenuation in different regions.

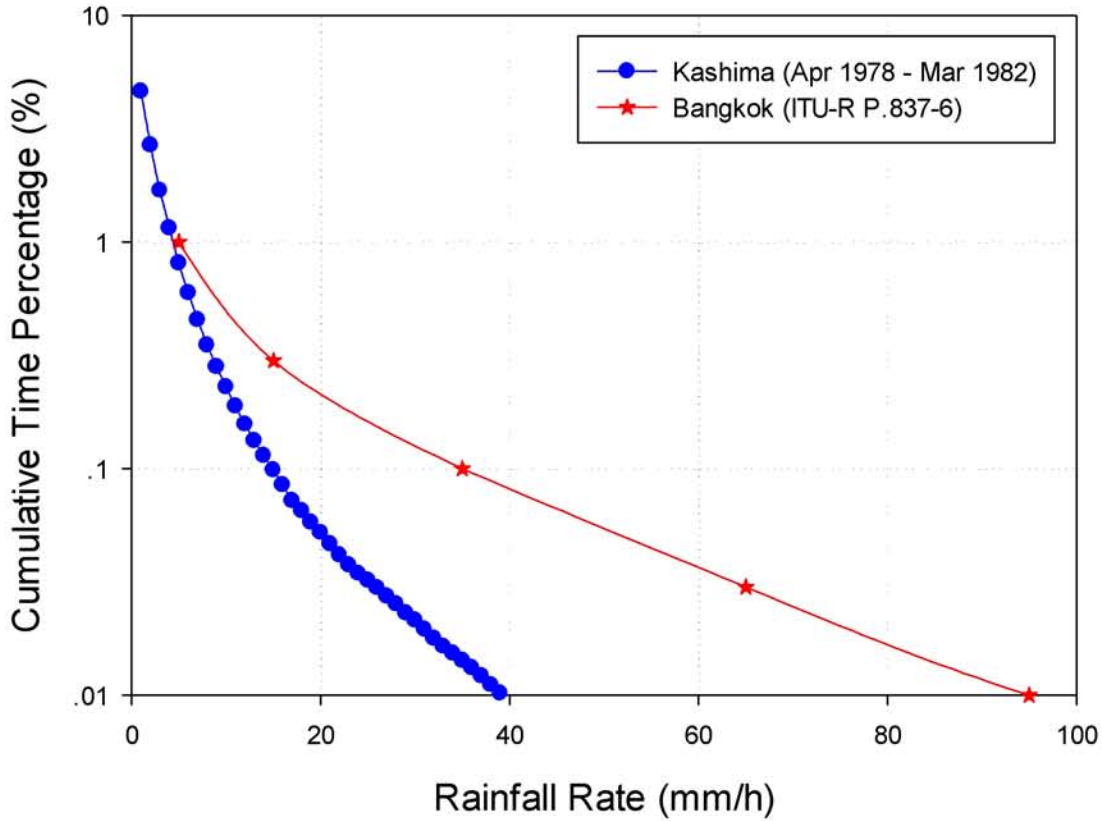


Figure 3.4: Annual cumulative time percentage of rainfall rate between Kashima, Japan and Bangkok, Thailand.

3.2.2 Frequency Scaling

As mentioned, the signals obtained from the Thaicom 2 and 3 satellites operate in the Ku-band, at frequencies of 12.57 and 12.59 GHz, respectively. To allow a comparison of the tropical and temperate region datasets, which were obtained at different frequencies, the Thaicom 2 and 3 satellite datasets were scaled up to 19.45 GHz (the CS satellite frequency). The ITU R. P.618-12 frequency scaling formula from the Ku- to Ka-band was used:

$$A_2 = A_1 (\varphi_2 / \varphi_1)^{1-H(\varphi_1, \varphi_2, A_1)} \quad (3.2)$$

$$\varphi(f) = \frac{f^2}{1 + 10^{-4} f^2} \quad (3.3)$$

$$H(\varphi_1, \varphi_2, A_1) = 1.12 \times 10^{-3} (\varphi_2 / \varphi_1)^{0.5} (\varphi_1 A_1)^{0.55} \quad (3.4)$$

where A_1 and A_2 are the equiprobable values of excess rain attenuation (dB) at frequencies f_1 and f_2 (GHz), respectively.

Figure 3.5 shows the attenuation of the Thaicom 2 satellite increasing from 9 to 19 dB, and the Thaicom 3 satellite increasing from 12 to 25 dB, after the scaling formula was applied. Thus, a significant rain attenuation difference of 10 dB and 13 dB for Thaicom 2 and 3, respectively, was observed when the frequencies are adjusted to 19.45 GHz.

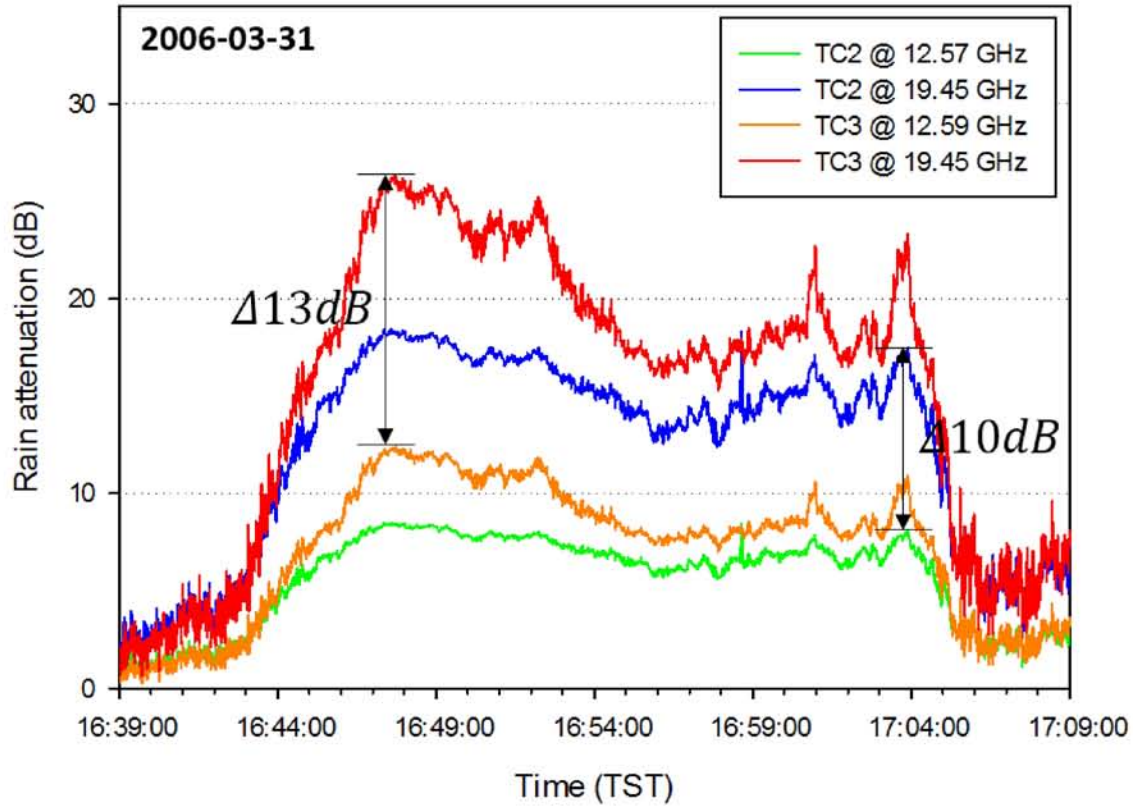


Figure 3.5: Rain attenuation sample of Thaicom 2 and 3 compared between frequency of 12.57 and 12.59 GHz, and 19.45 GHz.

3.2.3 Statistic Property

3.2.3.1 Cumulative Time Percentage

As for the satellite communication link, yearly service availabilities were observed from 0.01 to 0.1% of the cumulative time percentage (P), which corresponds to the duration of the downtime periods. In this section, the cumulative time percentage was used to derive the rain attenuation from the Thaicom 2, 3 and CS receiver beacons at 1-second time intervals. As was mentioned previously, there is 1 year of receiver beacon data from Thaicom

2 and 3, and 2 years of CS receiver beacon data, which made it necessary to rearrange some portions of the data to make them suitable for comparison purposes.

Figure 3.6 shows a comparison of rain attenuation between Thaicom 2, 3 and CS against the cumulative time percentage. In order to make clear comparisons, Thaicom 2 and 3 rain attenuation was scaled up to 19.45 GHz, which is the same frequency used by CS. This result shows the rain attenuation behavior at frequency of 19.45 GHz on an annual scale. Particularly, it can be seen that the curves are separated into tropical (Thaicom 2 & 3) and non-tropical (CS) areas. The first consideration is given at 0.01% of cumulative time percentage, where it can be found that CS beacon rain attenuation is about 15 dB. In contrast, Thaicom 2 rain attenuation is 19 dB and Thaicom 3 reached 24 dB. These results show that at 0.01% of time, the rain attenuation differences between tropical and non-tropical zones are at least 4 to 9 dB. Moreover, attenuations observed at 0.1% had genuine impacts on satellite service availabilities since Ka-band and above. Figure 3.6 shows that there are significant differences in rain attenuation between tropical and non-tropical zones above the 0.01% level. From these results, it can be seen that CS rain attenuation is about 5.4 dB, Thaicom 2 is 13 dB, and Thaicom 3 is 16.5 dB. Thus, the gap between tropical and non-tropical zone rain attenuation is at least 7.6 to 11.1 dB in the case of 1 year's data at 0.1%. More specifically, the difference attenuation values between Thaicom 2 and 3 is due to difference polarization effect. It is well known that the horizontal polarization is more attenuated with raindrop shape (oblate) than vertical polarization especially in tropical areas.

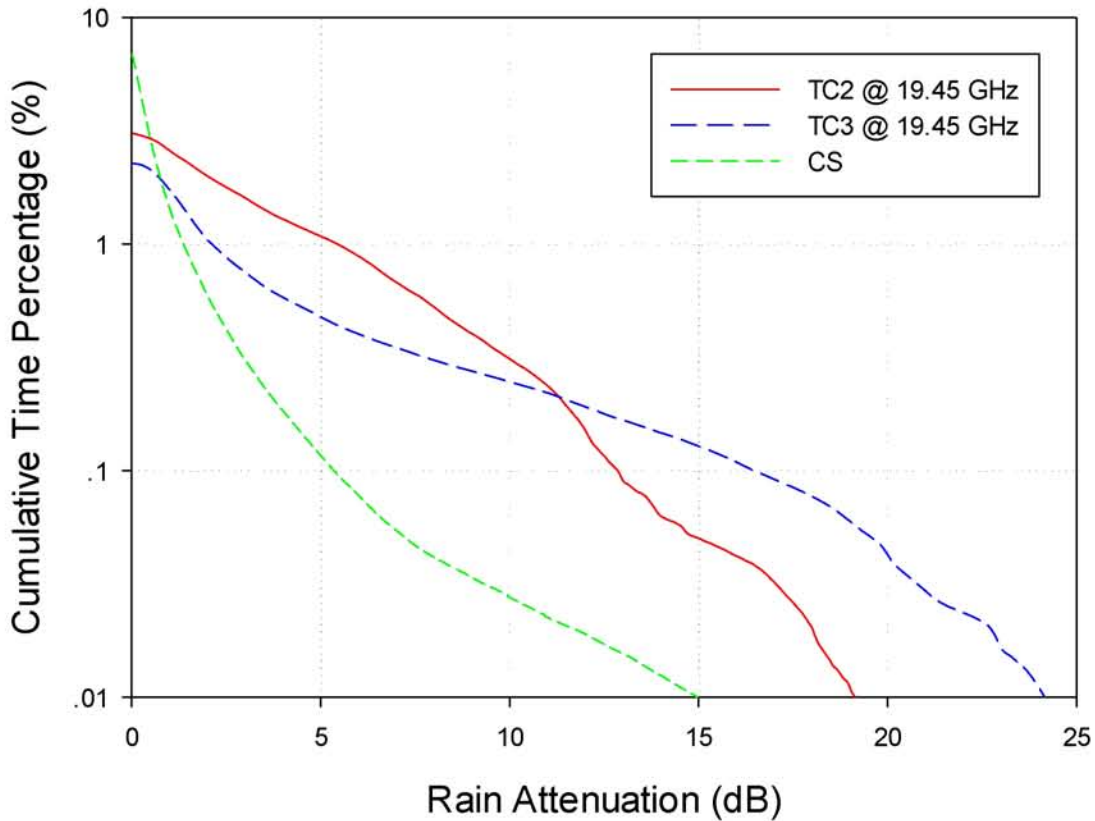


Figure 3.6: Yearly cumulative time percentage (P) against rain attenuation of Thaicom 2, 3 and CS.

3.2.4 Dynamic Properties

Understanding the dynamic properties of rain fade is very important for the development of rain attenuation mitigation methods. These dynamic properties can be derived from the data, including the rain drop size distribution, path length and rain type. Fade duration as investigated by Mandeep [6] and others [7][8] can express the frequency of rain events and the total attenuation time for each threshold level of concern. Another property of interest is fade slope. In Matriccioni's paper [9], statistics for the rate of change of attenuation at 11.6 GHz were calculated, and shown to be

log-normally distributed [10]. Van de Kamp found that the standard deviation of the rain attenuation was proportional to attenuation value, as well as being dependent on the rain type [11]. Studies have shown the fade slope varies with region, likely due to changes in local climate and elevation angle [12]-[21]. Fade duration and slope provide good indicators of the properties of the rainfall distribution.

Figure 3.7 shows a sample of receiver beacon rain attenuation data collected over 1 hours and illustrates the attenuation exceeded threshold level, fade duration and fade slope. The CS beacon operating in the Ka-band in Figure 3.7 shows that rainfall has degraded the KSTC receiver beacon almost 20 dB at the non-tropical Kashima site. In contrast, the results of Thaicom 2 beacon and Thaicom 3 beacon operating in Ku-band indicate that KMITL in Bangkok, which is located in a tropical zone, is being hit by severe rain and that signal attenuation will become more dominant over the Ka band satellite signal.

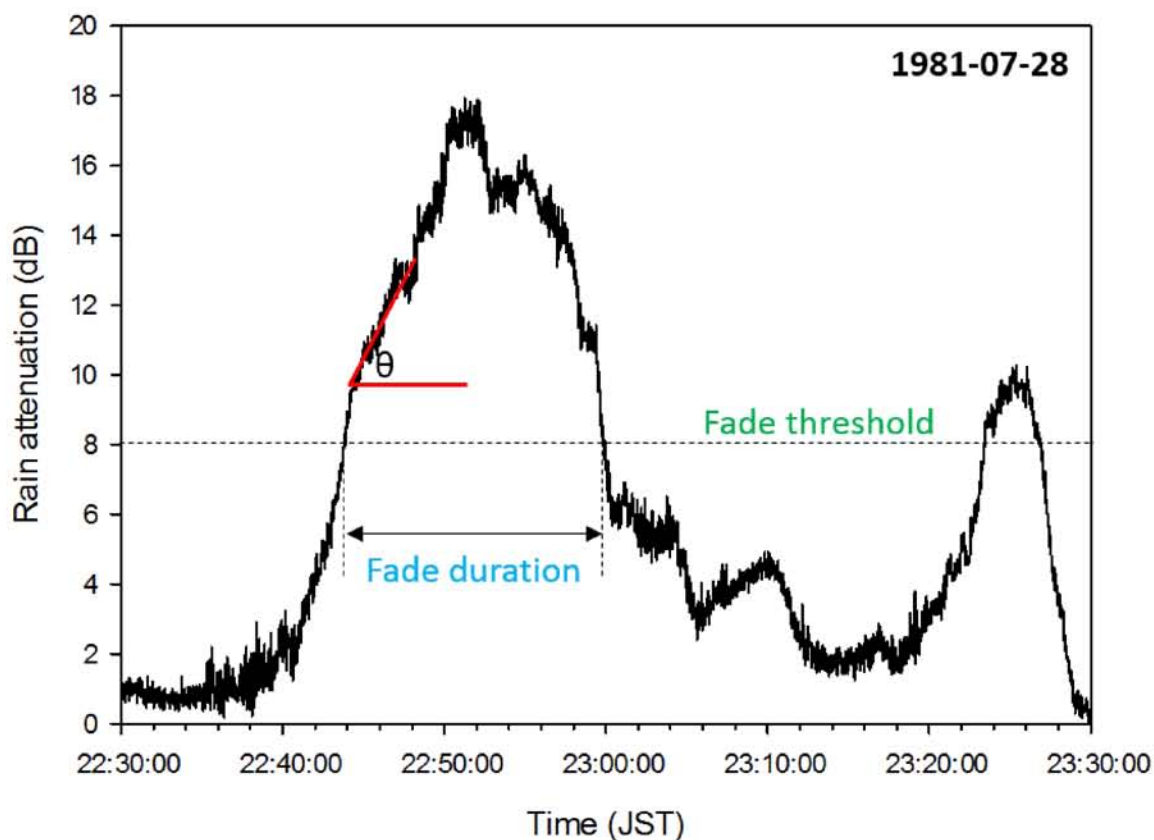


Figure 3.7: Sample of CS beacon attenuation time series with example of the attenuation threshold, fade duration and illustrated fade slope.

3.2.4.1 Fade Duration

Fade duration is defined as the length of an outage due to rain attenuation. In this paper, fade duration statistics are calculated from events with attenuations exceeding 1, 2, 4, 6, 8, 10, 12, 16, 20 and 24 dB and durations of 1, 2, 4, 6, 8, 10, 20, 40, 60, 80, 100 and 200 seconds. The point of concern here is taken into account to be the signal quality is substantially degraded for attenuations levels exceeding 15 dB. It can be shown the amount of the outage occurrence by rain attenuation in Ka-band.

3.2.4.1.1 CS Satellite

Table 3.2 shows the number of fade events for the CS satellite obtained over a two-year period, for the above exceedance levels and durations. It is shown that rain attenuation events exceeding 15 dB often occurred and the single longest duration of the largest rain attenuation threshold of 24 dB was 600 s.

Table 3.2: Event number of CS beacon derived for 2 years.

Duration (s)	Event number of the attenuation exceeded									
	1 dB	2 dB	4 dB	6 dB	8 dB	10 dB	12 dB	16 dB	20 dB	24 dB
1	45659	13181	2566	1202	463	364	192	63	34	29
2	24230	7288	1592	802	317	257	130	45	27	22
4	11238	3777	1012	504	217	177	94	41	24	18
6	7326	2695	766	389	178	143	86	35	21	16
8	5406	2164	671	334	155	125	82	33	20	14
10	4347	1824	590	301	144	117	78	33	20	12
20	2456	1200	465	232	115	83	62	26	18	10
40	1550	827	343	172	90	61	49	21	13	8
60	1225	666	284	139	79	52	38	17	9	7
80	1049	570	245	121	64	47	33	16	8	5
100	924	515	218	104	55	43	28	15	7	5
200	654	343	140	65	38	31	22	9	5	3
400	431	207	74	28	22	18	11	4	3	3
600	326	155	44	19	12	7	6	3	2	1
800	245	110	24	12	8	5	2	2	0	0
1000	188	86	18	9	4	3	1	1	0	0
2000	94	28	4	4	3	3	0	0	0	0
3000	44	10	1	2	2	0	0	0	0	0
4000	26	5	1	2	2	0	0	0	0	0
5000	21	2	1	2	2	0	0	0	0	0

The statistics presented in Table 3.2 are plotted in Figure 3.8(a). The average fade duration can be seen to decrease with increasing attenuation threshold due to the fact that large rain attenuation happens in a short

duration of time. The percentage of events exceeding a given duration is shown in Figure 3.8(b). For the CS satellite, an attenuation level greater than 16 dB is seen during 0.01% of rain events.

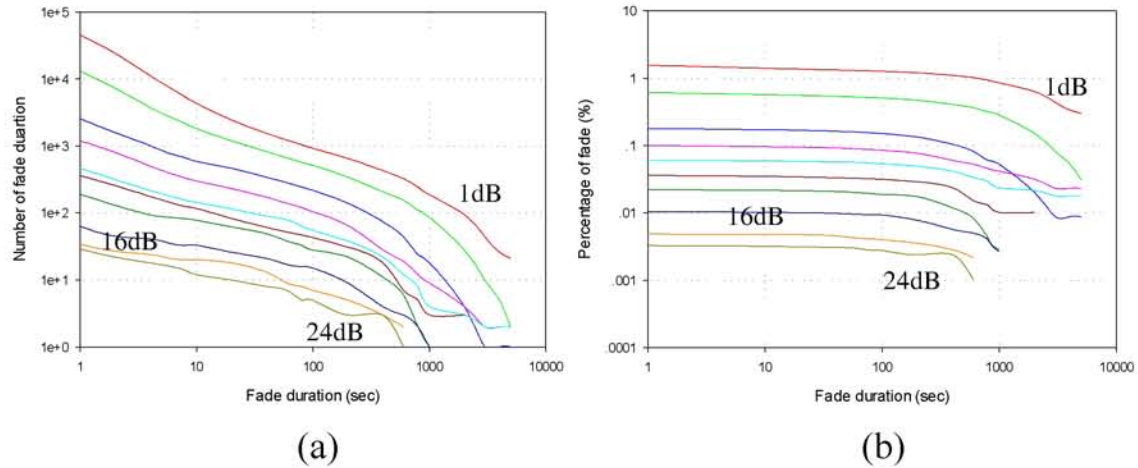


Figure 3.8: Fade duration statistic of CS beacon observed at 19.45 GHz. (a) event number of rain fade, (b) total time of rain fade in percentage.

3.2.4.1.2 Thaicom 2 Satellite

The fade durations in the Thaicom 2 satellite data were obtained over a one-year period, and the frequency was scaled from 12.57 to 19.45 GHz. Table 3.3 shows the number of rain fade events, which is representative of the average activity level for tropical areas. Attenuation levels exceeding 16 dB are observed more frequently than for the CS satellite. The data for attenuation levels of 20 and 24 dB are unreliable due to the collecting beacon data system errors.

Table 3.3: Event number of Thaicom 2 beacon derived for 1 years.

Duration (s)	Event number of the attenuation exceeded							
	1 dB	2 dB	4 dB	6 dB	8 dB	10 dB	12 dB	16 dB
1	8794	7048	3218	3165	1270	692	581	147
2	4970	4156	1911	1942	842	471	375	84
4	2617	2233	1045	1113	529	302	227	50
6	1827	1551	766	796	405	235	175	43
8	1392	1198	609	622	330	199	154	39
10	1137	977	513	508	294	172	134	38
20	657	541	338	318	213	134	90	32
40	384	337	227	230	166	110	64	27
60	285	274	190	196	152	98	58	24
80	254	234	176	176	139	87	52	23
100	240	222	167	167	132	84	50	20
200	199	179	137	126	102	63	39	15
400	163	140	118	100	69	40	21	6
600	133	114	98	74	52	29	16	2
800	115	95	83	62	38	19	11	2
1000	99	88	66	49	31	17	9	1
2000	62	55	34	21	11	5	1	0
3000	46	35	24	13	6	3	0	0
4000	37	27	19	6	1	1	0	0
5000	29	21	11	4	1	0	0	0

Figure 3.9(a) shows the trends in fade duration in the Thaicom 2 data. The average fade duration shown in Figure 3.9(b) is higher than that of the CS satellite data for attenuation exceedance levels of 2 to 16 dB. The percentage of time during fade events that had an attenuation exceeding 16 dB is 0.03%.

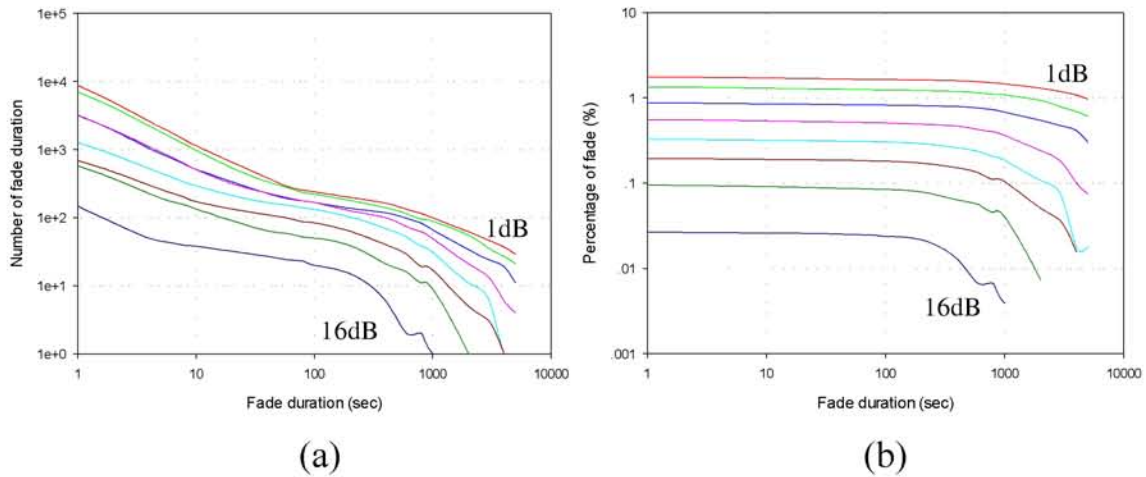


Figure 3.9: Fade duration statistic of Thaicom 2 beacon observed at 19.45 GHz. (a) event number of rain fade, (b) total time of rain fade in percentage.

3.2.4.1.3 Thaicom 3 Satellite

The observation period and scaling of the Thaicom 3 satellite data were the same as for the Thaicom 2 satellite data. Table 3.4 shows clearly that the number of fade events in tropical areas is much higher than in temperate areas, observed at an attenuation exceeding 2 dB to avoid any surrounding interference that can induce into the system where considered at the attenuation of 1 dB. From Table 3.4 it can be seen that there were more events exceeding an attenuation of 15 dB in one year in the Thaicom 3 data than in two years in the CS data.

Table 3.4: Event number of Thaicom 3 beacon derived for 1 years.

Duration (s)	Event number of the attenuation exceeded									
	1 dB	2 dB	4 dB	6 dB	8 dB	10 dB	12 dB	16 dB	20 dB	24 dB
1	19386	13310	6020	3548	2343	1557	1184	678	448	169
2	11008	6870	3377	1938	1303	822	682	382	277	105
4	5626	3400	1761	989	676	446	383	202	142	70
6	3708	2261	1169	661	468	304	276	160	102	56
8	2764	1725	872	504	376	256	221	131	72	46
10	2198	1369	716	413	312	217	190	115	66	42
20	1127	724	406	270	200	161	138	95	45	26
40	631	424	259	195	152	130	114	78	33	14
60	469	333	209	168	136	119	101	64	31	12
80	386	296	192	148	125	108	95	60	27	9
100	338	258	178	135	114	101	89	51	27	9
200	251	196	137	110	86	82	63	34	18	2
400	190	148	99	74	61	51	40	22	7	1
600	154	122	76	52	42	35	27	13	4	0
800	137	95	54	38	30	24	19	10	3	0
1000	120	75	42	29	27	19	12	6	1	0
2000	51	24	10	6	3	3	3	1	0	0
3000	28	12	4	3	1	0	0	0	0	0
4000	15	6	1	0	0	0	0	0	0	0
5000	13	3	1	0	0	0	0	0	0	0

Figure 3.10(a) illustrates trends in the fade duration of the Thaicom 3 satellite data. The interpretation of Figure 3.10(b) is the same as for Figure 3.9(b). The percentage of time during fade events that had an attenuation exceeding 16 dB is 0.1%. This is 10 times higher than the CS satellite data.

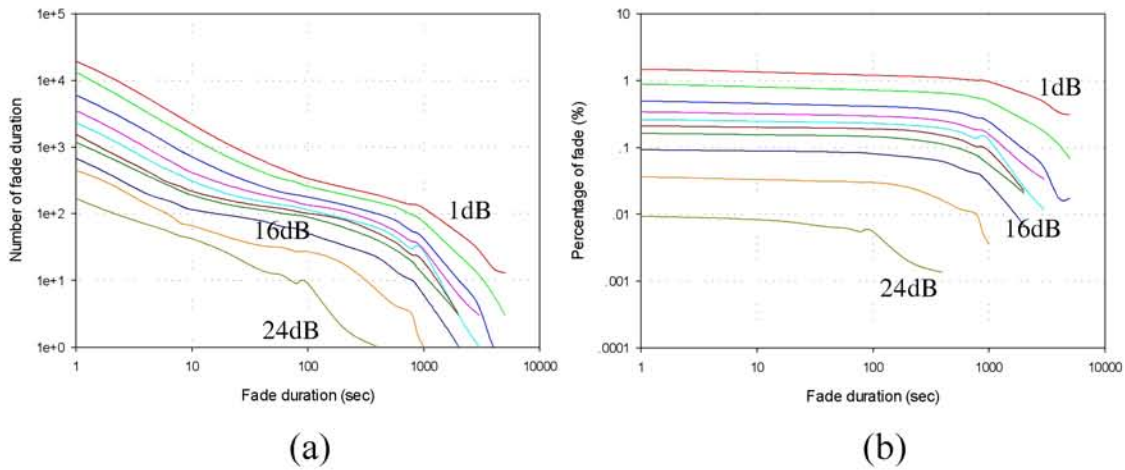


Figure 3.10: Fade duration statistic of Thaicom 3 beacon observed at 19.45 GHz. (a) event number of rain fade, (b) total time of rain fade in percentage.

3.2.4.2 Fade Slope

Fade slope is defined as the rate of change of attenuation in dB/s. Time intervals of 1 second were used. The distribution of fade slope shows general symmetry around zero for positive and negative slopes. Two parameters are commonly used to express the distribution of the fade slope: the standard deviation (σ_{ζ}) and the skewness (S). Positive skewness represents the occurrence of convective rain in a tropical area. On the other hand, negative skewness is evidence of widespread rain or a low rate of change in attenuation. Fade slope can be calculated with the following equation:

$$\zeta(i) = \frac{A(i+1) - A(i-1)}{2} \quad (\text{dB/s}) \quad (3.5)$$

where A is the attenuation in dB and i is the sample time in seconds.

In this research, we derived the fade slope using the CS, and the Thaicom 2 and 3 satellite datasets with time intervals of 1 second. To reduce

noise from ground equipment or other unknown sources, a minimum attenuation threshold of 2 dB at 19.45 GHz was selected for the calculations. The observation period for the CS (Thaicom 2 and 3) data was two (one) years. The Thaicom 2 and 3 satellites were located at a longitude of 78.5 °E in orbit and used the same receiver station but different polarizations. Figure 3.11 shows a comparison of the attenuations for the Thaicom satellites.

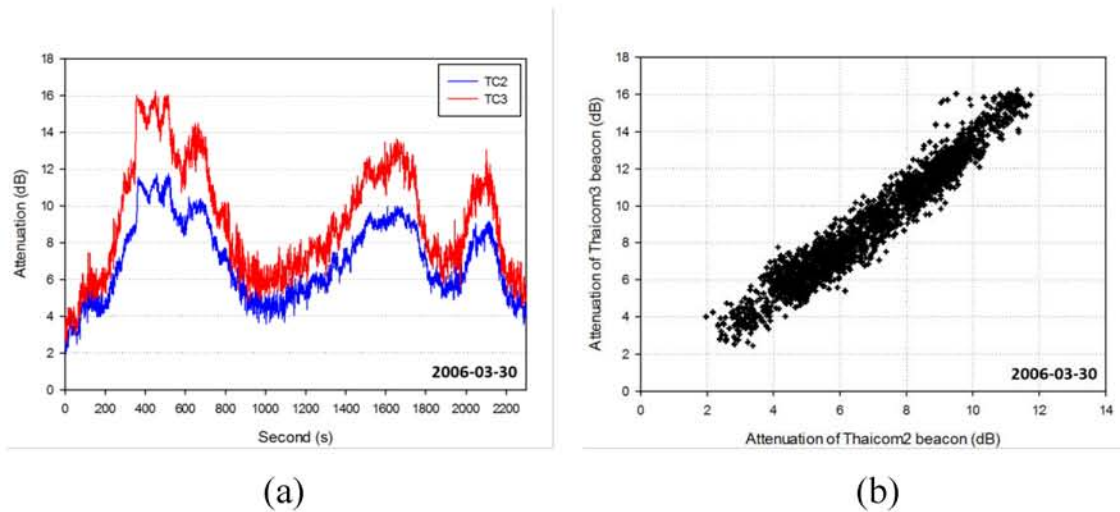


Figure 3.11: Rain attenuation comparison of Thaicom 2 and 3. (a) sample of consideration period, (b) scatterplot of attenuation.

3.2.4.2.1 Fade Slope Results

Figure 3.12 shows the estimated probability density function of the fade slopes of the CS, Thaicom 2 and 3 data. The standard deviation (σ_{ζ}) and skewness (S) are shown in Table 3.5. Here, if the value of σ_{ζ} is small, the narrow band of fade slope is happened. It is meant that the rate of change of attenuation is low as confirming the rain behavior in temperate areas. And it is shown another rain type in tropical areas where the value of σ_{ζ} is large. From Figure 3.12, there is a low (high) rate of change in the attenuation in temperate (tropical) areas. To further explore the differences in rain

attenuation between tropical and temperate areas, the skewness was also considered. Table 3.5 shows negative S in the CS data, consistent with widespread rain. The positive S obtained from the Thaicom 2 and 3 data confirms the high frequency of attenuation events in tropical areas.

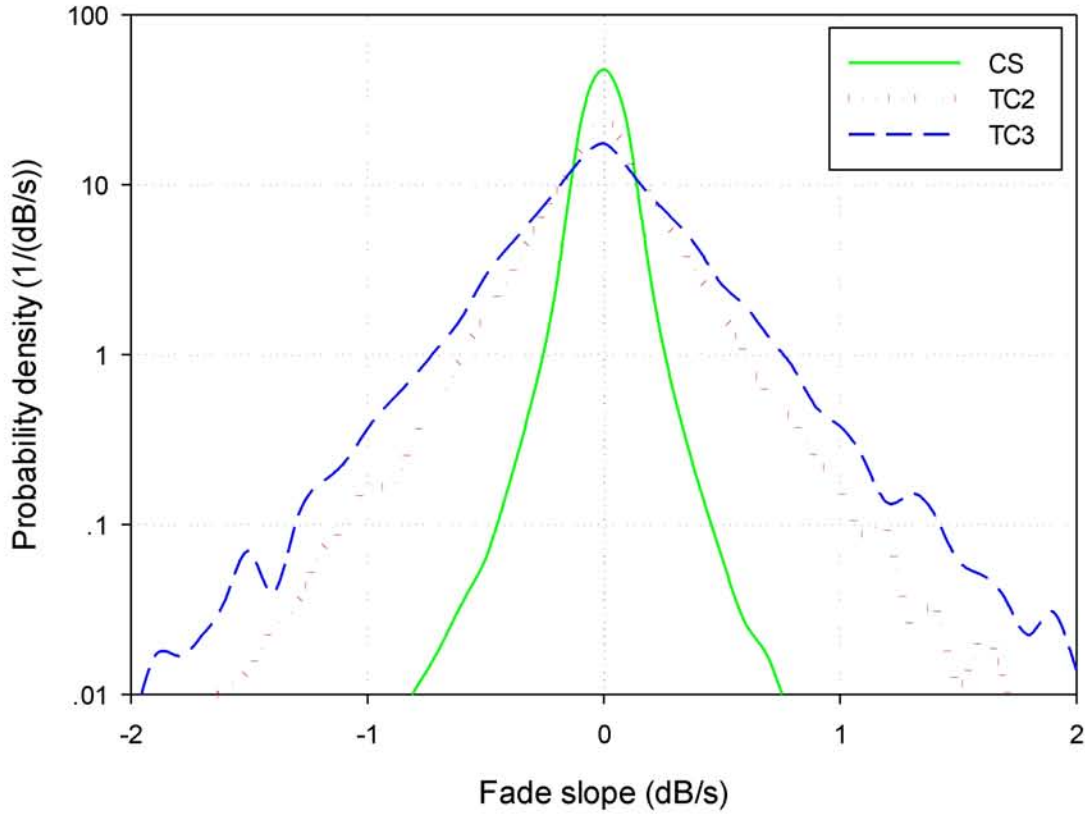


Figure 3.12: Fade slope comparison of Thaicom 2, 3 and CS.

Table 3.5: Parameters describes the rain attenuation behavior derived from fade slope.

	CS	Thaicom2	Thaicom3
Standard deviation (σ_{ζ})	0.09065	0.26721	0.36103
Skewness (S)	-0.11783	0.12172	0.09379

3.2.4.2.2 Comparison between Measured Data and the ITU

Prediction Model

The fade slope probability density function from ITU R. P.1623 [22] is shown in Eq. (3.6). The fade slope probability distribution depends on climatic parameters, drop size distribution and type of rain event. Therefore, in Eq. (3.6) the probability distribution mainly characterize the standard deviation of slope of rain attenuation.

$$p(\zeta|A) = \frac{2}{\pi\sigma_\zeta \left(1 + (\zeta / \sigma_\zeta)^2\right)^2} \text{ (dB/s)}^{-1} \quad (3.6)$$

where $p(\zeta|A)$ is the probability density of the fade slope, σ_ζ is the standard deviation of the conditional fade slope at a given attenuation level and ζ is the fade slope, which is varied here from -2 to 2 dB/s. The mean value of this distribution is 0 dB/s (symmetrical around zero).

Figure 3.13 shows the estimates of the fade slope distribution from the observations, and from Eq. (3.6) using the standard deviations presented in Table 3.5. The results show that the shapes of the distributions predicted by Eq. (3.6) are similar to the observations, but underestimate the probabilities. This suggests the probability density function given in Eq. (3.6) is not appropriate for modeling the properties of rain attenuation in these regions.

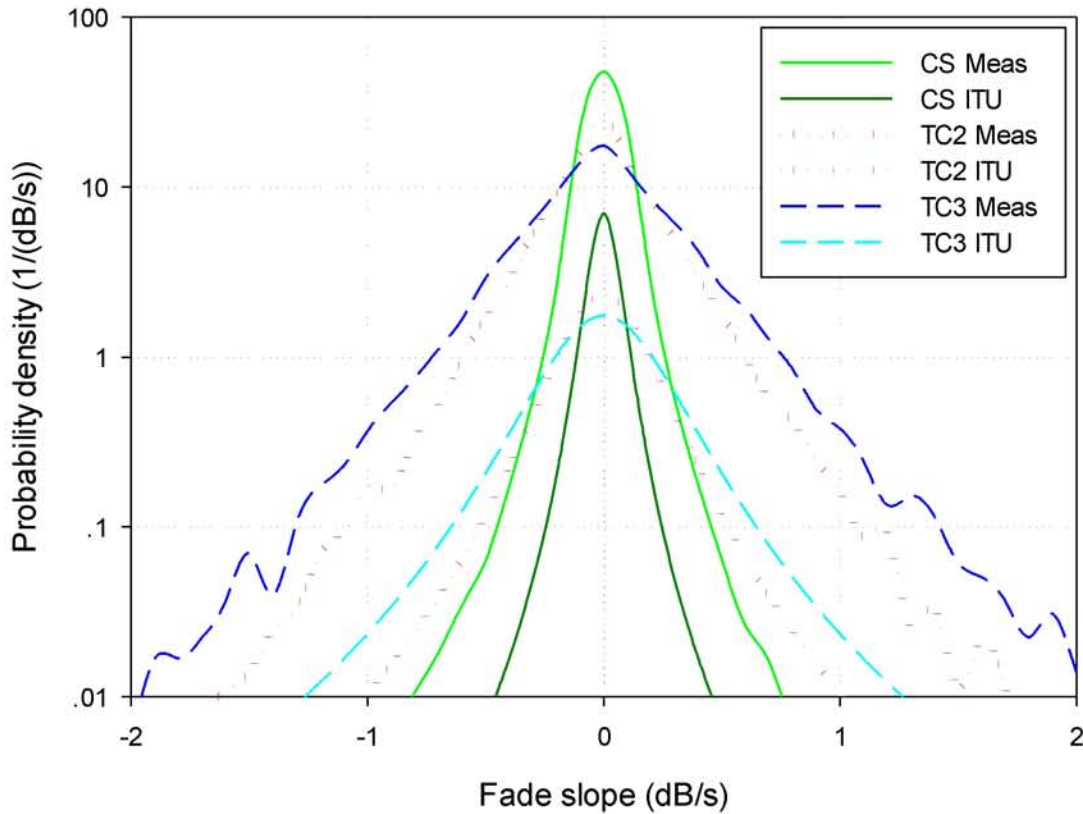


Figure 3.13: Comparison of fade slope of Thaicom 2, 3 and CS with ITU prediction model.

3.2.5 Time Diversity Results

3.2.5.1 Time Diversity with CS Beacon

Figure 3.14 shows the effectiveness of time diversity as applied to the CS beacon in the Ka-band at 19.45 GHz. Applying Eq. (3.1), we found that the diversity gains at 0.01% of time are 1.3, 4.4, 6.4, 8.8 and 9.9 dB when following the time diversities of 1, 5, 10, 30 and 60 minutes, respectively. The diversity gains at 0.1% show 0.5, 1.3, 1.8, 2.6 and 3.1 dB for the same times and other diversity gains are shown in Table 3.6.

The gain step of time diversity for the CS beacon in Japan or other non-tropical zones does not appear to show sudden changes; that is, it tends to match the rainfall characteristic mentioned above. However, this result also shows that time diversity trends exceeded 0.01% or 0.1% of the time probabilities for frequency of 19.45 GHz.

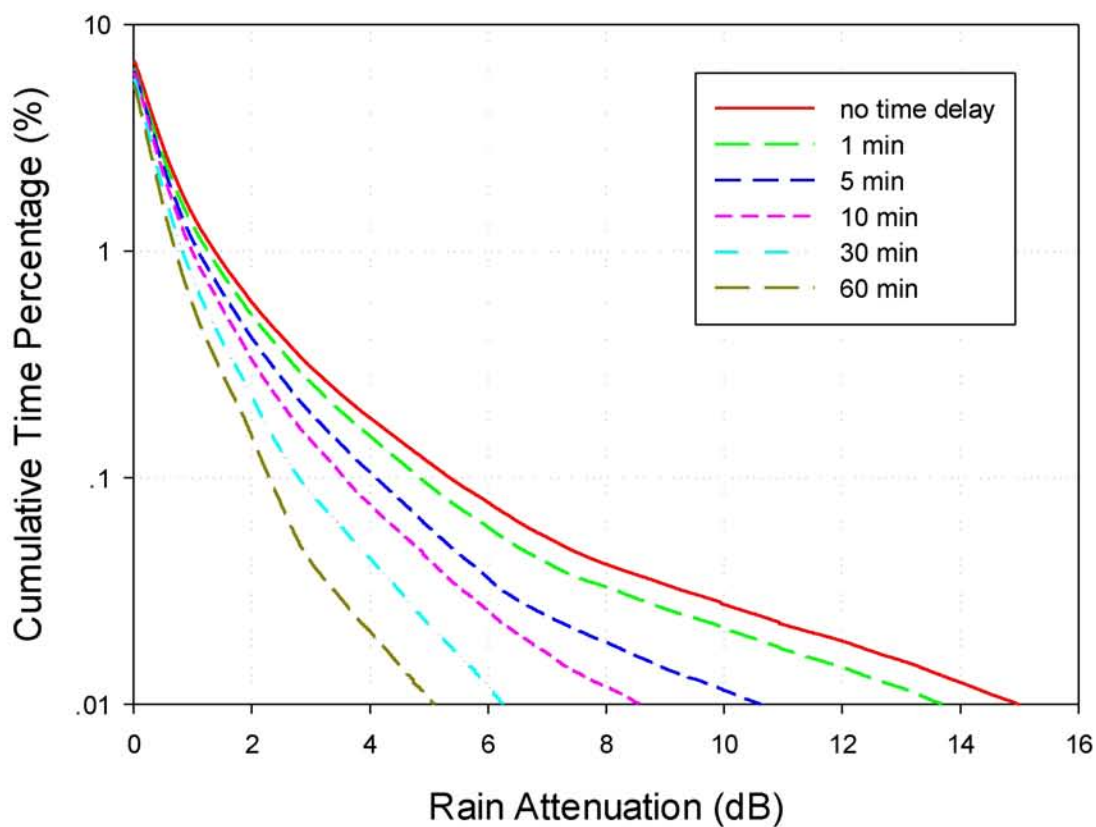


Figure 3.14: Performance of time diversity of CS beacon with several time delays.

Table 3.6: Diversity gain with various cumulative time percentage of CS beacon.

Cumulative time percentage (%)	Diversity gain with time delays				
	1 min	5 min	10 min	30 min	60 min
1	0.12	0.29	0.39	0.56	0.67
0.5	0.19	0.45	0.64	0.94	1.16
0.1	0.5	1.25	1.78	2.55	3.06
0.05	0.81	1.93	2.51	3.48	4.45
0.01	1.30	4.39	6.40	8.75	9.90

3.2.5.2 Time Diversity with Thaicom 2 Beacon

Figure 3.15 depicts the performance of time diversity under tropical region conditions by (a) the real receiver beacon in terms of Ku-band attenuation at 12.57 GHz, and (b) the beacon attenuation of Thaicom 2 obtained in the Ka-band at 19.45 GHz. First, the derived diversity gains of Thaicom 2 at 12.57 GHz as shown in Figure 3.15(a) at 0.01% of time are noted as 0.2, 0.9, 1.8, 3.5 and 4.2 dB for the times of 1, 5, 10, 30 and 60 minutes, respectively. In contrast, the diversity gains at 0.1% of time were noted as 0.2, 0.5, 0.8, 1.9 and 2.7 dB, for the same time delays. However, we found that the rain attenuation in the Ka-band at 19.45 GHz is actually much stronger than that experienced in the Ku-band at 12.57 GHz. After frequency scaling up to 19.45 GHz, as shown in Figure 3.15(b), we found that attenuation increased more than twice the time and the obtained diversity gains are 0.4, 1.8, 3.8, 7.3 and 8.8 dB at 0.01% of time and 0.3, 1.1, 1.8, 4.1 and 5.8 dB at 0.1% of time with 1, 5, 10, 30 and 60 minutes of time delays. Moreover, the diversity gains both in Ku-band at 12.57 GHz and Ka-band at 19.45 GHz with various time percentage are listed in Table 3.7.

More specifically, the diversity gain gap is defined as time diversity gain difference between each delay time cases, for example, 1 min to 5 min,

5 min to 10 min and so on. We can observe that diversity gain gap in Thaicom 2 case is larger than CS case. In other words, time diversity gain in Thaicom 2 case increases more steeply as delay time increases than CS case. This may be due to different rain property in tropical and non-tropical regions. For example, the diversity gain gap between 10 and 30 minutes shown in Figure 3.15 is larger than any other gap, whether at 12.57 GHz or 19.45 GHz, or even between those observed at 0.01% or 0.1% compared to the CS beacon. This gap indicates the rain characteristics in the tropical region that are most likely to occur during convective rain.

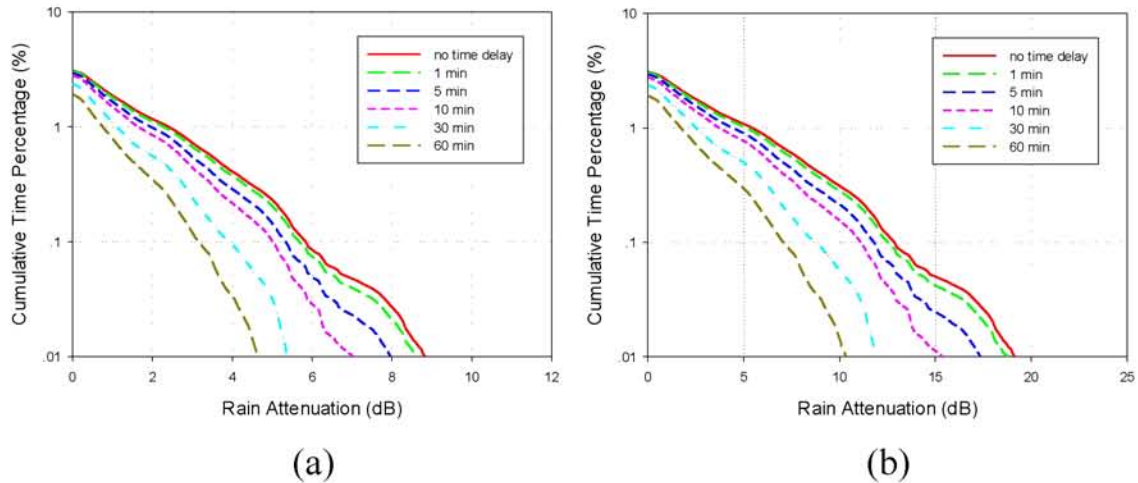


Figure 3.15: Performance of time diversity of Thaicom 2 for vertical polarization with several time delays. (a) In Ku-band at frequency 12.57 GHz, (b) In Ka-band at frequency 19.45 GHz.

Table 3.7: Diversity gain with various cumulative time percentage of
Thaicom 2 beacon.

Cumulative time percentage (%)	Diversity gain (dB) with time delays									
	12.57 GHz					19.45 GHz				
	1 min	5 min	10 min	30 min	60 min	1 min	5 min	10 min	30 min	60 min
1	0.13	0.45	0.77	1.31	1.66	0.31	1.02	1.73	2.93	3.72
0.5	0.14	0.50	0.80	1.44	2.14	0.31	1.13	1.77	3.18	4.75
0.1	0.16	0.50	0.82	1.91	2.69	0.34	1.07	1.76	4.09	5.79
0.05	0.31	0.89	1.38	2.24	3.21	0.64	1.87	2.93	4.76	6.86
0.01	0.17	0.86	1.81	3.46	4.17	0.37	1.80	3.79	7.31	8.81

3.2.5.3 Time Diversity with Thaicom 3 Beacon

Using the same simulation as described above, Figure 3.16(a) shows the curves for each delay times at 12.59 GHz and Figure 3.16(b) shows same property at 19.45 GHz. Considering the same rainfall rate statistics used for the Thaicom 2 beacon, we found that the Thaicom 3 beacon experiences more attenuation due to the difference in signal polarization. It should also be noted that the diversity gain step of Thaicom 3 beacon is not significantly different from that of the Thaicom 2 beacon. For example, at 0.01% time at 19.45 GHz as seen in Figure 3.16(b) the diversity gains obtained are 0.8, 2.6, 4.4, 11.8 and 15 dB for the time delays of 1, 5, 10, 30 and 60 minutes, while at 0.1% the diversity gains are 0.9, 3.5, 6.3, 11.5 and 13.1 dB for the same delays. However, the rain attenuation and diversity gain at 12.59 GHz are definitely lower than 19.45 GHz. To clarify the diversity gains of Thaicom 3 beacon both in Ku-band at 12.59 GHz and Ka-band at 19.45 GHz, diversity gains with various time percentage are listed in Table 3.8.

From the Thaicom 3 results, it can be seen that the diversity gap of 10 to 30 minutes is clearly expressed. This confirms that the behavior of rainfall in tropical areas occurs as heavy rain over short time periods. Looking at

Figure 3.16, we can see how the diversity gain improved about 7.4 dB between a 10-minute time delay and a 30-minute time delay, a passage of 20 minutes, whereas the diversity gain between time delays of 30 minutes and 60 minutes, a change of 30 minutes, is only 3.2 dB when observed at 0.01% of time at 19.45 GHz. The results indicate that the intensity of the rainfall declined during the period from 10 minutes to 30 minutes.

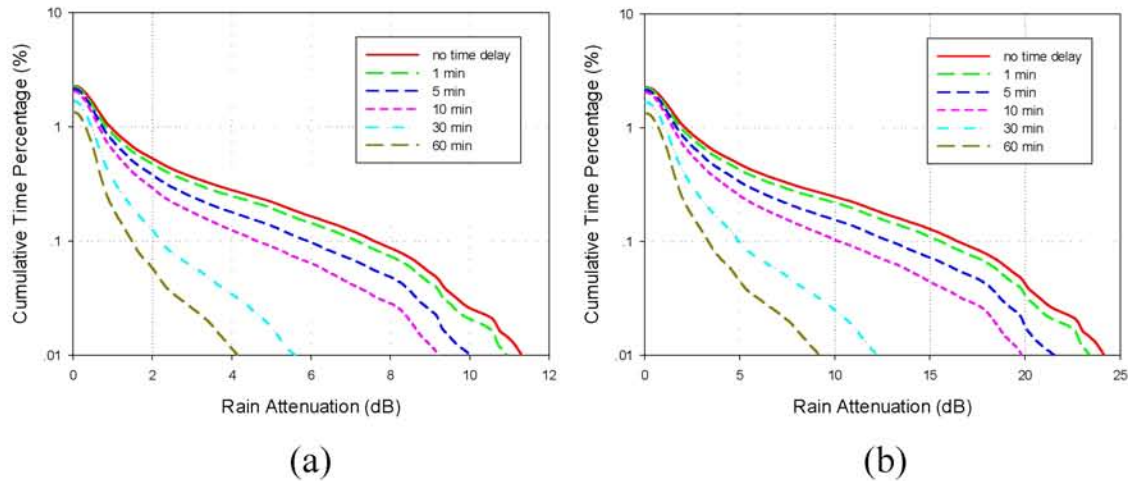


Figure 3.16: Performance of time diversity of Thaicom 3 vertical polarization with several time delays. (a) In Ku-band at frequency 12.59 GHz, (b) In Ka-band at frequency 19.45 GHz.

Table 3.8: Diversity gain with various cumulative time percentage of Thaicom 3 beacon.

Cumulative time percentage (%)	Diversity gain (dB) with time delays									
	12.59 GHz					19.45 GHz				
	1 min	5 min	10 min	30 min	60 min	1 min	5 min	10 min	30 min	60 min
1	0.11	0.20	0.29	0.47	0.62	0.22	0.43	0.64	1.05	1.4
0.5	0.24	0.62	0.88	1.34	1.52	0.54	1.38	1.96	3.00	3.41
0.1	0.44	1.68	2.96	5.37	6.1	0.91	3.54	6.26	11.51	13.12
0.05	0.35	1.21	2.50	5.76	6.97	0.72	2.50	5.20	12.19	14.83
0.01	0.38	1.27	2.12	5.7	7.16	0.77	2.60	4.35	11.84	14.96

3.2.5.4 Summary of Diversity Gain

We summarized all diversity gains for each time delay observed at 0.1%. Due to the brevity of the observation period, 0.1% was deemed more suitable than 0.01%, as shown in Figure 3.17. The results show the time diversity gain step increasing when delays from 1 minute to 60 minutes are applied. The interesting point here is considered to be the slope between 10 and 30 minutes, where it can be seen that the slope of the Thaicom 2 and 3 beacon is steeper than the CS beacon due to rain behavior between tropical and temperate areas are totally difference.

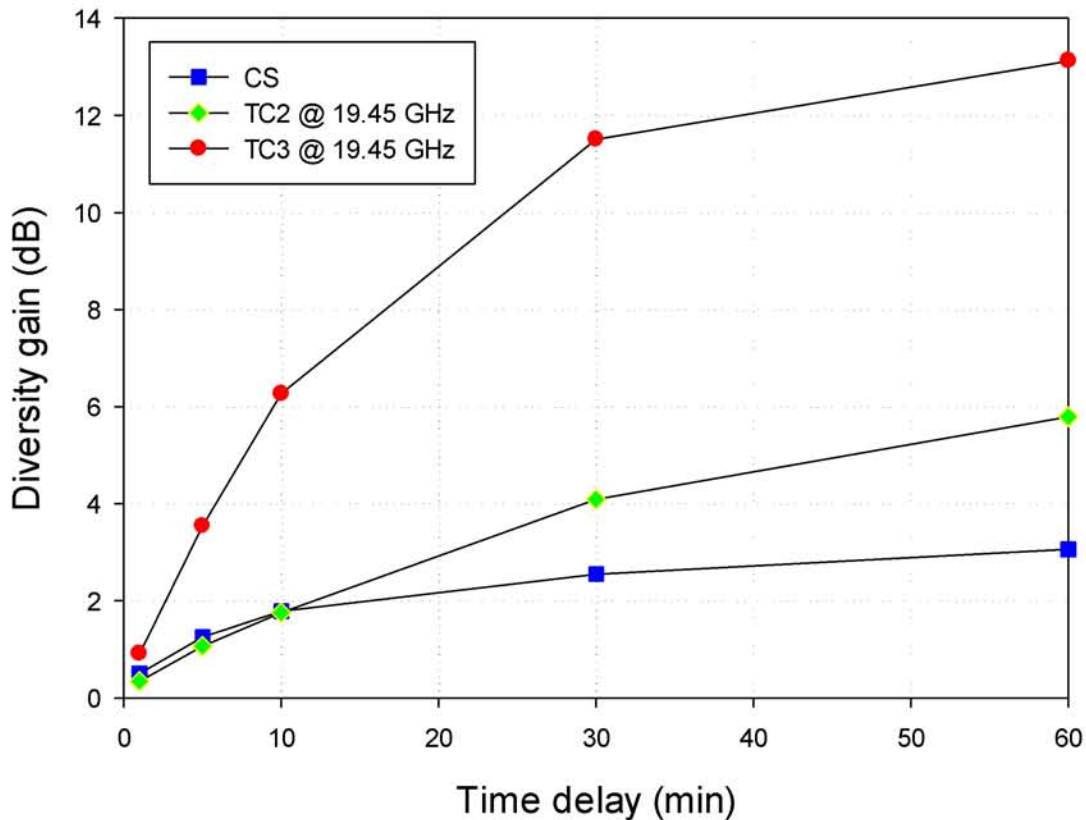


Figure 3.17: Diversity gain observed at 0.1% of cumulative time percentage against time delays. TC2 and TC3 results represent the diversity gain of Figs 8(b) and 9(b) at 19.45 GHz.

3.3 Time Diversity Method Applied with Rain Radar

Data

3.3.1 Data Analysis

This study used rain radar and AMeDAS data from across Japan produced by the Japan Meteorological Agency. The rain radar data are available in a 2560×3360 grid with a mesh size of approximately $1 \text{ km} \times 1 \text{ km}$, and at 5 min intervals. However, to cover mainland Japan and the southwestern islands, it was sufficient to extract 1481×1921 and 801×961 grids, respectively. As regards 5 min interval, shorter interval such as 1 min is preferable because very large attenuation normally change quite rapidly. However, at present time 5 min is the shortest time interval for all over high density $1 \text{ km} \times 1 \text{ km}$ rain map. The rainfall intensity can be determined using a combination of radar echoes and surface rain gauge data. Therefore, the Japan Meteorological Agency measures the precipitation at approximately 1300 ground stations in addition to radar observation points across Japan. The flow of analysis is shown in Figure 3.18. This study considered data spanning four years from July 2009 to June 2013. We applied time diversity with five time delays of 10, 20, 30, 60, and 120 min. Furthermore, we selected 23 observation points, 15 points on the mainland and 8 points on the southwestern islands of Japan, as shown in Figure 3.19. To evaluate the time diversity effect and predict the time diversity gain, the behavior of the rainfall and the rain intensity at each observation point across Japan were obtained and considered. Moreover, the analysis highlights different diversity gains for similar rain rate statistics in different sites arguably due to the different characteristics of rain and it leads to find

the importance of new parameter such as time correlation property of rainfall rate time series.

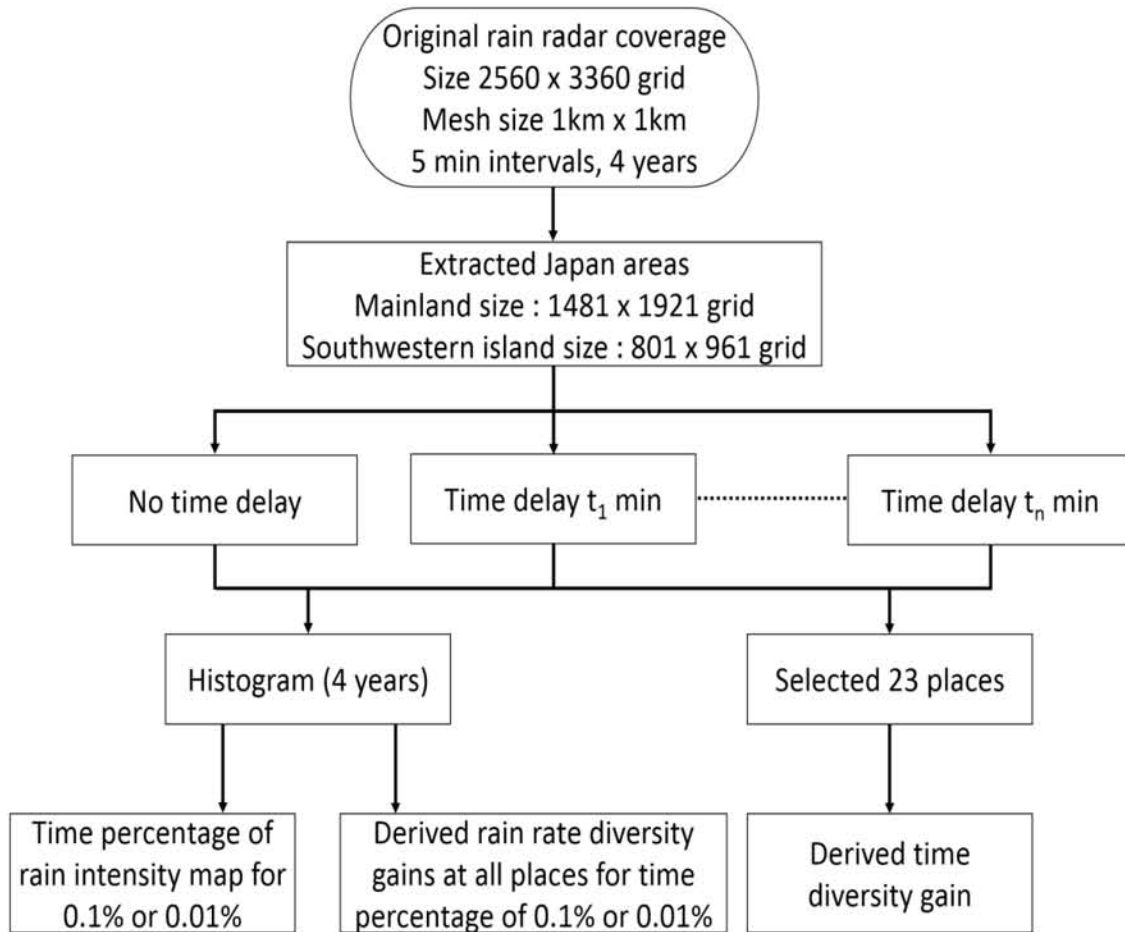


Figure 3.18: Simulation analysis flow.

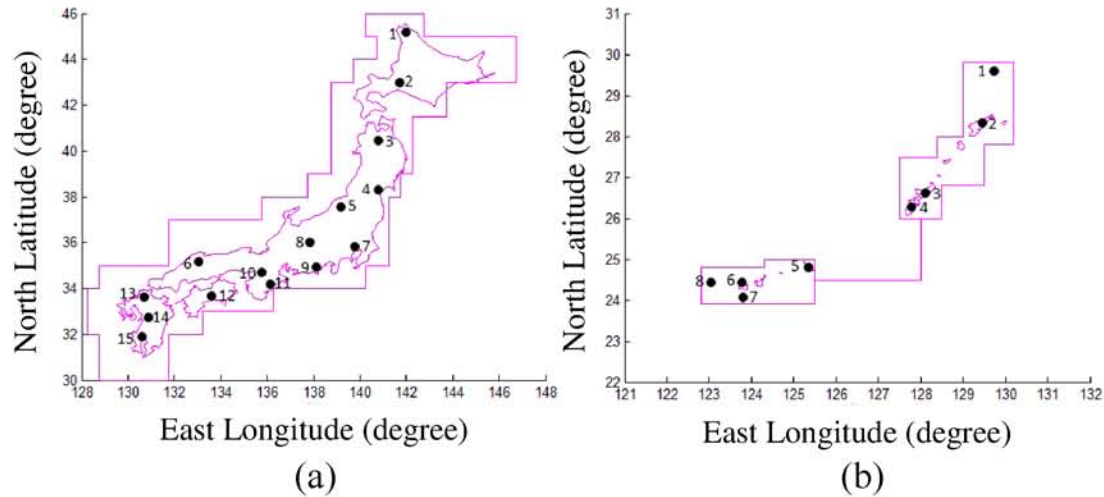


Figure 3.19: 23 observation points on (a) mainland and (b) southwestern islands of Japan.

3.3.2 Simulation Results

3.3.2.1 Estimated Rain Distribution across Japan

In this section, we derive the rain intensity with respect to the cumulative time percentage (P), as outlined in the International Telecommunication Union (ITU) recommendation (ITU R. P618-12), and the related link performance. A cumulative time percentage is derived as total time included rainy and dry season over Japan with no time delay was used, and the results are shown in Figure 3.20. The value of 0.01% is appropriate, especially for link calculations for the C band (6/4 GHz) because this band is less affected by rain attenuation; however, a value of 0.01% indicates 99.99% service availability each year. In the same way, for higher-frequency bands, such as the Ku, Ka, and Q/V bands, a cumulative time percentage of 0.1% is suitable, rather than 0.01%, because the rain attenuation more significantly affects higher-frequency bands than lower-frequency bands. The rain

intensity results for a cumulative time of 0.1%, or 99.9% service availability, are shown in Figure 3.20 using the same color scale as in Figure 3.21, for a cumulative time percentage of 0.01%. These figures provide complete coverage for all of Japan. The results show that high rain intensity appeared in the south and along the east coast of Japan for cumulative times of both 0.01% and 0.1%.

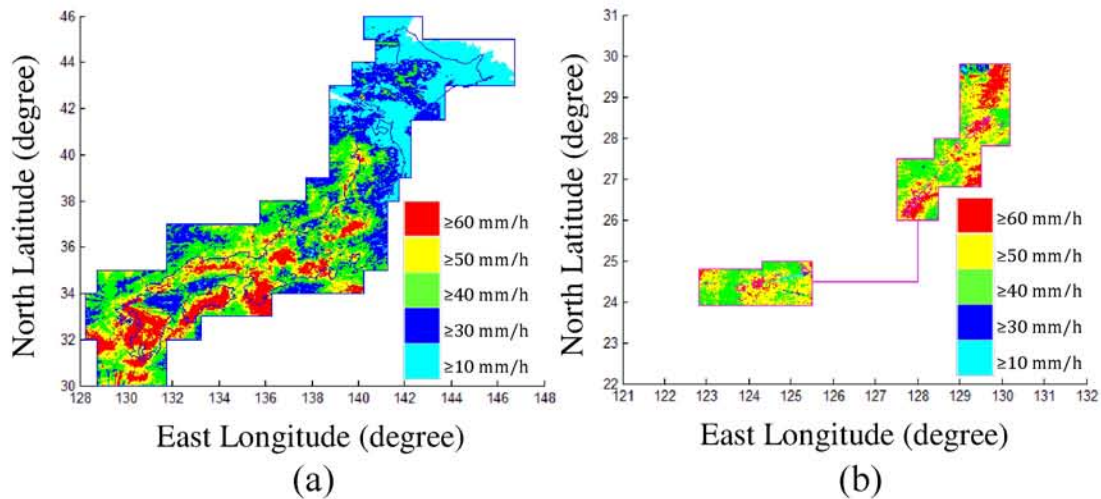


Figure 3.20: Four-year cumulative distribution of rain intensity for $P = 0.01\%$ with no time diversity for (a) mainland and (b) southwestern islands of Japan.

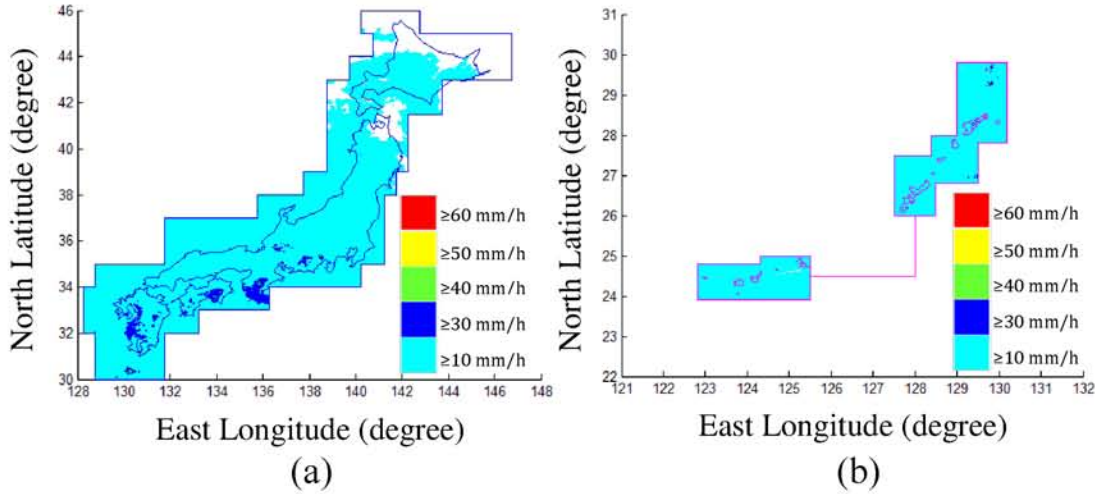


Figure 3.21: Four-year cumulative distribution of rain intensity for $P = 0.1\%$ with no time diversity for (a) mainland and (b) southwestern islands of Japan.

Furthermore, a time diversity simulation was conducted in which information was transmitted twice with time delays of 10 and 120 min. It is noted that the suitable time delays should be greater than the median duration of rain attenuation [23], D_0 which is given by:

$$D_0 = 80\phi^{-0.4} f^{1.4} A^{-0.39} \quad (3.7)$$

where D_0 is in seconds, ϕ is the elevation angle in degree, f is the frequency in GHz and A is the attenuation in dB.

In this analysis, we used appropriate time delays from 10 to 120 min. The effective rainfall rate time series in which time diversity is applied can be obtained by selecting the smaller rainfall rate between the original and the delayed time series. Figure 3.22 shows the four-year cumulative distribution of rain intensity for $P = 0.01\%$ and a time delay of 10 min. It can be seen

that the intensity is significantly reduced compared to that in Figure 3.20. Thus, most severe rain intensity phenomena are eliminated when the time diversity method is applied with a short time delay, and a large diversity gain can be expected at each location. This technique can avoid incomplete or missing data during rain events and, as previously mentioned, it is not necessary to make changes to either the satellites or their power supplies. Thus, the time diversity method may reduce operating costs in comparison with other methods.

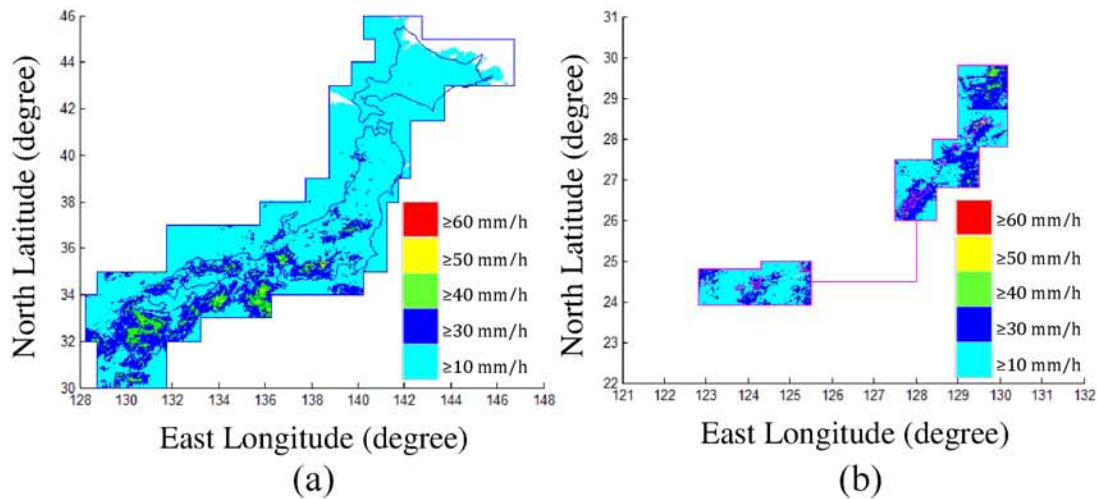


Figure 3.22: Four-year cumulative distribution of rain intensity for $P = 0.01\%$ with a time diversity of 10 min for (a) mainland and (b) southwestern islands of Japan.

3.3.2.2 Performance Evaluation

The performance of the time diversity technique was evaluated for all of the grid locations considered in this study. Figure. 3.23 show scatter plots of the diversity gain versus the rainfall rate for time delays of 10 and 120 min, respectively. The color of each point indicates the number of locations,

N , corresponding to that point, and the straight line is the limitation curve for the time diversity gain assuming no correlation between rainfall time series with time delay. The black points, which correspond to more than 1000 locations, are seen to fall close to a straight line, and the slope of this line increases with increasing time delay, approaching the limitation curve for a delay of 120 min. This indicates that the rain attenuation effect decreases with increasing time delay.

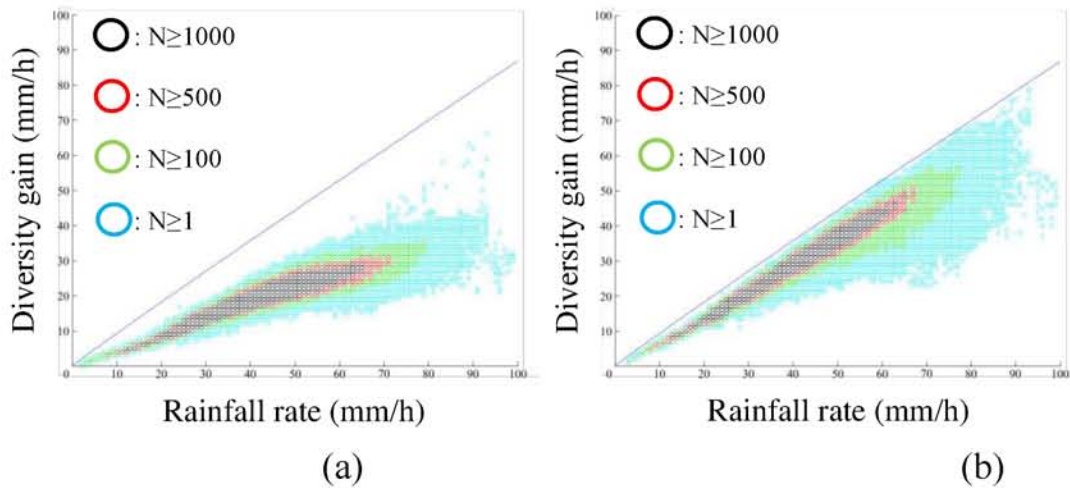


Figure 3.23: Diversity gain vs. rainfall rate for $P = 0.01\%$ with a time diversity of (a) 10 min and (b) 120 min.

When considering the design of satellites for the Ka band and higher-frequency bands, the cumulative rainfall occurrence rate by location is a significant factor. Figure 3.24 shows the cumulative rainfall occurrence rate for a total of 729,700 locations determined using different time delays and $P = 0.01\%$. The vertical axis represents the percentage of locations in Japan that received a given rainfall rate, which can be statistically determined from all scenes for 4 years. Here, we consider a cumulative rate of 50% in order to

allow comparison between the different time delays. In the absence of time diversity, the rainfall rate is approximately 45 mm/h. When time diversity is adopted, the rainfall rates for time delays of 10 and 120 min are 24 and 13 mm/h, respectively, corresponding to diversity gains of 21 and 32 mm/h, respectively. Thus, the diversity gain increases with increasing time delay.

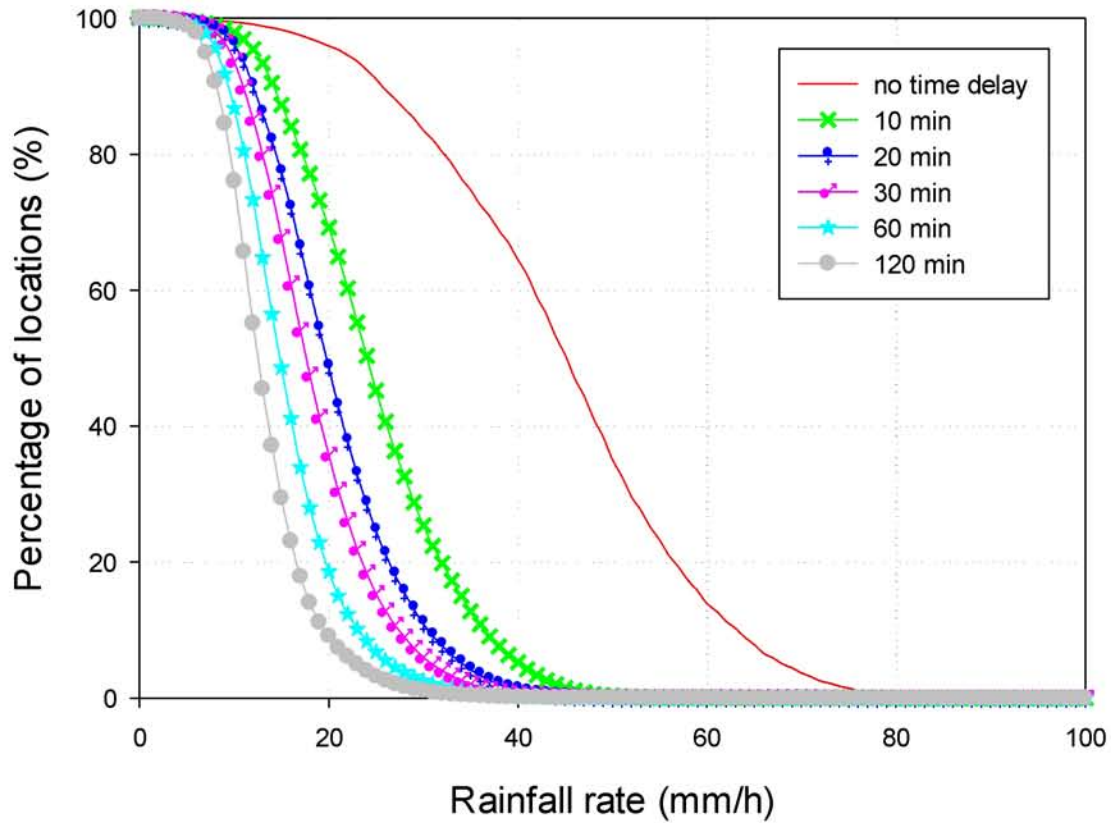


Figure 3.24: Cumulative rainfall occurrence rate by location for $P = 0.01\%$ and various time delays.

3.3.2.3 Rain Rate Diversity Gain

Data from 23 observation points across Japan were separately collected at 15 points on the mainland and 8 points in the southwest islands. The cumulative distribution of the rainfall rate over four years indicates the differences in

rainfall rates from place to place. Among these 23 points, Owase is the highest rainfall rate as shown in Table 3.9 and its cumulative distribution is shown in Figure 3.25. The average rainfall rate was approximately 78 and 39.1 mm/h for cumulative time percentages of 0.01% and 0.1%, respectively. The diversity gains for different time delays were derived from the results in Figure 3.26(a). For a cumulative time percentage of 0.01%, the diversity gains for time delays of 10, 20, 30, 60, and 120 min were 29.5, 33.3, 35.8, 48.8, and 42.2 mm/h, respectively. For a cumulative time percentage of 0.1%, the average rainfall rate was 39.1 mm/h, and the diversity gains were 13.1, 15.4, 16.3, 18, and 19.9 mm/h for time delays of 10, 20, 30, 60, and 120 min, respectively.

To transform the rainfall rate into rain attenuation [24]-[30], ITU-R recommendation P.618-12 is followed using a frequency of 22 GHz (the highest frequency in the 21.4–22 GHz band which is allocated next satellite broadcasting in ITU region 1 and 3). The rainfall rate exceeded at 0.01% of the time is used for predicting the rain attenuation value. Additionally, each sites parameters such as location, rainfall rate, elevation angle and so on are used to calculate for satellite orbit at 145° E longitude with the circular polarization to evaluate the effect of rain attenuation using the following equation.

The specific rain attenuation, γ_R (dB/km) is given by:

$$\gamma_R = k(R_{0.01})^a \quad (3.8)$$

where k and a are frequency-dependent coefficients given by ITU-R recommendation P.838-3 [31]. $R_{0.01}$ is the rain rate exceeded at 0.01% of time.

The prediction attenuation exceeded for 0.01% of an average year is obtained from:

$$A_{0.01} = \gamma_R L_S r_{0.01} v_{0.01} \quad (3.9)$$

where $r_{0.01}$ is the horizontal reduction factor, $v_{0.01}$ is the vertical adjustment factor and L_S is the slant-path length which is calculated the rain height from ITU-R recommendation P.839-4 [32].

The estimated attenuation to be exceeded for other percentages of an average year, in the range 0.001% to 5%, is determined from the attenuation to be exceeded for 0.01% for an average year:

$$A_p = A_{0.01} \left(\frac{p}{0.01} \right)^{-(0.655+0.033 \ln(p) - 0.045 \ln(A_{0.01}) - \beta(1-p) \sin \theta)} \quad (3.10)$$

where

$$\beta = \begin{cases} 0 & : p \geq 1\% \\ -0.005(|\varphi| - 36) & : p < 1\% \end{cases}$$

where A_p is the attenuation for different cumulative time percentages for an average year as a function of $A_{0.01}$ and the cumulative percentage of total time of concern p . We applied this equation to each of the 23 observation points across Japan as shown in Table 3.9.

Figure 3.26(b) shows the comparison of rainfall rate transformed to rain attenuation between ITU and Capsoni parameters [23]. Capsoni proposed the transformation rainfall rate to specific attenuation at the frequency of interest through the exponential relation $\gamma = kR^a$ and their parameter is $k=0.0701$, $a=1.0730$ at 20 GHz. The comparison results at 20 GHz show that ITU and Capsoni parameters are appropriately used in the rain attenuation transformation due to the values is insignificantly different.

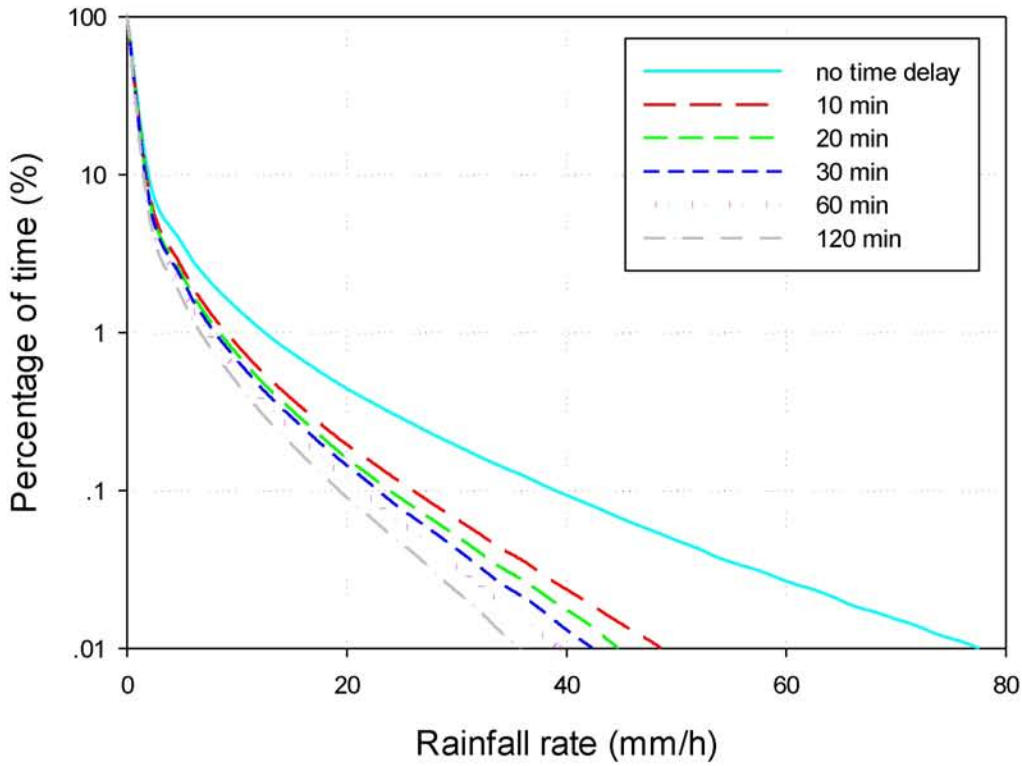


Figure 3.25: Cumulative time percentage of rainfall rate over four years at Owase for various time delays.

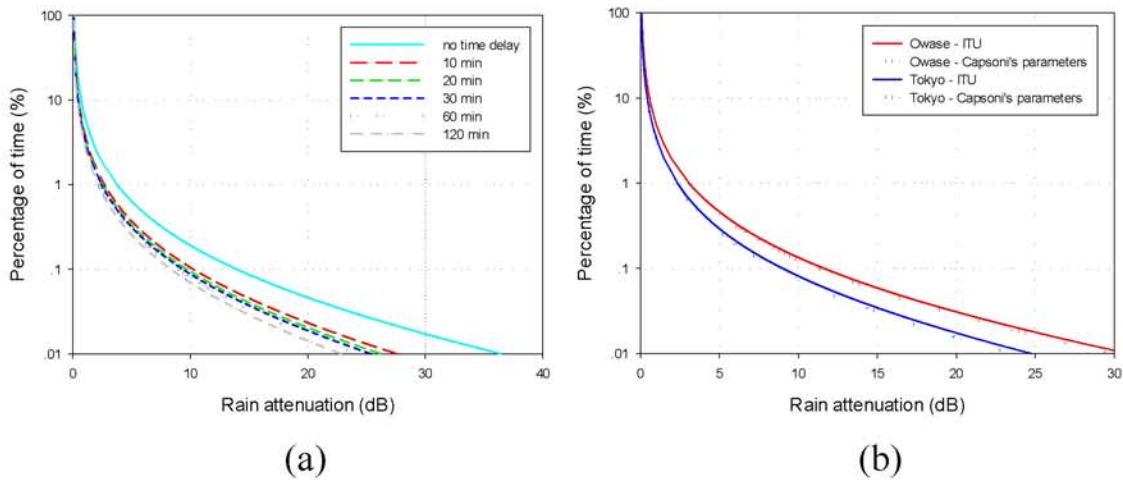


Figure 3.26: Cumulative time percentage versus rain attenuation for (a) rain attenuation in Owase with time delays at 22 GHz and (b) comparison of ITU and Capsoni's parameters in Owase and Tokyo at 20 GHz.

Table 3.9: Rainfall rate and rain attenuation at 22 GHz of 23 observation points of 0.01% and 0.1% of time.

Place no.	Place name	P = 0.1%		P = 0.01%	
		Rainfall rate (mm/h)	Attenuation (dB)	Rainfall rate (mm/h)	Attenuation (dB)
ML-1	Wakkankai	10.8	6.65	31	19.77
ML-2	Sapporo	11.8	6.58	29.9	19.41
ML-3	Aomori	11.4	6.51	28.6	19.01
ML-4	Sendai	15.4	7.56	34.1	21.48
ML-5	Niigata	17.1	8.82	42	24.64
ML-6	Matsue	21.2	11.33	56.9	30.46
ML-7	Tokyo	20.4	10.8	54.9	29.23
ML-8	Matsumoto	14.1	9.04	42.2	24.95
ML-9	Shizuoka	27.3	11.85	62.1	31.64
ML-10	Osaka	20.5	11.23	56.2	30.09
ML-11	Owase	39.1	13.94	78	36.45
ML-12	Kochi	29	12.47	64	32.84
ML-13	Fukuoka	25	12.99	67	34.09
ML-14	Kumamoto	27	13.7	71.9	35.58
ML-15	Kagoshima	28.5	12.96	64.4	33.57
SW-1	Suwanosejima	24.3	10.26	56.5	29.26
SW-2	Amami	18.4	8.06	39.2	23.4
SW-3	Nago	22.8	8.95	44.3	25.51
SW-4	Naha	23	9.61	49	27.19
SW-5	Hirara	18.5	8.15	37.2	23.24
SW-6	Taketomi	22	9.2	43.6	25.86
SW-7	The offing of Taiwan	23.7	11.03	56	30.29
SW-8	Yonaguni	19	8.13	36.2	23.13

From Figure 3.27, we show the diversity gain obtained from Eq. (3.1) for a cumulative time percentage of 0.1%; the rain attenuation are given in Figure 3.26(a) using Owase as an example. The power law relationship as described in the ITU-R recommendation P.838-3 [31] is used as the prediction method and is given

$$G_d = \alpha R^\beta \quad (3.11)$$

where G_d is the diversity gain (dB), R (mm/h) is the rainfall rate, α and β are frequency and time delay dependent coefficients that can be derived using the linear least squares fitting method after transformed Eq. (3.11) into logarithm scale. Table 3.10 gives the combinations of α and β for each time delay.

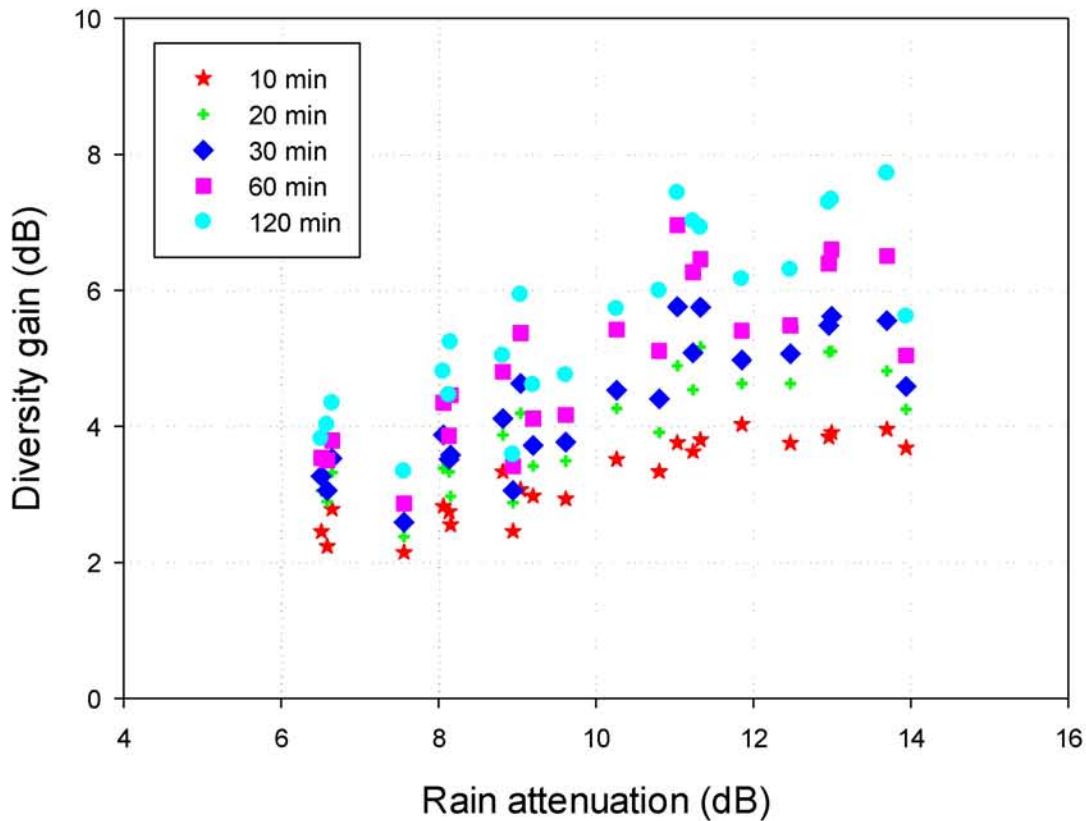


Figure 3.27: Diversity gain versus rain attenuation for 23 observation points in Japan for $P = 0.1\%$ with various time delays at 22 GHz.

Table 3.10: Frequency-dependent coefficients of time delays for $P = 0.1\%$ at 22 GHz.

P:0.1%	α	β
10 min	0.585	0.739
20 min	0.646	0.784
30 min	0.653	0.820
60 min	0.674	0.863
120 min	0.746	0.869

Figure 3.28 shows the comparison of the predicted diversity gain [33]–[35] between Matricciani’s model derived for Spino, Italy [1] and our proposed model derived for Japan determined from the frequency-dependent coefficients of time delays in Table 3.10 and from Eq. (3.11). The results in Figure 3.28(a) and (b) show that Matricciani’s model overestimates and it gives more error than our proposed model, for example at 10 min delay prediction, Matricciani’s model error is 0.894 but our proposed model error is 0.256 and other quantitative errors are shown in Table 3.11. Additionally, this prediction method can be adopted for use across Japan depending on the occurrence of rainfall or rain attenuation in each area, in order to determine appropriate time delays.

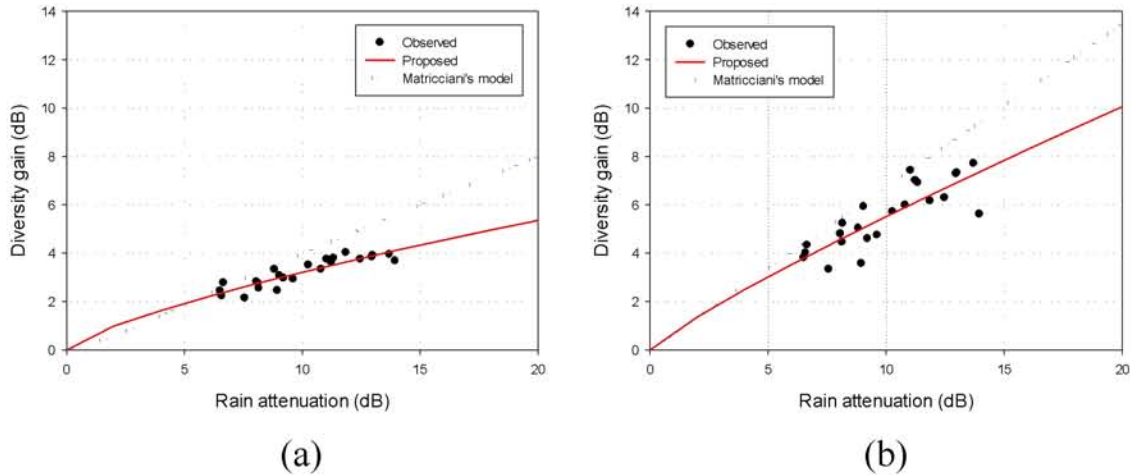


Figure 3.28: Comparison prediction of time diversity gain between our proposed and Matricciani models for $P = 0.1\%$ for (a) 10 min, proposed model used $\alpha = 0.585$ and $\beta = 0.739$, and (b) 120 min, proposed model used $\alpha = 0.746$ and $\beta = 0.869$.

Table 3.11: Prediction errors comparison.

Models	RMSE				
	10 min	20 min	30 min	60 min	120 min
Proposed	0.256	0.438	0.517	0.698	0.734
Matricciani	0.894	1.818	2.107	1.974	1.474

3.3.3 Time Diversity Gain Prediction Model

The previous section only considered the predicted time diversity gain [36]-[38] determined from the cumulative distribution of the rainfall rate or rain attenuation for $P = 0.01\%$ and 0.1% . However, we found that for a time delay of 120 min, the cumulative distribution graphs differed for some regions that had the same average cumulative rainfall rates, as shown in Figure 3.29.

Figure 3.29 shows the results for no time delay, a 120 min time delay,

and the probability maximum gain. The maximum gain was determined from the probability of the cumulative distribution of the real rainfall rate, which is given by

$$P_T[\%] = \left(\frac{P_1[\%]}{100} \right) \times \left(\frac{P_2[\%]}{100} \right) \times 100\% \quad (3.12)$$

where P_T is the probability with maximum diversity gain, P_1 is the measured cumulative distribution of the rainfall rate, and P_2 assuming the same value of P_1 as the probability distribution function for gain compensation.

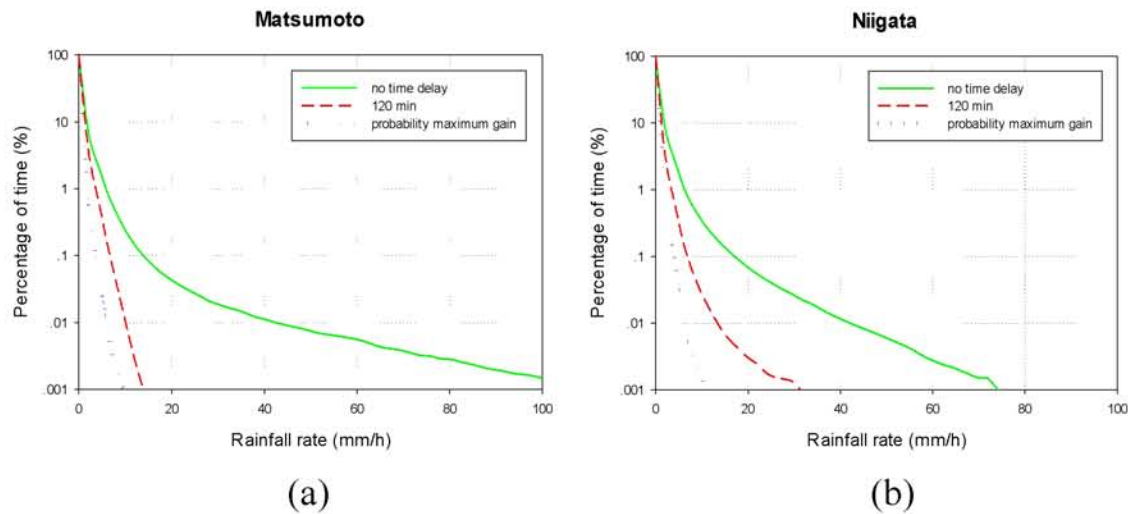


Figure 3.29: Cumulative time percentage versus rainfall rate for no time delay, a time delay of 120 min, and the probability maximum gain at (a) Matsumoto and (b) Niigata.

As shown in Figure 3.29, the curves for the 120 min delay for Matsumoto and Niigata differ from each other. The solid line is the cumulative distribution of the rainfall rate over four years, the dashed line includes a 120 min time delay, and the dotted line is the probability

maximum gain determined from Eq. (3.12). These two locations are considered because they have very similar rainfall rates for the same cumulative time percentages; for cumulative time percentages of 0.01% and 0.1%, the rainfall rates are approximately 42 and 15–17 mm/h, respectively, at both Matsumoto and Niigata. According to this, the curves should be approximately equivalent, but they are in fact different. Therefore, we conclude that the diversity gain may not depend only on the cumulative distribution of the rainfall rate; there are likely additional parameters involved that must be considered to obtain the most accurate prediction of the diversity gain. We suspect that G_d may be approximated as in the following equations:

$$G_d = f(R, \rho) \quad (3.13)$$

where G_d is the diversity gain, R is the rainfall rate and ρ is the time correlation coefficient of rainfall rate at each location.

3.4 Summary of Chapter 3

A time diversity method is proposed as an alternative method for mitigate rain attenuation effects in future satellite communications systems using the Ka band or higher-frequency bands. Such systems will aim to provide support beyond ground information technologies, such as super hi-vision television, next-generation compression technology, and new modulation techniques. This proposed method used the receiver beacons of Thaicom 2 and 3 in Bangkok, Thailand as the representative for tropical zone time diversity estimations and the CS receiver beacon in Kashima, Japan for non-

tropical zone estimations. Moreover, also used rain radar data over Japan with AMeDAS data spanning four years.

Time diversity is applied with all beacon data to confirm the efficiency of this method. From the simulation results, it can be seen diversity gain increases depend on the increasing time delays. Those time delays can also be linked to the rainfall rate occurring at those times. Nevertheless, this chapter provides a straightforward overview of the performance of time diversity in the Ku- and Ka-bands for the tropical region of Bangkok, Thailand, which means the results can reasonably be considered representative of tropical regions. Finally, we note that the large difference of rain attenuation between vertical and horizontal polarization of Thaicom 2 and 3 measured at Bangkok is observed. Then, it is also suggested that in tropical region such as Bangkok polarization diversity is effective in both cases with and without time diversity.

Fade durations were calculated for attenuation exceedance thresholds of 1, 2, 4, 6, 8, 10, 12, 16, 20 and 24 dB. Attenuation exceeding 16 dB was assumed to correspond to serious signal degradation in the Ka-band. The results showed that attenuation above 16 dB in tropical regions accounted for between 0.03% and 0.1% of the total rainy time, compared with 0.01% in temperate regions. This suggests rain attenuation has a greater impact, in terms of both the attenuation level and duration, in tropical regions.

Fade slope provides a good measure of rain attenuation in both regions, and can be expressed in terms of its standard deviation and skewness. The standard deviation of fade slope represents the speed of change of attenuation. From the estimated standard deviation and skewness, rain in the temperate region is widespread and characterized by a slow rate of change, while in the tropics it is convective and has a high rate of change.

Thus, it is found apparent difference of dynamic property of rain attenuation between temperate and tropical regions.

The cumulative distribution of the rain radar data was determined with respect to the rainfall rate in units of millimeters per hour and was also converted to rain attenuation following ITU recommendation P.618-12, based on parameters at 22 GHz. Furthermore, a time diversity gain prediction method was also proposed, which also uses the cumulative distribution of the rain attenuation. However, from our data analysis, the diversity gain does not depend only on the rainfall rate statistics; there are additional parameters that influence it. One such parameter we suspected is the time correlation coefficient of rainfall. To confirm our hypothesis and obtain greater accuracy, we plan to use a larger number of observation points in Japan and more precisely consider the time correlation coefficient; this will be addressed in subsequent studies. Moreover, the time diversity method that includes the time diversity gain prediction can be adopted for use in any location by using local rainfall rate statistics and can also be applied to any frequency band.

References of Chapter 3

- [1] E. Matricciani, “Time Diversity in Satellite Links Affected by Rain: Prediction of the Gain at Different Localities,” *Proc. European Conference on Antennas and Propagation (EuCAP)*, 2007.
- [2] H. Fukuchi, T. Saito, T. Shimomai and T. Kozu, “Time Diversity Method Evaluated by Rainfall Rate in Tropical Asian Region,” *Proc. AIAA Int. Comm. Satellite Systems Conf. (ICSSC)*, 2007.
- [3] C. Capsoni, M. D’Amico and R. Nebuloni, “Performance of Time-Diversity Satellite Communication Systems Investigated Through Radar Simulation,” *Proc. European Conference on Antennas and Propagation (EuCAP)*, 2007.
- [4] S. L. Jong, M. D. Amico, J. Din and H. Y. Lam, “Performance of Time Diversity Technique in Heavy Rain Region,” *Proc. Int. Symp. Antennas. Propag. (ISAP)*, pp. 575-576, 2014.
- [5] ITU-R, “Characteristics of precipitation for propagation modelling,” *Recommendation*, P.837-6, 2012.
- [6] J. S. Mandeep, “Fade duration statistics for Ku-band satellite links,” *Advances in Space Research*, vol. 52(3), pp. 445-450, 2013.

- [7] E. Matricciani, "Prediction of fade durations due to rain in satellite communication systems," *Radio Sci.*, vol. 32, pp. 935-941, 1997.
- [8] C. Amaya and T. Nguyen, "Fade Duration and Fade Slope Statistics Derived from Long-Term Anik-F2 Satellite Beacon Measurements in Ottawa-Canada," *Proc. General Assembly and Scientific Symposium*, 2011.
- [9] E. Matricciani, "Rate of change of signal attenuation from SIRIO at 11.6 GHz," *Electron. Lett.*, vol. 17, no. 3, pp. 139-141, 1981.
- [10] E. Matricciani, "Effects of filtering on rate of change of rain-induced attenuation," *Electron. Lett.*, vol. 18, no. 11, pp. 477-478, 1982.
- [11] M. M. J. L. van de Kamp, "Statistical analysis of rain fade slope," *IEEE Trans. Antennas Propag.*, vol. 51, no. 8, pp. 1750-1759, 2003.
- [12] F. Rucker, "Frequency and attenuation dependent fade slope statistics," *Electron. Lett.*, vol. 29, pp. 744-746, 1993.
- [13] B. Nelson and W. L. Stutzman, "Fade slope on 10 to 30 GHz earth-space communication links- measurements and modelling," *IEE Proc. Microw. Antennas Propag.*, vol. 143, no. 4, pp. 353-357, 1996.
- [14] K. I. Timothy, J. T. Ong and E. B. L. Choo, "Descriptive fade slope statistics on INTELSAT Ku-band communication link," *Electron. Lett.*, vol. 36, no. 16, pp. 1422-1424, 2000.
- [15] J. Feil, L. J. Ippolito Jr., H. Helmken, C. E. Mayer, S. Horan and R. E. Henning, "Fade slope analysis for Alaska, Florida and New Mexico ACTS propagation data at 20 and 27.5 GHz," *Proc. IEEE*, vol. 85, no. 6, pp. 926-935, 1997.

- [16] T. Maseng and P. M. Bakken, "A stochastic dynamic model of rain attenuation," *IEEE Trans. Commun.*, vol. COM-29, no. 5, pp. 660-669, 1981.
- [17] D. G. Sweeney and C. W. Bostian, "The dynamics of rain-induced fades," *IEEE Trans. Antennas Propag.*, vol. 40, no. 3, pp. 275-278, 1992.
- [18] W. Liu and D. G. Michelson, "Fade slope analysis of Ka-band earth-LEO satellite links using a synthetic rain field model," *IEEE Trans. Vehicular Tech.*, vol. 58, no. 8, pp. 4013-4022, 2009.
- [19] H. Dao, MD. R. Islam and K. AL. Khateeb, "Modification of ITU-R rain fade slope prediction model based on satellite data measured at high elevation angle," *IJUM Engineering Journal*, vol. 12, no. 5, pp. 53-59, 2011.
- [20] Z. Xin, Z. Zhenwei, L. Leke and L. Changsheng, "Rain fade slope on 12.5 GHz earth-space link at Qingdao," *Proc. Int. Conf. Microwave and Millimeter Wave Tech. (ICMMT)*, 2012.
- [21] R. K. Crane, "Modelling Attenuation by Rain in Tropical Regions," *Int. J. Satell. Commun. Network.* 1990; **8**:197-210. doi:10.1002/sat.4600080312.
- [22] ITU-R, "Prediction method of fade dynamics on Earth-space paths," *Recommendation*, P.1623, 2003.
- [23] C. Capsoni, M. D'Amico and R. Nebuloni, "Radar Simulation and Physical Modeling of Time Diversity Satellite Systems," *Radio Sci.*, vol. 44, 2009.

- [24] Y. Abayomi I.O and N. Hisham H. K, “Rain Attenuation Modelling and Mitigation in the Tropics,” *Int. Journal of Electrical and Computer Engineering (IJECE)*, vol. 2, no. 6, pp. 748-757, 2012.
- [25] S. Nakazawa, S. Tanaka and K. Shogen, “A Method to Transform Rainfall Rate to Rain Attenuation and its Application to 21GHz Band Satellite Broadcasting,” *Proc. Int. Symp. Antennas. Propag. (ISAP)*, pp. 1386-1389, 2007.
- [26] Badron K, Ismail AF, Islam MR, Sbdullah K, Din J and Tharek AR, “A modified rain attenuation prediction model for tropical V-band satellite earth link,” *Int. J. Satell. Commun. Network*. 2015; **33**:57-67. doi:10.1002/sat.1071.
- [27] D. Lakanchanh, A. Datsong, N. Leelaruji and N. Hemmakorn, “Rainfall Rate and Rain Attenuation in Ku-Band Satellite Signal in Thailand and Laos,” *SICE-ICASE Int. Joint Conf.*, pp. 3928-3932, 2006.
- [28] Y. Abdulrahman, T. A. Rahman, S. K. A. Rahim and M. R. Ul Islam, “A New Rain Attenuation Conversion Technique for Tropical Regions,” *Progress In Electromagnetics Research B*, vol. 26, pp. 53-67, 2010.
- [29] V. Ramachandran and V. Kumar, “Modified Rain Attenuation Model for Tropical Regions for Ku-Band Signals,” *Int. J. Satell. Commun. Network*. 2007; **25**:53-67. doi:10.1002/sat.846.
- [30] J. S. Mandeep, S. I. S. Hassan and M. F. Ain, “Rain Rate Conversion for Various Integration time for Equatorial and Tropical Climates,” *Int. J. Satell. Commun. Network*. 2008; **26**:329-345. doi:10.1002/sat.918.

- [31] ITU-R, “Specific attenuation model for rain for use in prediction methods,” *Recommendation*, P.838-3, 2005.
- [32] ITU-R, “Rain height model for prediction methods,” *Recommendation*, P.839-4, 2013.
- [33] J. X. Yeo, Y. H. Lee and J. T. Ong, “Rain Attenuation Prediction Model for Satellite Communications in Tropical Regions,” *IEEE Trans. Antennas Propag.*, vol. 62, no. 11, pp. 5775-5781, 2014.
- [34] A. Dissanayake, J. Allnutt and F. Haidara, “A Prediction Model That Combines Rain Attenuation and Other Propagation Impairments Along Earth Satellite Paths,” *IEEE Trans. Antennas Propag.*, vol. 45, no. 10, pp. 1546-1558, 2014.
- [35] D. Y. Choi, J. Y. Pyun, S. K. Noh and S. W. Lee, “Comparison of Measured Rain Attenuation in the 12.25 GHz Band with Predictions by the ITU-R Model,” *Int. J. Antennas Propag.*, 2012.
- [36] Surat K. K, Vijaya B. R. S and D N. Rao, “Prediction of Ku Band Rain Attenuation Using Experimental Data and Simulations for Hassan India,” *Int. Journal of Computer Science and Network Security (IJCSNS)*, vol. 8, no. 4, pp. 10-15, 2008.
- [37] C. Capsoni, L. Luini, A. Paraboni, C. Riva and A. Martellucci, “A New Prediction Model of Rain Attenuation That Separately Accounts for Stratiform and Convective Rain,” *IEEE Trans. Antennas Propag.*, vol. 57, no. 1, pp. 196-204, 2009.
- [38] R. K. Crane, “Modelling Attenuation by Rain in Tropical Regions,” *Int. J. Satell. Commun. Network.* 1990; **8**:197-210. doi:10.1002/sat.4600080312.

Chapter 4

Adaptive Satellite Power Control

Method

4.1 Concept and System Configuration

Regarding satellite communication in higher frequency bands [1][2], such as the Ku- and Ka-bands, rainfall has a much greater effect on satellite propagation paths, both from the gateway to the satellite and from the satellite to the users. For this reason, adaptive satellite power control [3] using power boost beams is proposed to maintain the satellite potential, as shown in Figure 4.1. The boost beam can be used in areas that experience difficulties from rain attenuation. In this method, precipitation is observed and predicted several hours before rainfall occurs in a given area using changes in the rain radar pattern. This information is also shared with all involved. If the rainfall rate reaches a point at which communication becomes unreliable, gateways or base stations take command of the satellite to increase the power in the affected areas. The power boost is varied in real time according to the effect of the current rainfall.

For areas in Japan, the designed boost beam sizes are 50, 100, 150, and 200 km (effective areas on ground). Because these boost beam sizes correspond to the diameters of the antennas in the 22 GHz band [4], the antenna size range was calculated between 2 to 10 m which can cover our beam sizes proposed.

In this study, a phased array antenna is considered because it can make several boost beams within wide beam by controlling the phase of the signal emitted from each radiating element as proposed in reference [5]. In preliminary analysis, we used one to four beams because in Japan, the probability that the number of simultaneous peaks in the rainfall rate or impacted areas exceeds this number is small. Therefore, one to four beams are sufficient to compensate for rain attenuation in Japan. However, if rain occurs over a wide area, we also use four different beam sizes as appropriate for such areas. In this simulation, the position of the local maximum rainfall rate in Japan is determined, and the boost beam center is then set to be located at the peak rainfall rate position. The boost areas are assumed to be square regions with side lengths equal to the beam sizes, i.e., 50 km \times 50 km, 100 km \times 100 km, 150 km \times 150 km, and 200 km \times 200 km. When more than one beam is used, the next peak rainfall rate is continuously searched for. As mentioned above, it is assumed that there are no simultaneously impacted areas, and thus we set our simulation to not allow the overlapping of boost areas because we do not want to waste boost power. To prevent beam collision, this system setup includes a guarded area, which is a square region with sides half the beam size in which the subsequent beam center cannot be positioned. The next peak rainfall rate is then searched outside the guarded area

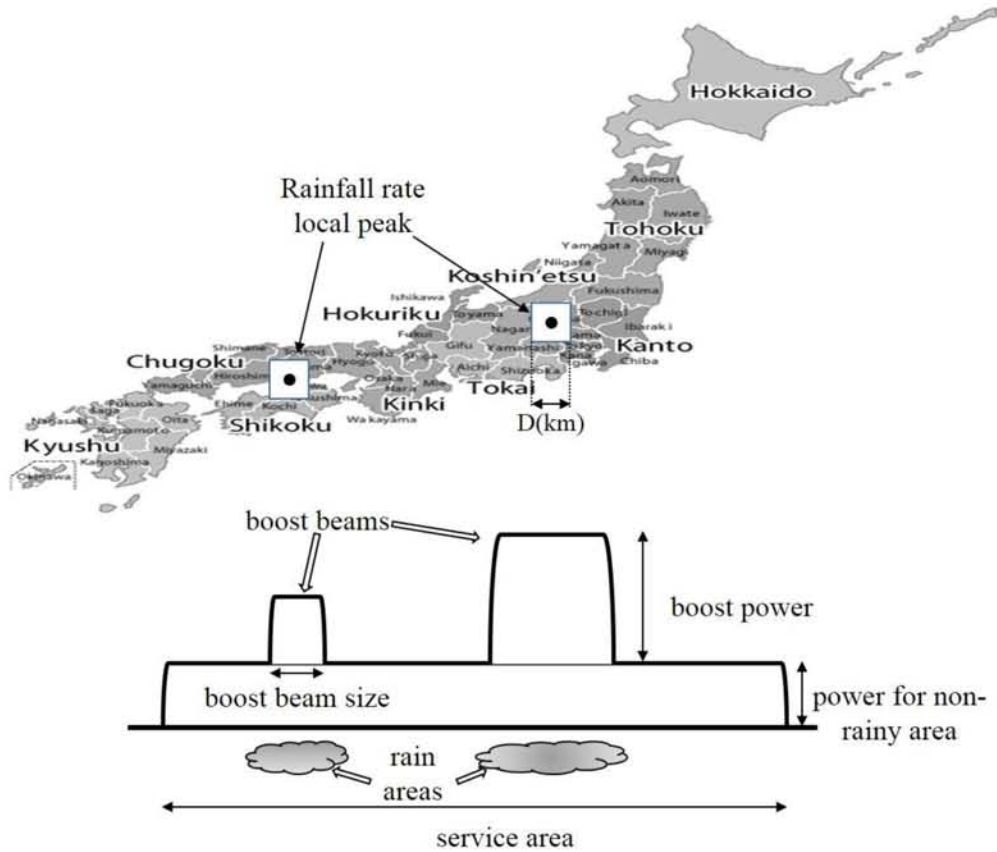


Figure 4.1: Attenuation mitigation using boost beam concept.

4.2 Rain Rate Observation and Simulation Parameters

The boost beam simulations in this study were performed using rain radar data collected throughout Japan by the Japan Meteorological Agency (JMA). Rain radar data are collected at time intervals of 5 min and at the mesh points of a grid of approximately 1 km that covers the whole of Japan. However, the main areas of Japan are covered by 1481×1921 matrices, excluding the southern island, the data of which are extracted from original JMA 2560×3360 matrices of radar coverage. The rainfall intensity was derived from radar precipitation maps, and the data were calibrated using surface rain gauge observation data from over 1,300 stations throughout Japan. The data used in this study were collected over four years starting in

July 2009. Basically, the overall image of the rainfall for all considered data is derived using a cumulative distribution function. This procedure is shown in Figure 4.2. The parameters used for the simulation were as follows.

- Rain radar data collection period: July 2009 to June 2013
- Boost beam sizes: 50, 100, 150, and 200 km
- Boost beam numbers: 1, 2, 3, and 4
- Boost amount (fixed): 20 mm/h
- Boost point searching: Local maximum rain intensity
(Boost beam overlap was not allowed.)

To indicate the number of beams and their size in each case considered in this study, “case n - m ” is hereafter used to refer to a case with n boost beams and a beam size given by m , where 1, 2, 3, and 4 correspond to beam sizes of 50, 100, 150, and 200 km, respectively.

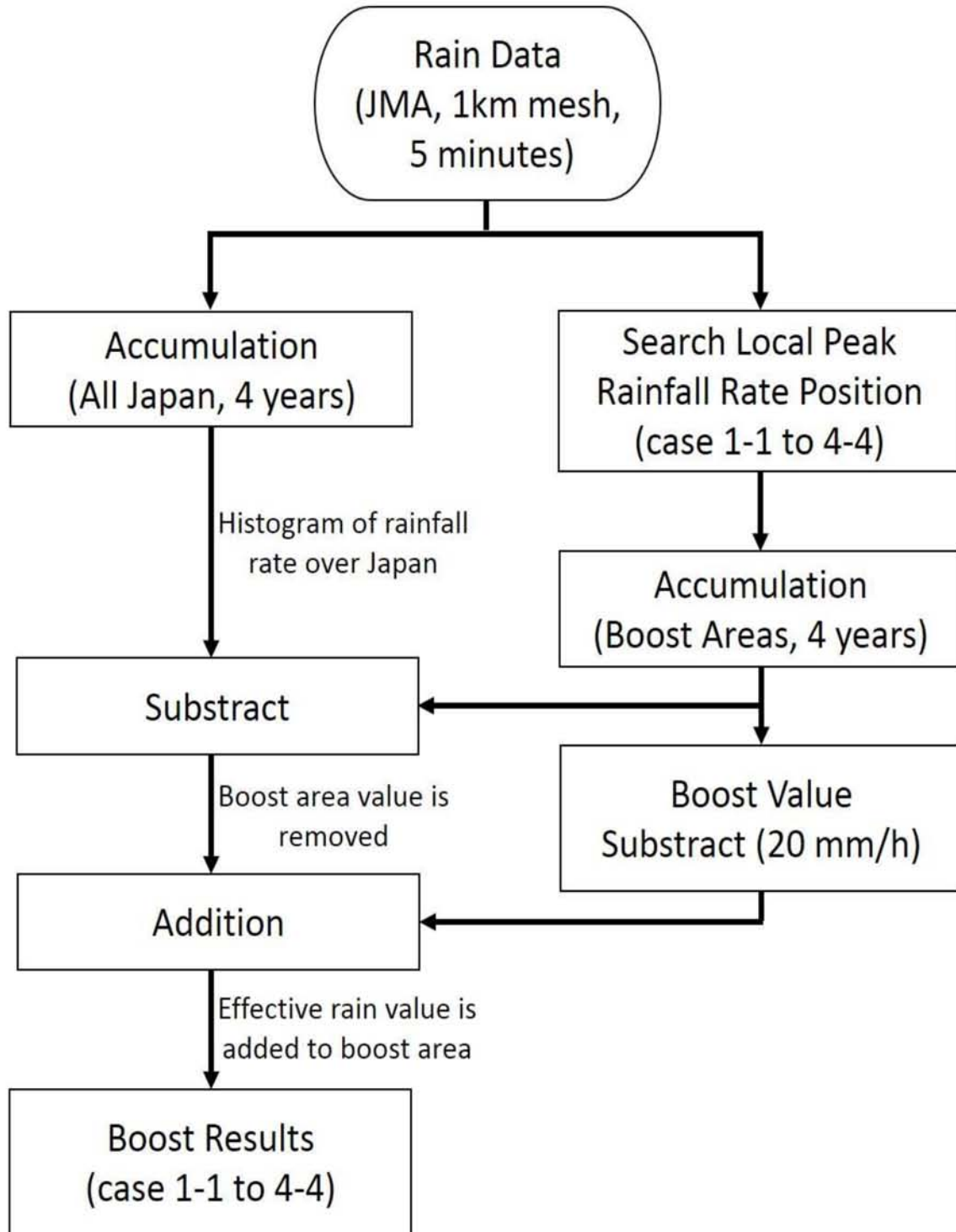


Figure 4.2: Analysis flow.

4.3 Simulation Results

4.3.1 Boost Beam Efficiency

ITU-R recommendation P.618-12 concerns rainfall rate values at cumulative time percentages (P) of 0.1% and 0.01%, which correspond to 99.9% and 99.99% service availability throughout the year, respectively. On the other hand, the cumulative time percentages of 0.1% and 0.01% means acceptance agreement of the outage times between satellite regulator and satellite operator for the effective usage. For instance, $P = 0.1\%$ equal to 525.6 minutes and $P = 0.01\%$ equal to 52.56 minutes outage times throughout the year, respectively. Moreover, rainfall rate at $P = 0.01\%$ has been used to calculate link budget for C-band and Ku-band, but due to much more rain attenuation impacts in Ka-band, rainfall rate at $P = 0.1\%$ is also useful value. In this paper, we proposed both consideration on rainfall rate values at 0.1% and 0.01%. Figure 4.3 shows the rain intensity derived from rain radar data collected throughout Japan over four years at intervals of 5 min.

The rainfall rate data derived from the radar data available in Japan at 5-min intervals contains some areas that cannot be observed because of radar wave obstructions, such as mountainous areas; however, the data for these areas are not used in this analysis.

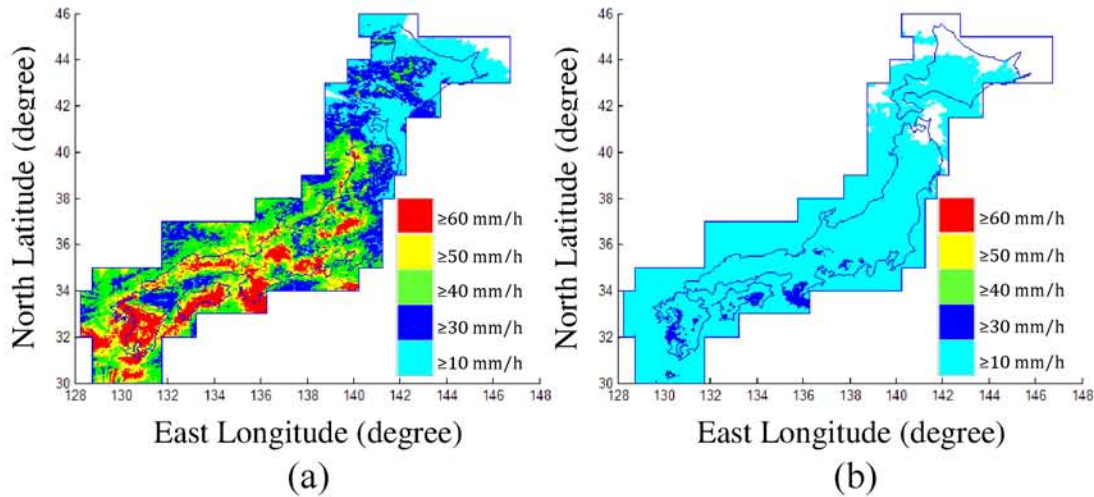


Figure 4.3: Rain intensity for cumulative time percentage of (a) 0.01% and (b) 0.1%

Figure 4.3 illustrates the observed rain intensity within the border that represents the coverage of mainland Japan, which has been calibrated except over the ocean. The color scale represents different rainfall rate levels; red, yellow, green, blue, and cyan correspond to regions where rainfall rates were equal to or exceeded 60, 50, 40, 30 and 10 mm/h, respectively. These divisions were adopted based on the fact that the largest rain intensity (≥ 60 mm/h), which most commonly occurred in the south and along the east coast of Japan, was observed only for $P = 0.01\%$ and that rainfall rates under 30 mm/h covered almost the entirety of Japan for $P = 0.1\%$. Moreover, the rainfall rates that occurred in the northern areas were quite small: 10–40 mm/h for $P = 0.01\%$, and 0–10 mm/h for $P = 0.1\%$. In addition, no rainfall occurred in some areas. As a result, the north of Japan has suffered little from rain attenuation, and there is likely no need for power boosting in these areas.

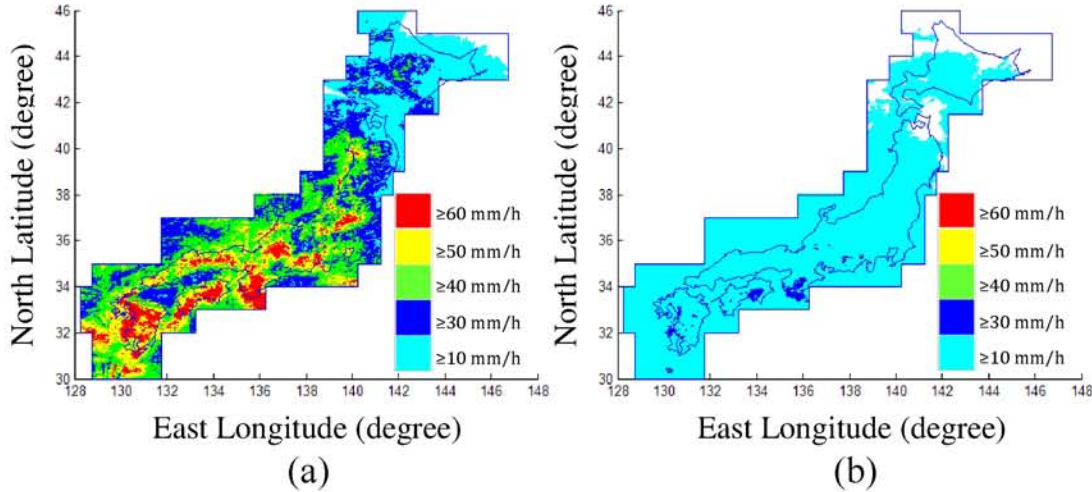


Figure 4.4: Rain intensity for case 1-1 with cumulative time percentage of
(a) 0.01% and (b) 0.1%

In this study, the effective rain intensity was evaluated with a constant boost beam of 20 mm/h. A power backup for reduce the rainfall rate effects up to 20 mm/h is sufficient and may be used for the adaptive power control method in areas of Japan. Examples of all boost beam simulation results of are shown in Figures 4.4 and 4.5. These results illustrate the reduction in the rain intensity in the maximum (case 4-4) and minimum (case 1-1) boost cases, as explained below. The maximum case, shown in Figure 4.5, used four beams with a boost beam diameter of 200 km; as explained in Section 4.1, this is referred to as case 4-4. Conversely, the minimum case, shown in Figure 4.4, used one beam with a boost beam diameter of 50 km; this is referred to as case 1-1. Both cases also show the effective rainfall rates for cumulative time percentages of 0.01% and 0.1% considering the importance of the satellite link design.

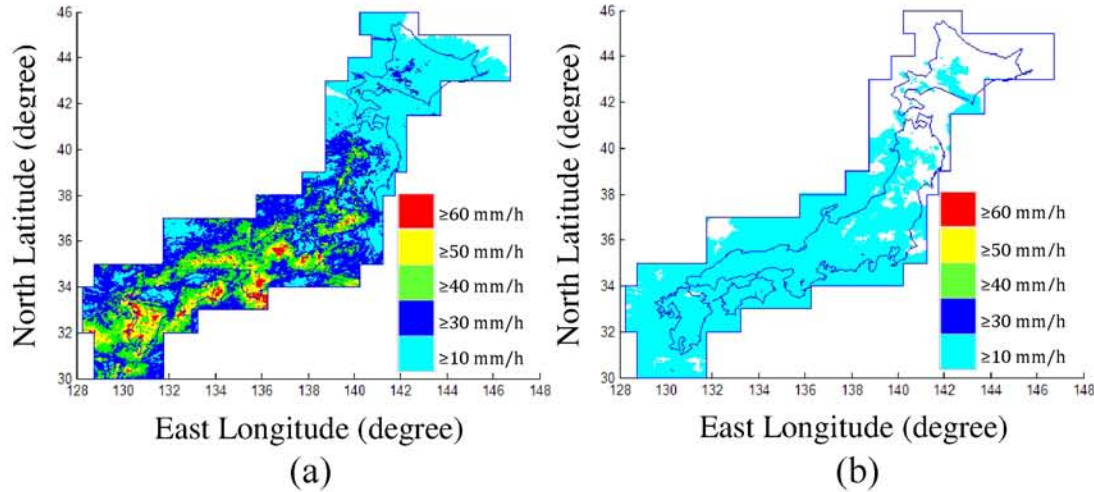


Figure 4.5: Rain intensity for case 4-4 with cumulative time percentage of
(a) 0.01% and (b) 0.1%

To describe the situation in greater detail, case 1-1 is represented by a boost area equivalent to $1 \times 50 \text{ km} \times 50 \text{ km} = 2500 \text{ km}^2$. Additionally, case 4-4 is represented by a total boost area equivalent to $4 \times 200 \text{ km} \times 200 \text{ km} = 160,000 \text{ km}^2$, which means that the total boost area in case 4-4 is approximately 64 times larger than that of case 1-1. These effective rain intensity features indicate that the effect of rain attenuation is reduced by the decrease in the rain intensity, particularly in areas that experience severe rain and nearby areas.

There are some cases which have the same effective areas such as 1-4 and 4-2 cases which have $40,000 \text{ km}^2$. Figure 4.6 shows rain intensity both cases 1-4 (a) and 4-2 (b) only for cumulative time percentage of 0.01% to consider the reduction of rain intensity, it is shown that the reduction of rain intensity of case 4-2 is clearly improved than case 1-4.

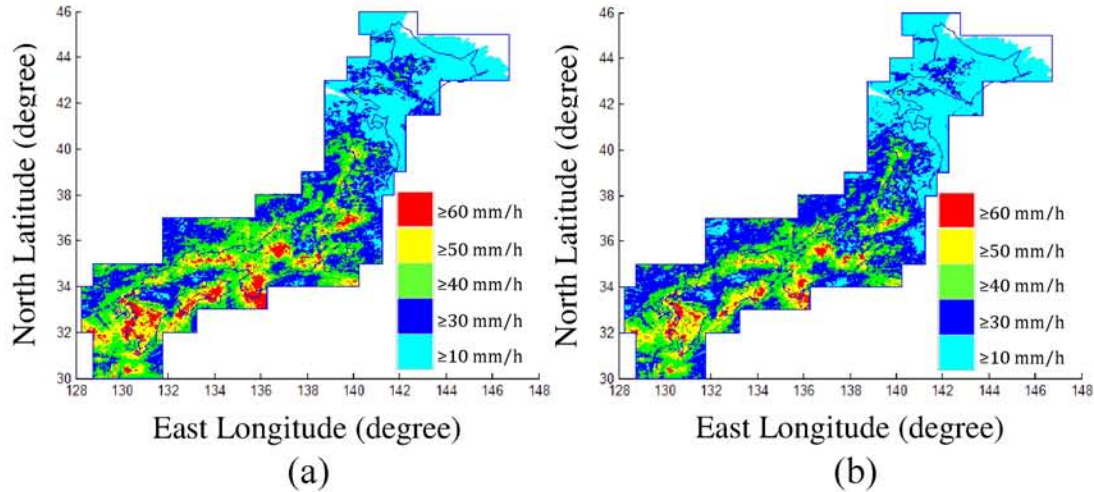


Figure 4.6: Rain intensity for cumulative time percentage of 0.01% with (a) case 1-4 and (b) case 4-2

4.3.2 Effective Rainfall Rate Reduction Factor throughout

Japan

The effective rainfall rate reduction factor (ERF) is expressed as the difference between the effective rainfall rate in the case where no power boost is applied and that in each case where a boost is applied in cumulative distribution. The ERFs throughout Japan are shown in Figures 4.7 - 4.10 with respect to the rainfall rate without a boost (mm/h). The scatterplots were obtained in all places for cases 1-1 (minimum), 4-4 (maximum), 1-4 and 4-2 (same effective areas). These figures show the density of places as a histogram with different colors representing the number of places at which the ERF is equal to a given value. Specifically, black, red, green, and cyan represent cases in which the number of places is at least 1000, 500, 100, and 1 places, respectively. The slope of the black data points indicates the significant increase in the ERF. In case 4-4, this slope is the highest in comparison with other cases; this means that most areas are boosted.

Conversely, most places receiving a boost in case 1-1 have maximum ERFs of approximately 4 mm/h because in the majority of the areas experiencing rainfall at a rate of 30-60 mm/h, the signal reception is not corrected when one boost beam is applied. This is because the boost beam prioritizes the areas with a maximum rainfall rate of nearly 100 mm/h. For deeper consideration, this scatterplot is limited by the provided boost amount, and for the value of 20 mm/h used in this paper, there are no boosted places that can achieve a gain exceeding 20 mm/h. Furthermore, the observation results shown in Figures 4.7 - 4.10 indicate that the degree of improvement of the ERF in most places is better following the increase in the boost area. The ERFs in all other boost cases considered in this study (cases 1-2 to 4-3) are similarly improved.

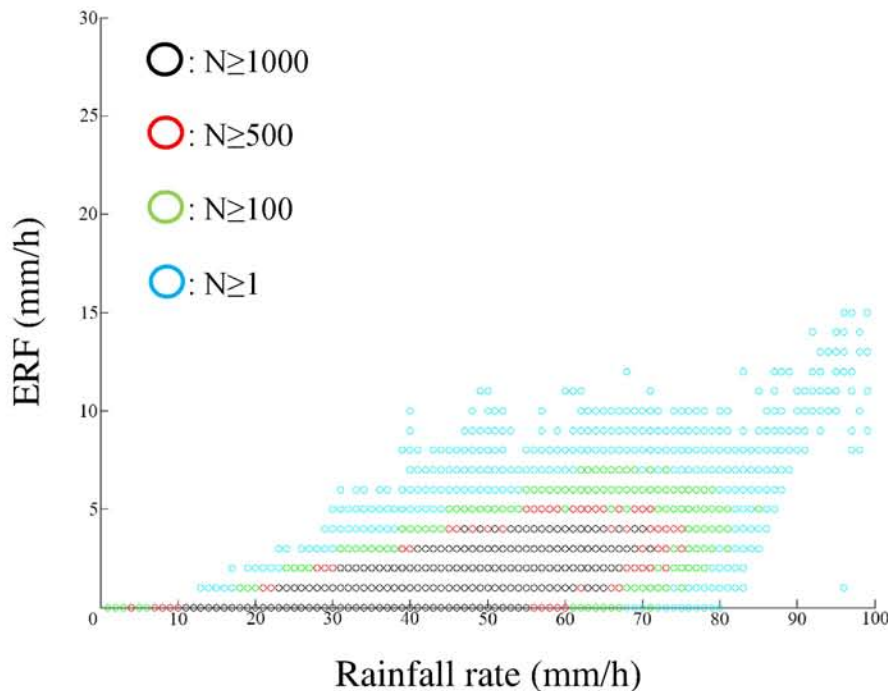


Figure 4.7: ERFs in case 1-1 for a constant boost beam of 20 mm/h at a cumulative time percentage of 0.01%.

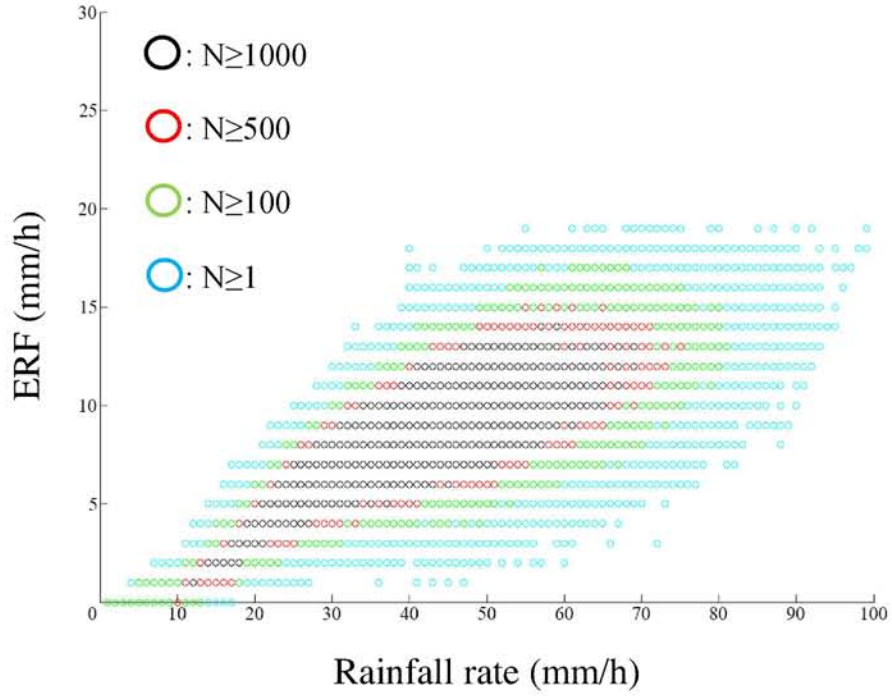


Figure 4.8: ERFs in case 4-4 for a constant boost beam of 20 mm/h at a cumulative time percentage of 0.01%.

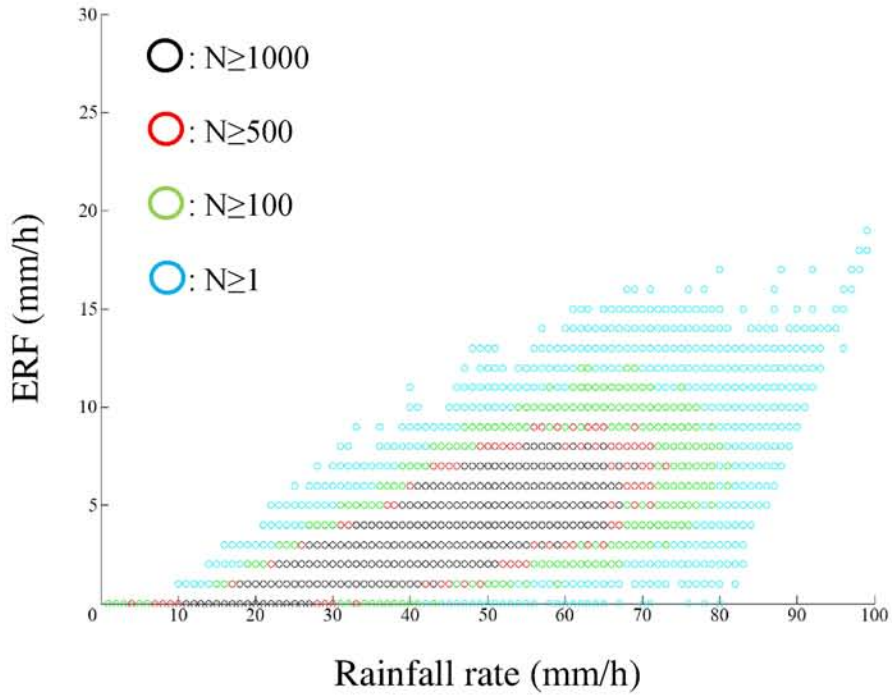


Figure 4.9: ERFs in case 1-4 for a constant boost beam of 20 mm/h at a cumulative time percentage of 0.01%.

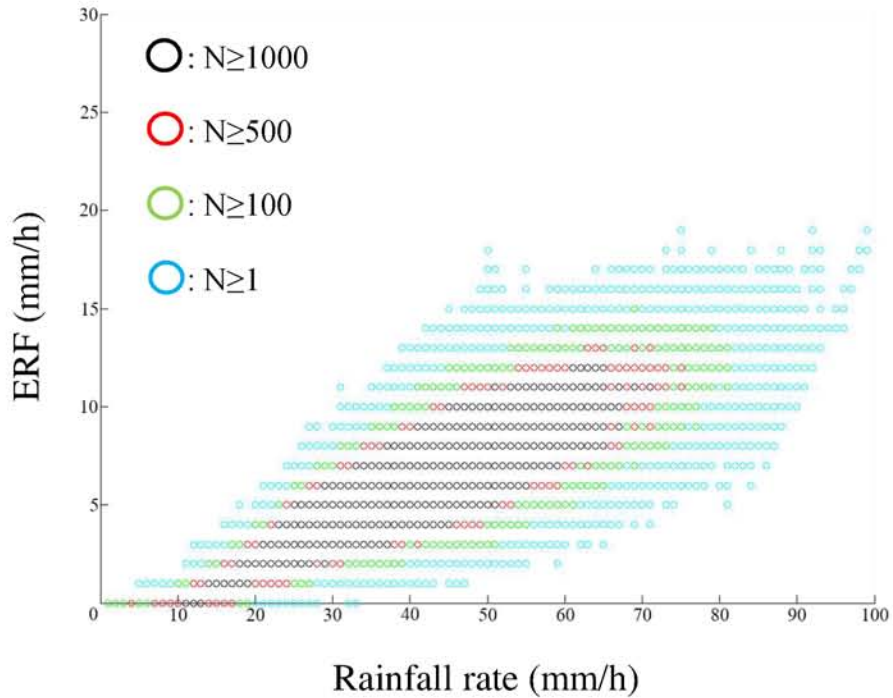


Figure 4.10: ERFs in case 4-2 for a constant boost beam of 20 mm/h at a cumulative time percentage of 0.01%.

However, Figures 4.9 and 4.10 show the scatterplots of ERF versus rainfall rate for cases 1-4 and 4-2 those have the same effective areas. The slope of the most boosted areas in case 4-2 is higher than case 1-4. It is evidence that case 4-2 can reduce the effect of rain more than case 1-4.

4.3.3 ERF and Boost Parameters

Using the ERF results described in the previous section, Figures 4.11 and 4.12 summarize the place dependence of the observed effective rain rate for approximately 729,700 places located throughout Japan using a cumulative place percentage. These results show the place percentage with respect to the effective rainfall rate at a cumulative time percentage of 0.01%. Figure 4.11 shows the results obtained using one boost beam for each considered boost

beam size (cases 1-1, 1-2, 1-3, and 1-4), and Figure 4.12 shows the results obtained using four boost beams for each considered beam size (cases 4-1, 4-2, 4-3 and 4-4). In the cases using one beam, the trends were somewhat improved in comparison with the case where no boost was applied. In the same manner, in the cases using four beams, a clear improvement was observed.

Figure 4.13 shows the boost gain with respect to the effective area in each boost case at cumulative time percentages of 0.01% and 0.1%; these data were collected for a cumulative place percentage of 50%. The ERFs ranged from approximately 2 to 10 mm/h in each boost area analyzed under a constant boost power of 20 mm/h. For example, the maximum ERF in case 4-4 was 9.47 mm/h, whereas the minimum ERF in case 1-1 was approximately 1.46 mm/h, both of these cases correspond to a cumulative time of 0.01%.

These results demonstrate that cases 1-4 and 4-2 have the same boost areas but different boost gains [6]. Case 1-4 has a ERF of approximately 4.04 mm/h, and case 4-2 has ERF of approximately 7 mm/h for the same effective area of 40,000 km². This difference in boost gain indicates that the performance of boost beams is more effective when more boost beams are used than when a larger beam size is used. This is due to that the dispersion of rainfall rates in larger boost beam is much bigger than that in smaller boost beam.

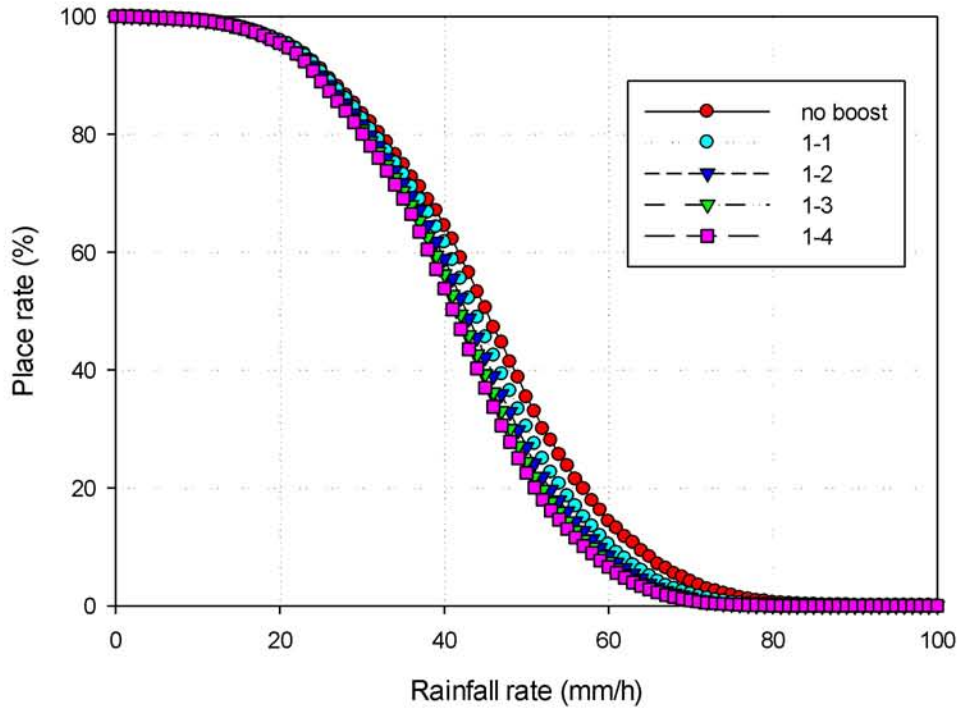


Figure 4.11: Cumulative place percentage in case 1-m.

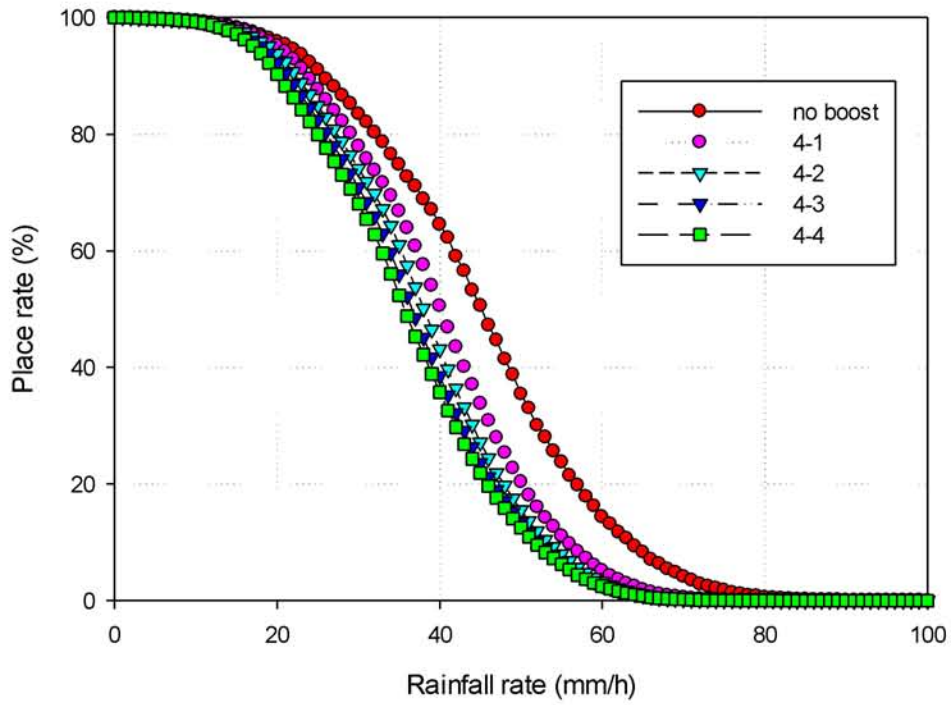


Figure 4.12: Cumulative place percentage in case 4-m.

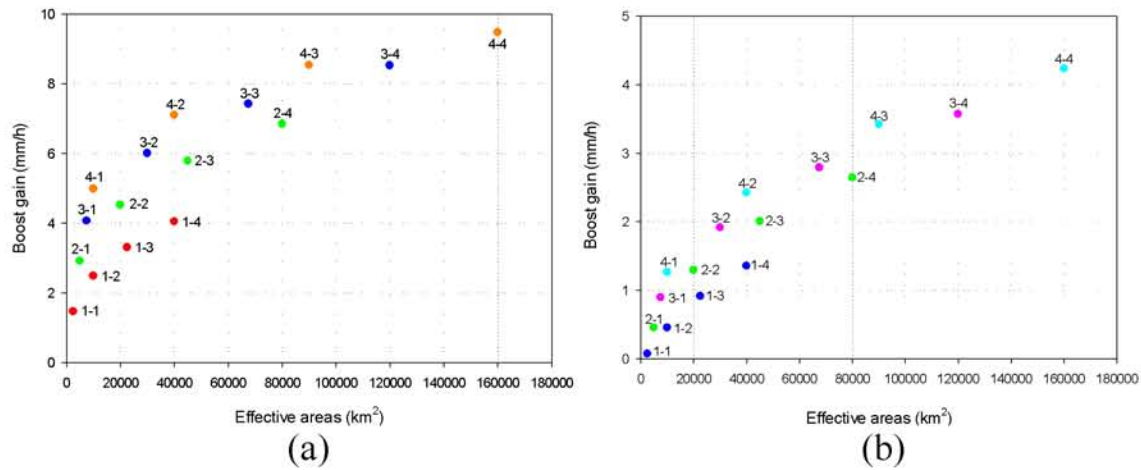


Figure 4.13: EFRs for cumulative time percentages of (a) 0.01% and (b) 0.1%

4.4 Summary of Chapter 4

In this Chapter, rain radar data were used to evaluate the performance of adaptive satellite power control for use in future satellite communication. Customized for areas of Japan using the Ka-band and higher frequency bands, the proposed boost beam method was designed to use up to four antennas of different beam sizes to ensure the coverage of areas severely affected by rain. Furthermore, we used a fixed boost value of 20 mm/h, because the maximum rain intensity at a cumulative time percentage of 0.01% is relatively low in Japan compared with that in the tropical region.

The boost beam simulation results are useful in the prediction of the power compensation required to reinstate functioning communication capabilities in areas experiencing severe rainfall. For each boost case considered in this study, varying the number of beams and the beam size, the cumulative distributions of the rain intensity for cumulative time percentages of 0.1% and 0.01% were observed following the ITU recommendation.

Scatterplots of the ERF results revealed largely boosted areas can be increased by increasing number and size of beams. Finally, dependence of the boost beam design on the target topography and climate was investigated.

In addition, the boost beam method can be used to improve satellite communication services not only in the case of rain attenuation but also in areas struck by natural disasters [7] to maintain the area's satellite connection to other areas in order to ask for help or to boost power to congested areas that require more power.

References of Chapter 4

- [1] M. Umehira, K. Kobayashi, Y. Yasui, M. Tanaka, R. Suzuki, H. Shinonaga and N. Kawai, "Recent Japanese R&D in Satellite Communications," *IEICE Trans. Commun.*, vol. E92-B, no. 11, pp. 3290-3299, 2009.
- [2] H. J. Lee, J. M. Kim, B. S. Lee, H. Lee and J. S. Ryoo, "Recent Korean R&D in Satellite Communications," *IEICE Trans. Commun.*, vol. E92-B, no. 11, pp. 3300-3308, 2009.
- [3] A. Paraboni, M. Buti, C. Capsoni, D. Ferraro, C. Riva, A. Martellucci and P. Gabellini, "Meteorology-Driven Optimum Control of a Multibeam Antenna in Satellite Telecommunications," *IEEE Trans. Antennas Propag.*, vol. 57, pp. 508-519, 2009.
- [4] S. Nakazawa, M. Nagasaka and S. Tanaka, "A Method to Estimate Outage for 21-GHz Band Satellite Broadcasting System," *Int. Symp. Elec Theory (IEICE)*, pp. 314-317, 2013.
- [5] M. Kamei, S. Nakazawa, S. Tanaka and K. Shogen, "Research for the Introduction of the 21GHz-band Satellite Broadcasting in Japan," *Proc. Int. Symp. Space Tech Sci. (ISTS)*, 2011.

- [6] P. Chodkaveekityada and H. Fukuchi, “On-broad Adaptive Attenuation Compensation Technique for Future Satellite Communication,” *Proc. Int. Symp. Antennas Propag. (ISAP)*, pp. 111-112, 2014.
- [7] N. Kadowaki, T. Takahashi, M. Akioka, Y. Fujino and M. Toyoshima, “Research and Development Issue of Satellite Communications Systems for Large Scale Disaster Relief,” *IEICE Trans. Commun.*, vol. E95-B, no. 11, pp. 3378-3384, 2012.

Chapter 5

Site Diversity Improvement Derived by Rain Gauge Network in Thailand

5.1 Overview

The site diversity concept [1]-[6] is to provide more stations in order to sustain communications with satellite and users when the main station is degraded by rain attenuation, especially in high-frequency bands. The distance between the main site and the diversity site is set as short as possible to reduce unnecessary connection costs. As observed in Thailand, when rain falls on both the main station and the diversity site in the receiving Ku-band, all contents are lost. It is evident that the diversity site is not placed in the appropriate areas to fully avoid the rain attenuation effects. To improve this problem, rain spatial correlation [7]-[9] will become a more significant factor to evaluate rainfall correlation behaviors, such as rainfall rate, distance and

direction dependences. This information can be derived from the precipitation data in each area.

5.2 Rain Gauge Network

This section analyzes the rain gauge network data provided by the Thai Meteorological Department. We selected 12 sites of rain gauges around the center of Bangkok, Thailand, as shown in Figure 5.1. The observed area covered the main and the diversity sites of the satellite operators of Thailand as well. The rain gauge data were available at intervals of every 3 hours. The data considered were the span of four years from 2010 to 2013. Table 5.1 shows the station names and locations of the installed rain gauges. These stations were selected to represent the rain behavior in the center of Thailand by evaluating the spatial correlation between each combination. The total number of combinations was 66.

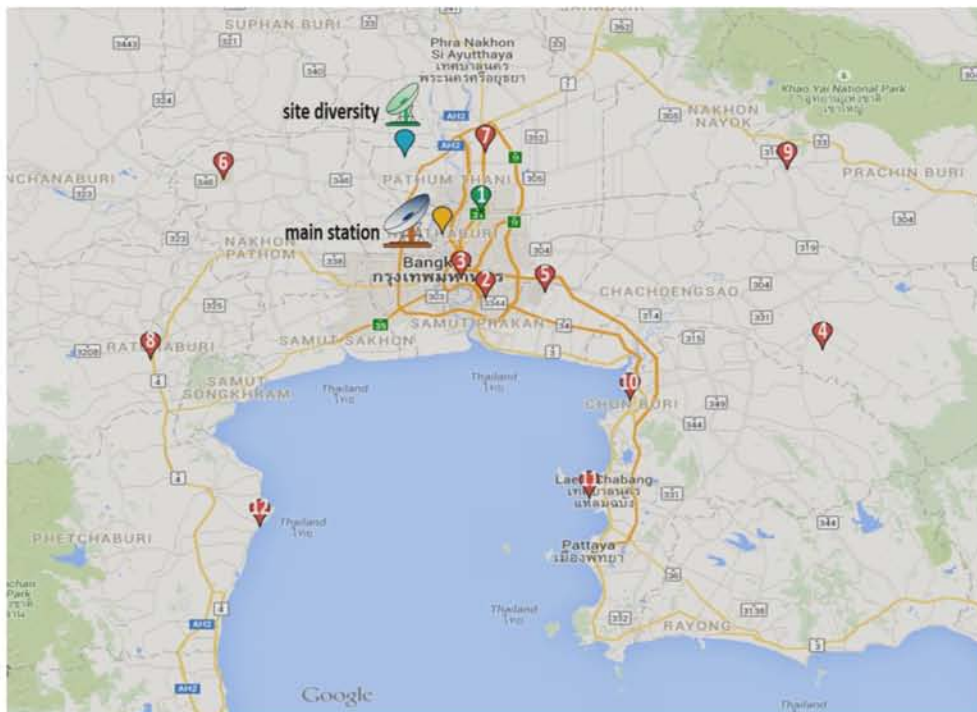


Figure 5.1: Map of locations of rain gauges.

Table 5.1: Site specifications of rain gauges.

Station name	Location (Lat,Long)
1. Donmuang Airport, Bangkok	13.92 N, 100.61 E
2. Bang Na, Bangkok	13.67 N, 100.62 E
3. Bangkok	13.73 N, 100.56 E
4. Chachoengsao	13.52 N, 101.46 E
5. Suvarnabhumi Airport, Samut Prakan	13.69 N, 100.77 E
6. Nakhon Pathom	14.02 N, 99.97 E
7. Pathum Thani	14.10 N, 100.62 E
8. Ratchaburi	13.49 N, 99.79 E
9. Prachin Buri	14.05 N, 101.37 E
10. Chon Buri	13.37 N, 100.98 E
11. Laem Chabang, Chon Buri	13.08 N, 100.88 E
12. Phetchaburi	13.00 N, 100.06 E

5.3 Spatial Correlation Estimation

5.3.1 Spatial Correlation Coefficient

In this analysis, we used the data of the 12 rain gauge stations over 4 years to evaluate the behavior of rainfall and to construct the site diversity formula for Thailand. Basically, we derived the spatial correlation coefficient in Eq. (5.1) to calculate the correlation in each distance for a total of 66 combinations. For example, Figure 5.2 shows a scattergram of rainfall rates between stations no. 1 and no. 2.

$$\rho = \frac{n \sum R_x R_y - (\sum R_x)(\sum R_y)}{\sqrt{n(\sum R_x^2) - (\sum R_x)^2} \sqrt{n(\sum R_y^2) - (\sum R_y)^2}} \quad (5.1)$$

where R is rainfall rate (mm/h), and subscripts x and y are station numbers. The correlation coefficient is calculated when R_x and R_y are both greater than 0 mm/h.

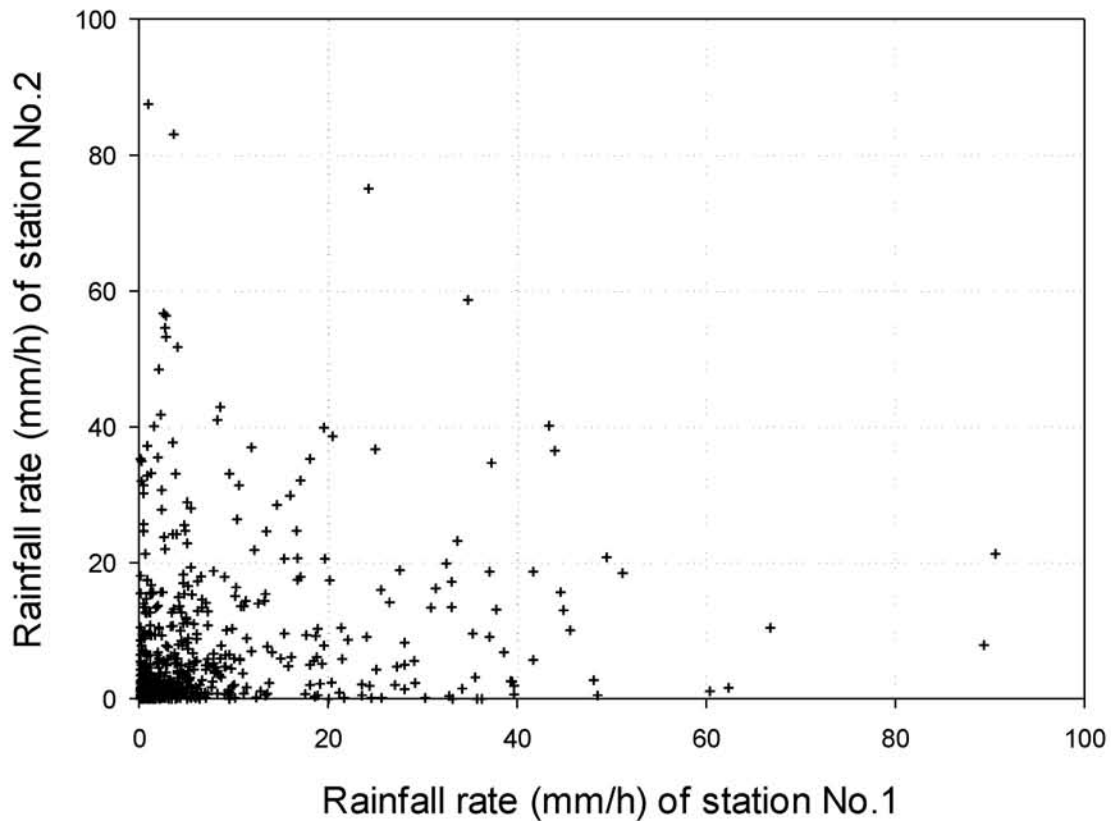


Figure 5.2: Example of rainfall rate scattergram between stations no. 1 and no. 2.

Then, we calculated the distance between two points from the latitude and the longitude of each station's location by using the Haversine formula. The spatial correlation coefficient and the distance are plotted in Figure 5.3. To find the relation between spatial correlation and distance, the conventional formula of distance dependence [7] is used as follows:

$$\rho = e^{-\alpha D^\beta} \quad (5.2)$$

where D is distance (km), and α and β are approximation coefficients of the model. If the correlation is approximated by Eq. (5.2), the relation between $\ln(D)$ and $\ln(-\ln \rho)$ becomes linear.

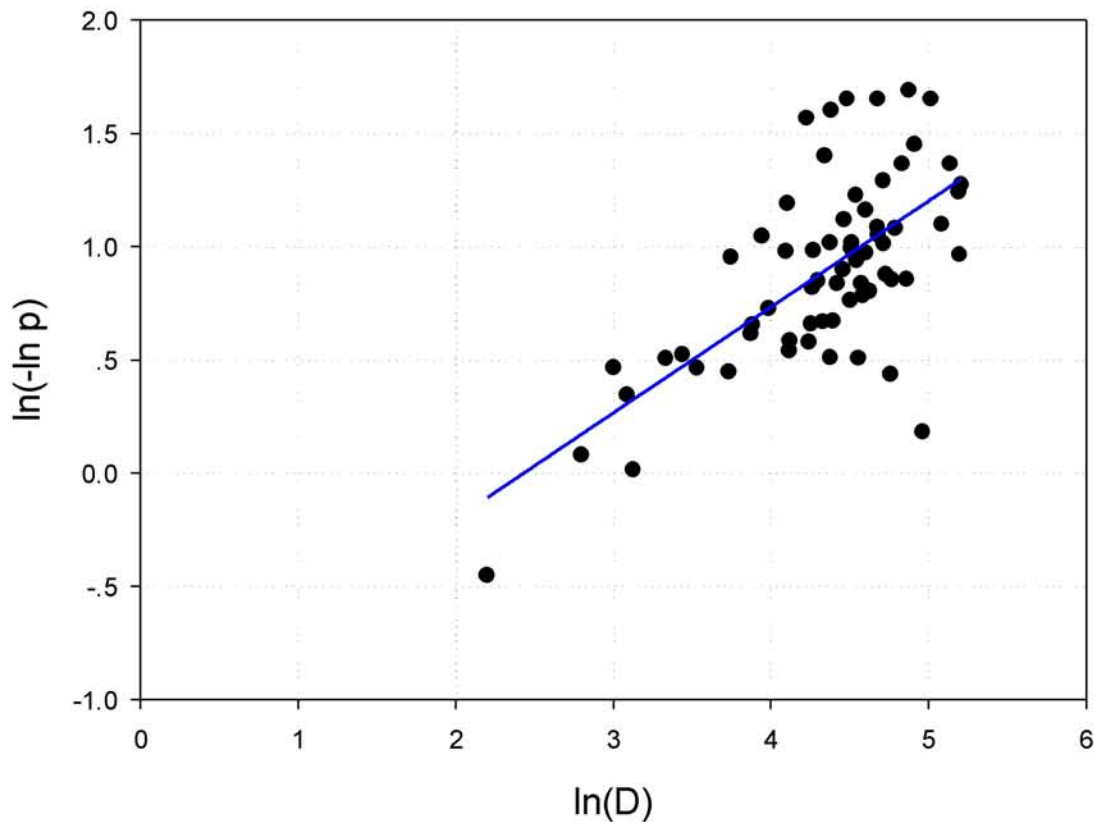


Figure 5.3: Relation of spatial correlation and distance on a linear scale.

A linear regression fitting method is used to estimate the approximation coefficients from Figure 5.3. Here, the approximated value of α is 0.321 and β is 0.468.

In Figure 5.4, the abscissa represents the distance (km) obtained from each pair of rain gauge results and the ordinate represents the spatial correlation. It is normal for the spatial correlation to peak at the same position (0 km) and to decrease as the distance increases. The results in Figure 5.4 show that the conventional formula with our approximation coefficient (solid line) fits well with the spatial correlation from the rain gauges.

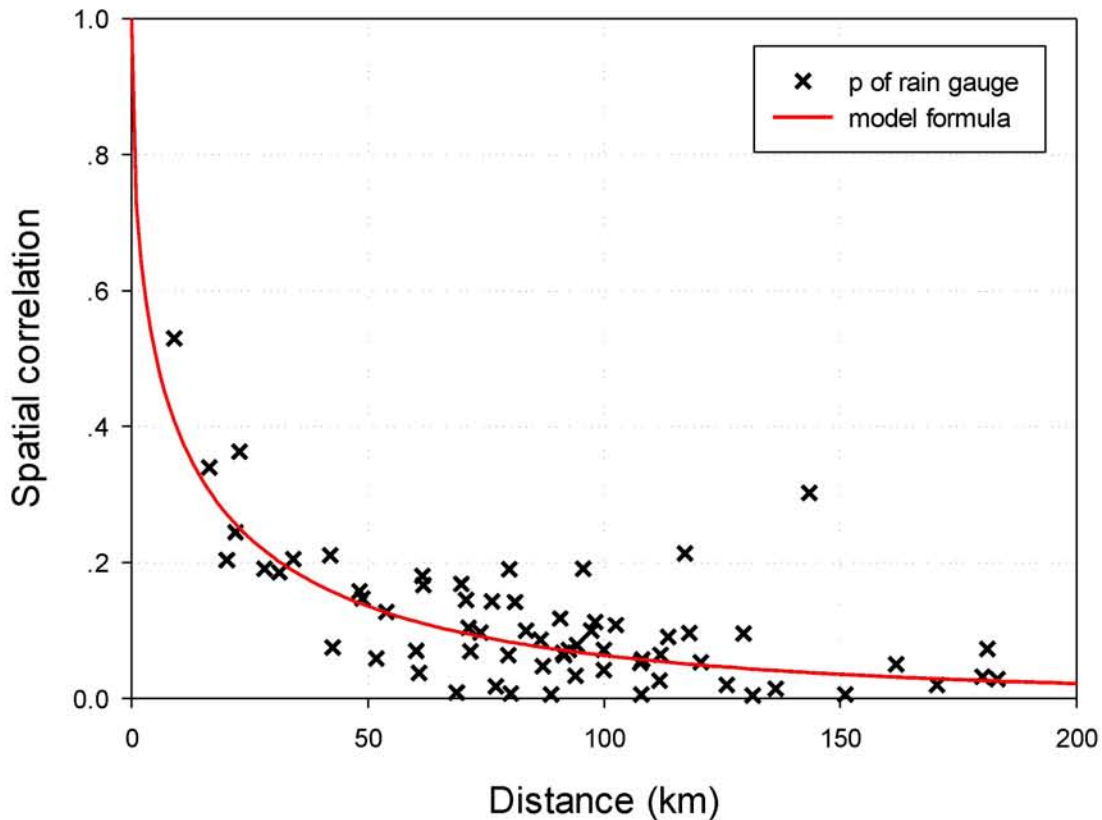


Figure 5.4: Comparison of approximation formula and spatial correlation coefficients of rainfall rates.

Table 5.2: Distance, spatial correlation and azimuth angle parameters.

D (km)	No.	1	2	3	4	5	6	7	8	9	10	11	12
1	1		28.11	21.98	102.52	31.27	69.73	20.15	99.95	83.46	73.79	98.12	118.01
2	2	28.11		9.03	92.51	16.44	80.25	48.18	91.26	91.50	51.81	71.32	95.52
3	3	21.98	9.03		99.87	22.85	71.73	41.99	87.05	94.22	60.78	79.89	97.23
4	4	102.52	92.51	99.87		77.04	170.47	111.73	180.17	60.25	53.97	79.70	161.80
5	5	31.27	16.44	22.85	77.04		93.94	48.79	107.66	76.28	42.53	68.77	108.10
6	6	69.73	80.25	71.73	170.47	93.94		70.72	61.55	151.07	131.45	143.45	113.57
7	7	20.15	48.18	41.99	111.73	48.79	70.72		111.94	81.08	90.65	117.16	136.34
8	8	99.95	91.26	87.05	180.17	107.66	61.55	111.94		181.09	129.55	125.93	61.77
9	9	83.46	91.50	94.22	60.25	76.28	151.07	81.08	181.09		86.54	120.51	183.26
10	10	73.79	51.81	60.78	53.97	42.53	131.45	90.65	129.55	86.54		34.25	107.93
11	11	98.12	71.32	79.89	79.70	68.77	143.45	117.16	125.93	120.51	34.25		88.74
12	12	118.01	95.52	97.23	161.80	108.10	113.57	136.34	61.77	183.26	107.93	88.74	
ρ	No.	1	2	3	4	5	6	7	8	9	10	11	12
1	1		0.191	0.244	0.108	0.185	0.168	0.204	0.071	0.099	0.097	0.112	0.096
2	2	0.191		0.530	0.071	0.340	0.007	0.157	0.067	0.063	0.058	0.104	0.191
3	3	0.244	0.530		0.041	0.363	0.069	0.210	0.047	0.078	0.037	0.190	0.099
4	4	0.108	0.071	0.041		0.017	0.020	0.026	0.032	0.070	0.127	0.063	0.050
5	5	0.185	0.340	0.363	0.017		0.033	0.147	0.052	0.142	0.075	0.008	0.057
6	6	0.168	0.007	0.069	0.020	0.033		0.145	0.180	0.005	0.004	0.302	0.091
7	7	0.204	0.157	0.210	0.026	0.147	0.145		0.064	0.141	0.117	0.213	0.014
8	8	0.071	0.067	0.047	0.032	0.052	0.180	0.064		0.073	0.095	0.020	0.166
9	9	0.099	0.063	0.078	0.070	0.142	0.005	0.141	0.073		0.086	0.053	0.028
10	10	0.097	0.058	0.037	0.127	0.075	0.004	0.117	0.095	0.086		0.204	0.005
11	11	0.112	0.104	0.190	0.063	0.008	0.302	0.213	0.020	0.053	0.204		0.005
12	12	0.096	0.191	0.099	0.050	0.057	0.091	0.014	0.166	0.028	0.005	0.005	
θ (deg)	No.	1	2	3	4	5	6	7	8	9	10	11	12
1	1		-177.77	-194.34	-115.75	-145.94	-279.22	-3.08	-241.74	-79.91	-146.78	-162.61	-210.24
2	2	177.77		-315.83	-100.31	-82.17	-299.09	0.00	-257.52	-62.35	-130.56	-156.76	-219.19
3	3	194.34	315.83		-103.39	-101.07	-299.92	-8.94	-252.31	-67.76	-131.35	-154.37	-213.74
4	4	115.75	100.31	103.39		-284.31	-289.24	-305.51	-269.14	-350.65	-252.24	-232.13	-249.28
5	5	145.94	82.17	101.07	284.31		-293.11	-340.47	-258.26	-58.21	-147.44	-170.04	-225.18
6	6	279.22	299.09	296.92	289.24	293.11		-82.69	-198.28	-88.57	-123.40	-136.63	-175.09
7	7	3.08	0.00	8.94	305.51	340.47	82.69		-232.98	-93.84	-154.36	-166.05	-206.40
8	8	241.74	257.52	252.31	269.14	258.26	198.28	232.98		-69.77	-95.78	-111.01	-151.76
9	9	79.91	62.35	67.76	350.65	58.21	88.57	93.84	69.77		-209.17	-206.21	-230.65
10	10	146.78	130.56	131.35	252.24	147.44	123.40	154.36	95.78	209.17		-198.57	-247.66
11	11	162.61	156.76	154.37	232.13	170.04	136.63	166.05	111.01	206.21	198.57		-264.37
12	12	210.24	219.19	213.74	249.28	225.18	175.09	206.40	151.76	230.65	247.66	264.37	

5.3.2 Spatial Correlation Pattern Analysis

In this section, we derive the rainfall spatial correlation pattern from 3 parameters: distance, spatial correlation and azimuth angle as shown in Table. 5.2. Each parameter is calculated from a pair of rain gauge data. Derivation of this pattern requires symmetrical information. However, the bearing angle can be calculated in both directions of a pair of rain gauge data and can use the same data of spatial correlation and distance. Finally, we obtain 132 combinations.

Figure 5.5 illustrates the spatial correlation pattern derived from rain gauge data around the center of Bangkok, Thailand. The abscissa represents the distance from West to East in kilometers and the ordinate represents the distance from South to North in kilometers. The result shows that a high correlation happens within 10-20 km of the center. To most effectively locate the site diversity for distances of more than 20 km, the direction should be considered.

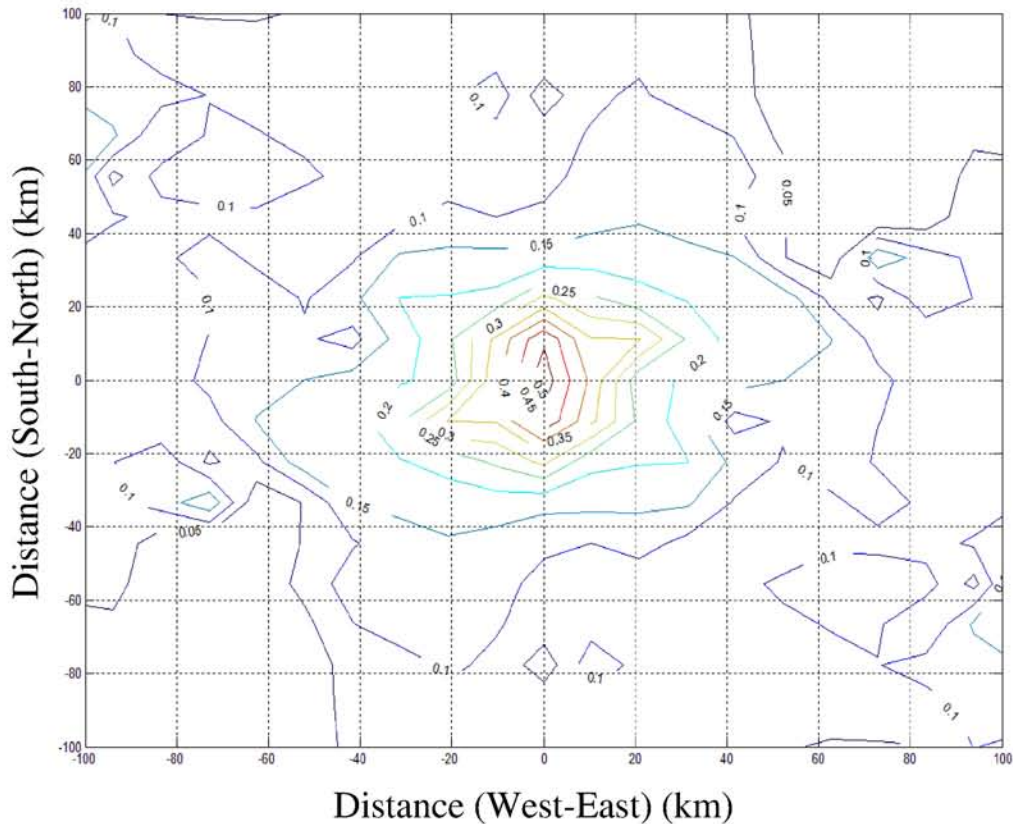


Figure 5.5: Rainfall spatial correlation pattern in the center of Thailand.

5.4 Site Diversity Gain Improvement

According to the derived results from the previous section, especially from the spatial correlation pattern, the existing site diversity formula should be improved. It is shown that the spatial correlation is not only dependent on the distance but also the direction. This dependence should be included, as shown in the following equation:

$$\rho(D, \theta) = \exp\left[-\alpha(D, \theta)D^{\beta(D, \theta)}\right] \quad (5.3)$$

The site diversity gain formula is expressed by ITU R P.618-12 as the equation below.

$$G_d = k(1 - \rho)^m \quad (5.4)$$

Then, Eq. (5.4) can be improved to estimate the diversity gain more accurately by using the spatial correlation that depends on both distance and direction. The new formula is rewritten as follows:

$$G_d = k\left(1 - \exp\left[-\alpha(D, \theta)D^{\beta(D, \theta)}\right]\right)^m \quad (5.5)$$

where G_d is diversity gain, and k and m are the approximation coefficients of diversity gain.

5.5 Summary of Chapter 5

The distance and direction dependences of the spatial correlation factor are shown. The spatial correlation can be used to consider the rain attenuation mitigation method, especially in tropical areas such as Thailand. The improvement of the site diversity gain contributes to a more precisely predictable formula. However, to mitigate the rain attenuation in future satellite communications in the high frequencies of the Ka-band and above, the number of diversity sites should be increased inversely to the size of the site diversity [10].

In this analysis, we used 3 hours of averaged rain rate data. It is known that data at shorter time intervals, such as 1 min intervals, are suitable for evaluation of rain attenuation mitigation methods. It is expected that shorter time intervals of rain rate measurement can provide smaller rain correlation coefficients between two sites.

References of Chapter 5

- [1] C. Kouroglogas, A. D. Panagopoulos, S. N. Livieratos and G. E. Chatzarakis, “Pico-Scale Dynamic Diversity Gain Evaluation in Broadband Satellite Communication System,” *Ka and Broadband Communication, Navigation and Earth Observation Conference*, pp. 621-627, 2014.
- [2] C. Nagaraja and I. Otung, “Statistical Prediction of Site Diversity Gain on Earth-Space Paths Based on Radar Measurements in the UK,” *IEEE Trans. Antennas Propag.*, vol. 60, no. 1, pp. 247-256, 2012.
- [3] J. X. Yeo, Y. H. Lee and J. T. Ong, “Performance of Site Diversity Investigated Through RADAR Derived Results,” *IEEE Trans, Antennas Propag.*, vol, 62, no. 10, pp. 3890-3898, 2011.
- [4] J. Poolsawut, T. Limpiti and N. Puttarak, “A study on Ka-band site switching using advanced prediction for rain-induced attenuation,” *The International Symposium on Antenna and Propagation (ISAP)*, pp. 157-158, 2014.

- [5] S. Begum, C. Nagaraja and I. Otung, “Analysis of Rain Cell Size Distribution for Application in Site Diversity,” *Proc. European Conference on Antennas and Propagation (EuCAP)*, 2006.
- [6] J. X. Yeo, Y. H. Lee and J. T. Ong, “Site Diversity Gain at the Equator: Radar-Derived Results Modeling in Singapore,” *Int. J. Satell. Commun. Network.* 2015; **33**:107-118. doi:10.1002/sat.1074.
- [7] M. Akimoto and K. Watanabe, “Study on Rain Attenuation Considering Rainfall-Intensity Dependent Spatial Correlation Characteristics,” *Global Telecommunications Conference*, pp. 2864-2868, 2004.
- [8] S. Maeda and H. Fukuchi, “Quantitative Assessment of Site Diversity from Rainfall Spatial Correlation Characteristics,” *The International Symposium on Antenna and Propagation (ISAP)*, 2012
- [9] P. Chodkaveekityada, Y. Inose and H. Fukuchi, “Modeling of Site Diversity Gain Using Rain Radar Data in Japan,” *33rd AIAA International Communications Satellite Systems Conference (ICSSC)*, 2015.
- [10] B. Roy, A. K. Shukla and M. R. Sivaraman, “Micro Scale Site Diversity Over A Tropical Site In India and Evaluation of Diversity Gain with Synthetic Storm Technique,” *Indian Journal of Radio & Space Physics*, vol. 40, pp. 211-217, 2011.

Chapter 6

Conclusion

6.1 Summary of Preceding Chapters

This thesis has revised and proposed improved attenuation mitigation methods to support the next generation of satellite communications operating in the Ka-band and above. The main results are summarized as follows.

Chapter 1 presented the roadmap of satellite communication and overall rain attenuation mitigation technologies.

Chapter 2 revised the cross-polarization effects due to rain from 10-100 GHz and discussed the relation between rainfall rate, attenuation and XPD. Moreover, homogeneous and inhomogeneous rain models were considered. According to the conventional raindrop size distribution of MP model it may overestimate small diameter raindrop number, on the other hand the latest Gamma model has convex shape distribution. Then, it is expected that the propagation parameter such as attenuation and XPD difference between MP

and Gamma models becomes apparent in higher frequency are such as 100 GHz which as short wave. This speculation is theoretically proved by attenuation and XPD relations.

Chapter 3 proposed that the most effective method is time diversity for non-real time satellite communication services. Regarding the time diversity strategy is to transmit the broadcasting contents twice with certain time difference. More specifically, if the exact real-time transmission is not needed such as broadcasting type transmission, the contents are transmitted in advance with certain time to the formal transmission time. This time advance contents are largely compressed to save frequency resource. In this research work, it is found that even several minutes time diversity, it is equivalent to double the transmission power or antenna area. The results were expressed well as a rain intensity map, a cumulative time percentage and a diversity gain. In addition, significant parameters that can improve the accuracy of the prediction system were found.

Chapter 4 proposed the adaptive satellite power control method for locations in Japan to preliminarily investigate the power consumption. The results revealed that boosted areas can be increased by increasing the beam number, beam size or even the boost power. More specifically, if the summation of boosted areas are the same, it is efficient to use many small boosted beams rather than one large boost beam because of rain confinement to small areas as rain intensity increases.

Chapter 5 described improvement of the site diversity method by using the Thai rain gauge network. Three factors, which are spatial correlation,

distance and direction, were taken into account to enhance the prediction of the site diversity gain formula. Regarding the spatial correlation pattern in Thailand look like no large correlated areas, it is due to rain behavior in the tropical areas as convective rain is happened in the short period of time with small areas. It is expected that the site diversity method is more effective in tropical areas than middle latitude areas because at the same distance difference rain spatial correlation in tropical areas may be much smaller than middle latitude. It is speculated from the fact that space correlation property derived in Thailand which use the 3 hour integrated time is nearly the same as Japan using several minutes integration time. It is well known that the integration time decreases as space correlation of rain decreases. That is why it becomes important to realize transformation method from correlation with longer integration time to shorter one. This becomes important for future work.

Note: 1.) To realize high-speed wireless network, one example is to use dual polarization link which uses orthogonal polarization with the same frequency. In the design for such dual-polarized link, it is important to consider the both effect of attenuation and XPD. For digital communication link, it is known that the effect of attenuation is larger than depolarization. Then, the following Chapter 3-6, author emphasize the analysis on attenuation mitigation technologies.

2.) For the tropical regions high speed satellite links, some attenuation mitigation technologies should be combined.

6.2 Comparison of attenuation mitigation technologies

The comparison of rain attenuation mitigation technologies in this research are shown in Table 6.1 to summarize the advantage and disadvantage among three methods. These methods are not exclusive and may be realize more effective attenuation countermeasure.

Table 6.1: Advantage and disadvantage of 3 mitigation methods.

Method	Advantage	Disadvantage
Time diversity	- The most effective method - Ground technologies	- Non-real time communication
Adaptive satellite power control	- Specific areas needed - Real time communication	- Limited power resource - Ineffective for large attenuation
Site diversity	- Good for large attenuation - Real time communication	- Cost expensive

6.3 Future Work

Specific rainfall rate information for Japan is very useful to improve the performance of rain attenuation mitigation technologies. It will be more useful if we can establish the following systems to obtain valuable information in tropical areas, especially Thailand. Our planned work is listed below:

- A collection system of the raindrop size distribution in Thailand should be established.

- It is very important to improve the rain gauge network in Thailand from a long duration (3 hours) to a suitable duration (1 minute). A shorter duration can be used to evaluate time diversity and site diversity performances.
- By using above additional valuable data, more detailed evaluation of attenuation mitigation technologies should be done.

Appendix A

List of Publications

Journals

1. **P. Chodkaveekityada** and H. Fukuchi, "Prediction Model of Time Diversity Using Rain Radar Data," *International journal of satellite communications and networking*, 2016, DOI: 10.1002/sat. 1182.
2. **P. Chodkaveekityada** and H. Fukuchi, "Time Diversity Evaluation for Attenuation Mitigation Method Using Attenuation Data in Thailand and Japan," *International journal of satellite communications and networking*, 2016, DOI: 10.1002/sat. 1184.
3. **P. Chodkaveekityada** and H. Fukuchi, "Evaluation of Adaptive Satellite Power Control Method Using Rain Radar Data," *IEICE Transaction on Communication*, Vol. E99-B, pp.-, No. 11, Nov. 2016.
4. **P. Chodkaveekityada** and H. Fukuchi, "Effect of Raindrop Size Distribution and Rain Rate Inhomogeneity on the Relationship between Attenuation and Depolarization," *International journal of satellite communications and networking*. (Major revision)

5. **P. Chodkaveekityada** and H. Fukuchi, “Differences in the Dynamic Properties of Rain Fade between Temperate and Tropical Regions,” *Advances in Space Research*. (Major revision)

International Conferences

1. **P. Chodkaveekityada** and H. Fukuchi, “On-board Adaptive Attenuation Compensation Technique for Future Satellite Communication”, *International Symposium on Antennas and Propagation (ISAP)*, Kaohsiung, Taiwan, December, 2nd – 5th, 2014.
2. H. Fukuchi, Y. Inose and **P. Chodkaveekityada**, “Spatial Correlation Property Derived from Radar Rain Map and Site-Diversity Effect Evaluation”, *International Symposium on Antennas and Propagation (ISAP)*, Kaohsiung, Taiwan, December, 2nd – 5th, 2014.
3. **P. Chodkaveekityada** and H. Fukuchi, “Improvement of Depolarization Formula Using Gamma Raindrop Size Distribution Up to 100GHz”, *Asia-Pacific Conference on Antennas and Propagation (APCAP)*, Bali Island, Indonesia, June 30th – July 3rd, 2015.
4. H. Fukuchi and **P. Chodkaveekityada**, “Propagation Impairments Along Satellite-To-Earth Path and Their Mitigation Technologies”, *Asia-Pacific Conference on Antennas and Propagation (APCAP)*, Bali Island, Indonesia, June 30th – July 3rd, 2015.
5. **P. Chodkaveekityada**, H. Fukuchi, T. Limpiti and P. Supnithi, “Time Diversity Evaluation for Attenuation Mitigation Method Using Attenuation Data in Thailand and Japan”, *International Symposium on Space Technology and Science (ISTS)*, Kobe-Hyogo, Japan, July, 4th – 10th, 2015.

6. **P. Chodkaveekityada**, Y. Inose and H. Fukuchi, “Modeling of Site Diversity Gain Using Rain Radar Data in Japan”, *33rd AIAA International Communications Satellite Systems Conference (ICSSC)*, Gold Coast, Australia, September 7th – 10th, 2015.
7. **P. Chodkaveekityada** and H. Fukuchi, “Combination Benefits of Short-Time Diversity and Adaptive Satellite Power Control”, *International Symposium on Antennas and Propagation (ISAP)*, Hobart, Tasmania, Australia, November, 9th – 12th, 2015.
8. **P. Chodkaveekityada** and H. Fukuchi, “Variation of Boost Constants Effects for Adaptive Satellite Power Control”, *10th International Conference on Information, Communication and Signal Processing (ICICS)*, Singapore, December, 2nd – 4th, 2015.
9. **P. Chodkaveekityada** and H. Fukuchi, “Spatial Correlation Property Using Rain Gauge Network in Thailand to Improve Site Diversity Effect”, *International Conference on Electrical Engineering/Electronic, Computer, Telecommunications and Information Technology (ECTI-CON)*, Chiang Mai, Thailand, June 28th – July 1st, 2016.
10. **P. Chodkaveekityada** and H. Fukuchi, “Fade Slope Comparison between Thailand and Japan for Ka band Rain Attenuation”, *International Technical Conference on Circuits/Systems, Computer and Communication (ITC-CSCC)*, Okinawa, Japan, July 10th – 13th, 2016.